THE UNIVERSITY OF CHICAGO

MECHANISMS OF ARP2/3 COMPLEX AND OTHER ACTIN BINDING PROTEINS

A DISSERTATION SUBMITTED TO
THE FACULTY OF THE DIVISION OF THE BIOLOGICAL SCIENCES
AND THE PRITZKER SCHOOL OF MEDICINE
IN CANDIDACY FOR THE DEGREE OF
DOCTOR OF PHILOSOPHY

GRADUATE PROGRAM IN CELL AND MOLECULAR BIOLOGY

BY
MEGHAN ERIN O'CONNELL

CHICAGO, ILLINOIS
AUGUST 2021

Table of Contents

List of Figures

List of Tables

ACKNOWLEDGMENTS

The road to completing this PhD has honestly been a difficult one. There's been setbacks, tears, stress, but there's many people who made every step of it easier, more entertaining, and sometimes downright fun.

To my mentor, David Kovar: whose guidance and constant support helped me have a successful PhD and allowed me every opportunity I wanted to explore in science and career along the way- even the one that involved me going to France before joining the lab.

To Kovar lab, new and old: You made it so I loved coming to work every day. From science discussions to Thursday treats and our Chicago adventures, my graduate school experience would not have been nearly as wonderful without you all. To Olivia Gray, Linsin Smith, and Christina Roman: thank you for being my support system through all of this. The three of you made the last few years some of the most enjoyable I've had.

To Katie Miller and Caroline Auger: the two of you have been my best friends for literally as long as I can remember. No matter how far apart we are, I can count on the two of you to always be there when needed, usually with Nintendo games and laughs.

To Elis Gifford: you kept me sane through hula hoops and craft days. Thank you for always encouraging me to be kind to myself, but also teaching me that sometimes it's okay to throw a hoop at the wall in frustration.

To my partner, Carlo Berti: you are my constant rock. Thank you for taking a leap with me in this wild graduate school journey and for not only supporting me, but pushing me always to be better than I ever think I can be. Every day, I'm excited to wake up next to you and our two cats, knowing we can conquer anything as long as we are together.

Lastly, to my parents, Joan Poirier and Daniel O'Connell: you raised me to be fierce and independent. You are the reasons I am where I am today. Without your support from day one, I would be nowhere near the person I am now.

ABSTRACT

How cells temporally and spatially form complex cellular structures within a crowded cytoplasm is a fundamental question in biology. The actin cytoskeleton is a dynamic cellular network that self-organizes into a range of networks to regulate diverse cellular processes, such as cytokinesis, polarization, endocytosis, and cell motility. Understanding how these diverse F-actin networks can be assembled and maintained from their shared pool of actin monomers at the right place and time is a long-standing question in our lab.

The actin cytoskeleton assembles dynamic networks of filamentous actin (F-actin) from shared G-actin monomers through the action of actin nucleators, such as formin and Arp2/3 complex. Additionally, the individual and combined presence and functions of a wide variety of actin binding proteins (ABPs) work to define an actin network's identity—regulating assembly and disassembly, network density, and architecture—all of which lead to specialized, unique network functions. Therefore, in order to fully understand each network, it is crucial to understand the mechanistic principles that drive ABP functions, both alone and in concert.

Previous studies in our lab have demonstrated that steady-state actin networks' size and density are maintained through actin nucleator's competition for actin monomers, and that this competition is uniquely tuned by the monomer binding protein, profilin. Our lab showed that profilin favors formin-mediated actin assembly, while directly inhibiting Arp2/3 complex branching; yet, the exact mechanism underlying this inhibition is unclear. Here, we built an optimal fluorescently-tagged fission yeast Arp2/3 complex and demonstrated it rapidly nucleates branching in vitro, with no significant defects when incorporated into fission yeast cells. This construct will now be used to directly examine the mechanism by which profilin inhibition of branching occurs, along with many other mechanistic investigations. As previous work to directly visualize Arp2/3 complex has been limited—and with no direct visualization of the fission yeast protein—this new construct will prove invaluable to the field.

Additionally, in looking to understand the mechanisms of actin nucleators, we found

that the fission yeast contractile ring formin, Cdc12, is specifically tailored for its function during cytokinesis. By building chimera proteins where the FH1 and FH2 domains of Cdc12 were replaced with formins with different or similar nucleation or elongation properties, we discovered that nucleation rate is the driving factor behind efficient contractile ring assembly.

Work in our lab has shown the importance of competitive and cooperative interactions of actin binding proteins (ABPs) [28, 133]. Here, we have expanded this work and found a competitive interaction between the crosslinking proteins fimbrin and α-actinin, in which they compete for binding both in vitro and in actin patches and the contractile ring [29]. Further, we showed that the side-binding protein tropomyosin can synergize with α-actinin to make it a better competitor against fimbrin [29].

Much work has been done by our lab and others to understand how fission yeast actin network assembly is regulated, yet little has been done to understand the mechanistic properties of fission yeast actin disassembly. Here, we engineered and purified fission yeast disassembly proteins. We found that fission yeast twinfilin and CAP1 synergize for rapid barbed and pointed end depolymerization of F-actin in vitro, similar to homologs in other systems.

Further, while our lab's previous work looked at what drives actin cytoskeleton self-organization during steady state, how network identity and self-organization is initially established in fission yeast is unclear. Here, we developed and optimized a microfluidic system for fission yeast, allowing us temporal control for actin network perturbations previously not available in this organism. Through temporally controlled treatment and washout with Latrunculin A, an actin sequestering protein, we were able to mimic an initial 'disassembled' rate that was rapidly reversible to monitor initial network assembly and self-organization. We observed that Arp2/3-mediated F-actin networks were always the first to re-assemble. Interestingly, formin-mediated F-actin networks did not re-assemble in the absence of Arp2/3-mediated networks, suggesting that endocytic actin patches or their associated proteins are required for the initial establishment of formin-mediated networks.

CHAPTER 1

INTRODUCTION

1.1 Introduction

This dissertation will examine the mechanisms of multiple actin binding proteins fission yeast to build a larger picture of how F-actin networks are assembled, organized, and maintained. Our lab focuses on how F-actin and its associated actin binding proteins mechanistically function and are able to self-organize into functionally distinct F-actin networks within a crowded cytoplasm.

How something as complex as a cell, with multiple variant parts, can assemble with remarkably consistent organization is a long-standing biological question. A cell is composed of varying, complex, component parts—a rapidly diffusing mixture of proteins, lipids, and nucleic acids all sharing the space of a crowded cytoplasm—that organize into higher order, dynamic structures, such as organelles and protein complexes, with high regularity. The organization of a cell's interior structure is paramount for its function and survival, but how is the cell able to provide this organization at such a microscopic, detailed level?

The actin cytoskeleton presents a great biological model for a self-organized system and the importance of understanding its component parts. The actin cytoskeleton is dynamic; actin filaments are constantly undergoing cycles of assembly, disassembly, and turnover. These dynamic actin filaments assemble into larger, more stable F-actin network structures, which continuously exchange with their surrounding environment. How building blocks of actin subunits can lead to the generation of a wide variety of structurally and functionally distinct networks which allow actin to fulfill its multitude of roles within the cell remains a fundamental question. Throughout this dissertation, I focus on both the mechanistic characterization of actin binding proteins, that have pivotal roles in the self-organization of the fission yeast cytoskeleton, as well as examine how self-organization can occur in an initial

state, where no actin networks currently exist, rather than in a steady state system.

1.2 Actin

Actin is one of the most abundant and well conserved proteins across diverse species, compromising up to 5-10% of total protein content in some cell types. Organisms such as fission yeast, budding yeast, and other single cell eukaryotes express a single actin protein from one gene to assemble a diverse range of actin networks [51]. In contrast, in some multicellular systems, like humans, cells can express different actin isoforms from multiple genes, allowing for distinct roles of each isoform in specific actin network assembly. Whether it is one or multiple genes, these vast array organisms utilize actin molecules which are both structurally and functionally similar [51].

1.2.1 Properties of actin assembly

The building block of actin networks in cells is the actin monomer (G-actin), a globular 43kDa protein with four distinct subdomains as well as a nucleotide binding cleft (Figure 1.1A). This medial cleft is able to bind to adenosine triphosphate (ATP), ADP-Pi, or adenosine diphosphate (ADP), but in the G-actin form will most tightly bind to ATP [140]. Under physiological conditions, monomeric ATP-bound actin will spontaneously polymerize into dynamic, filaments known as F-actin. However, actin polymerization has an initial lag period, due to a rate-limiting nucleation step at the beginning of polymerization [32]. Actin dimers are energetically unfavorable and thus dissociate back into actin monomers quickly [32]. Once a stable actin trimer is formed, an actin filament can polymerize from both ends of the filament, though this assembly occurs at different rates, generating polarity in the actin filament (Figure 1.1B). At a fast-growing barbed end, F-actin elongates rapidly compared to the slow-growing pointed end [109]. Upon addition of an actin monomer into an actin filament, an actin monomer undergoes a conformational change that rapidly promotes ATP

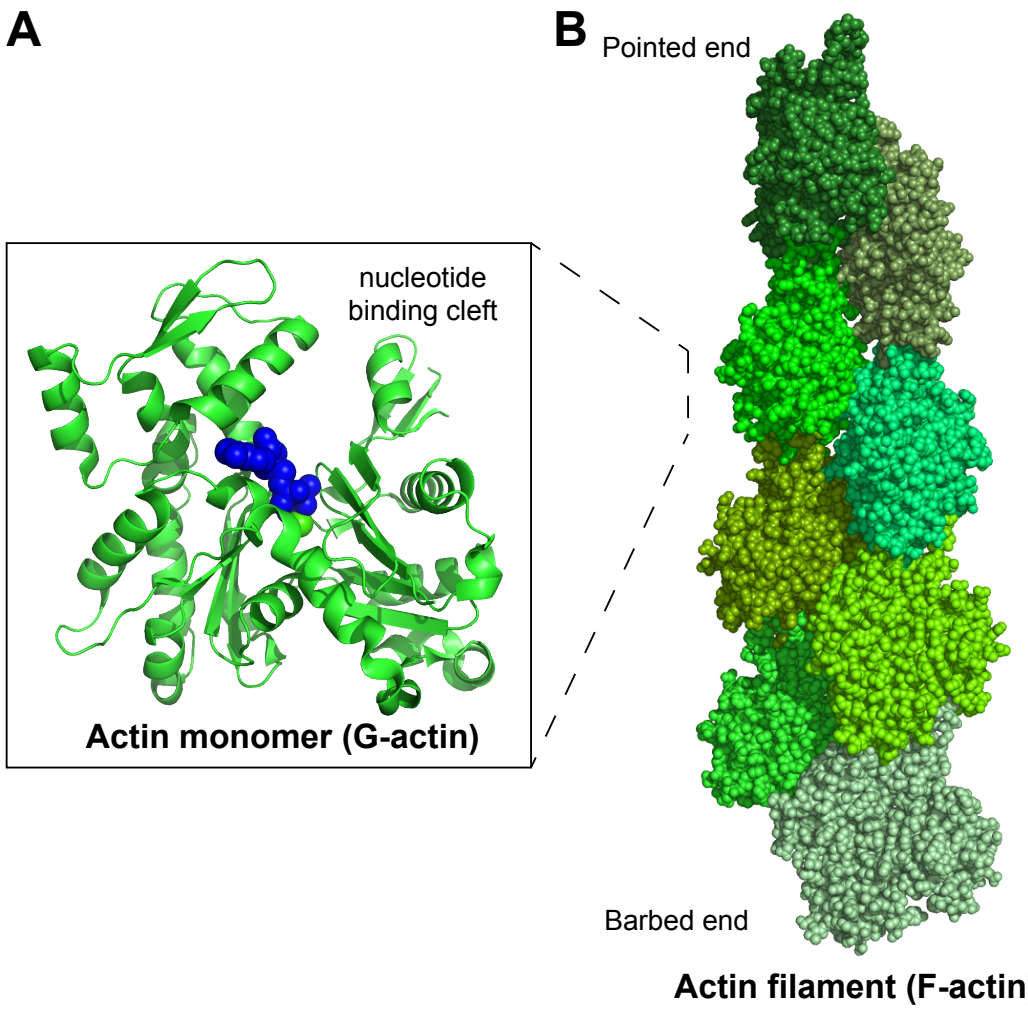

Figure 1.1: **Actin monomers (G-actin) polymerize to form actin filaments (F-actin). (A)** Structure of a globular actin monomer (PDB: 1NWK) (G-actin) with ATP (blue) at the nucleotide binding cleft. **(B)** Filamentous actin (F-actin) (PDB: 6BNO) is formed by the polymerization of G-actin monomers. F-actin is composed of a slow-growing pointed end (top) and fast-growing barbed end (bottom).

hydrolysis into the ADP-Pi form. The release of inorganic phosphate is slow, but upon release then forms ADP-actin [23]. ADP-actin dissociates easily from both filament ends, allowing for disassembly of the actin filament back to its monomeric form, where it can be recycled for later use.

The ability for actin monomers to polymerize is calculated in reference to the critical concentration (C_c), the concentration at which G-actin and F-actin are in equilibrium. If the concentration of actin is below the critical concentration, disassembly is favored and filament elongation is highly unfavorable. Above the critical concentration, assembly is highly favored and F-actin can polymerize. The rates of assembly and disassembly are also influenced by the critical concentration [109].

While actin rapidly polymerizes under physiological conditions in vitro, within cells, actin polymerization is highly restricted. Despite actin concentrations in the cytoplasm ranging between 50-200 μM, well above the critical concentration, approximately half of all actin exists as unpolymerized actin monomers. This cytoplasmic pool of available actin monomers is maintained through different actin assembly factors and actin binding proteins (ABPs). Profilin in particular is a small protein which can bind to actin monomers and inhibit nucleation of actin filaments, but allows for addition to the barbed end of a pre-existing actin filament [62, 112]. Most cytoplasmic free actin monomers are bound to profilin, thus controlling and regulating actin nucleation and elongation within cells [62]. Other ABPs work together to regulate actin networks [28, 29], maintain a pool of monomeric G-actin through regulation of the nucleation and elongation of F-actin [141, 142], or by building and maintaining higher order F-actin networks through mechanisms discussed later in this chapter.

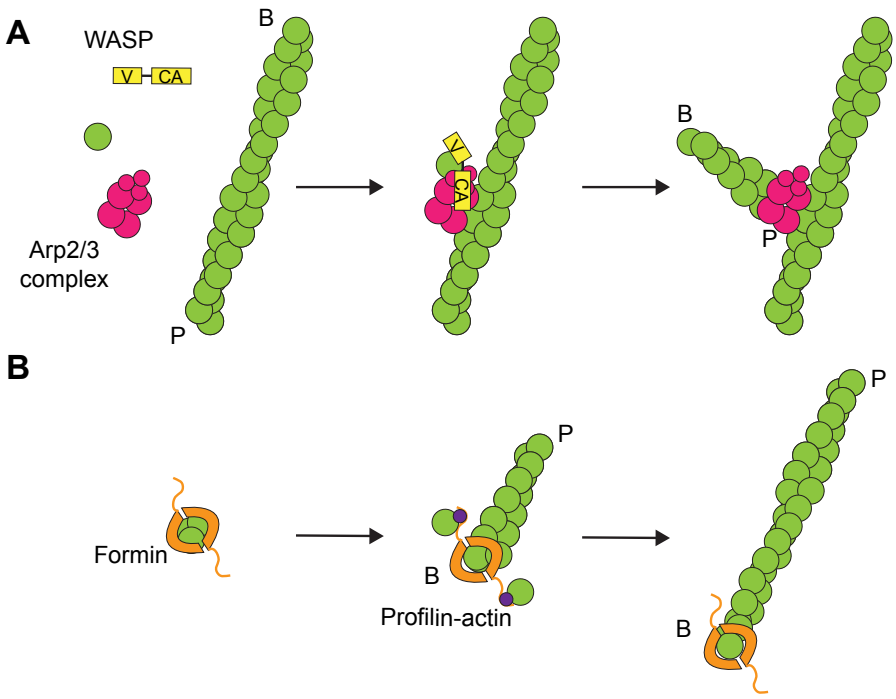

Figure 1.2: **Arp2/3 complex and formins are the primary actin assembly factors in fission yeast. A.** Arp2/3 complex forms a complex with WASP and an actin monomer. This complex (Arp2/3 complex, WASP, and an actin monomer) binds to the side of an existing actin filament to nucleate a branch upon dissociation of WASP. **B.** Formins stabilize an actin dimer or trimer. Upon seed formation, formins can then processively elongate actin filaments through the addition of profilin-actin complexes to the barbed end.

1.3 Actin assembly factors

In order to spatially and temporally control actin network assembly, cells employ actin assembly factors, which allow them to overcome energy barriers which discourage spontaneous F-actin nucleation. In fission yeast, there are two primary classes of actin assembly factors, formins and Arp2/3 complex, which are discussed in the following section.

1.3.1 Formin

Formins are a large class of proteins that are expressed across most eukaryotic species, with many expressing multiple different isoforms that have distinct functions within different

cell types and even subcellular locations. Formins are highly conserved and are classified by their ability to associate with the barbed end of F-actin filaments. The formin protein family consists of proteins with multiple domains, each with a distinct role in actin nucleation (FH2), actin elongation (FH1FH2), or regulation of either of these processes.

Formins are characterized by the presence of two types of formin homology domains (FH1, FH2) which each promote formin's role in F-actin nucleation and elongation [105]. The FH2 domain forms a donut-shaped homodimer which facilitates nucleation of F-actin filaments (Figure 1.2B) [105]. While the mechanism by which this occurs is not fully understood, it is hypothesized and there is evidence to suggest it does so by stabilizing the actin dimer or trimer nucleus, the highly energetically unstable intermediate in filament polymerization [104, 16]. Then, the FH2 domains will processively associate with the growing barbed end of an actin filament. During this elongation and processivity, the FH1 domains can bind profilin-actin through polyproline-rich motifs and promote G-actin addition to the barbed end (Figure 1.2B) [16]. It is unclear whether the FH1 domain directly incorporates G-actin, or simply promotes addition through increasing the local concentration of profilin-actin around the barbed end. In either case, FH1FH2 domains allow many formins to increase the barbed end elongation rate above that of actin alone. Through these mechanisms, formin is able to nucleate and rapidly elongate long, linear F-actin filaments, which are often structurally well-suited for networks which experience contractile stress or tension, such as the cytokinetic contractile ring or F-actin stress fibers.

However, despite the well-conserved mechanisms of formin's roles in F-actin nucleation and elongation, the rates at which these processes occur vary for different formins when characterized *in vitro* [126]. Partially, this is due to differences in both the sequence variance in FH1 and FH2 domains, the distance between FH1 and FH2 domains, or the number of FH1 domains in the particular formin. It is also due to a wide variety of less well-conserved regulatory or localization domains that directly tailor each formin for its particular role in

the cell [24]. In addition to variations in the FH1 and FH2 domains, many formins contain an autoinhibitory mechanism through the interaction of two domains: their diaphanous autoregulatory domain (DAD) and diaphanous inhibitory domain (DID). This interaction autoinhibits formin nucleation and elongation and is released by a Rho family GTPase binding to the DID [76, 99].

1.3.2 Arp2/3 Complex

The actin-related protein-2/3 (Arp2/3) complex is a 7-subunit protein complex that is essential for life through its role in cellular processes such as endocytosis and cell motility [46]. The two proteins for which Arp2/3 complex gets its name—actin-related proteins 2 and 3—are structurally similar to actin monomers and together mimic the structure of the actin dimer [90]. Unlike formins which nucleate linear F-actin, Arp2/3 complex primarily nucleates branched F-actin networks [45, 145]. These branched F-actin networks are often dense, and optimal for force-generating cellular processes—being able to internalize vesicles or push the lamellipodial membrane forward for cellular motility [145, 158].

To nucleate F-actin, Arp2/3 complex binds to the side of an existing actin filament (referred to as the mother filament) (Figure 1.2A). There, Arp2/3 complex acts as the nucleus for a new filament growth (the daughter filament) and anchors the pointed end of the newly growing daughter filament as the barbed end elongates. This results in a 70 degree angle branch structure of the daughter filament from the side of the mother filament (Figure 1.2A) [46, 45, 145].

However, in many eukaryotic systems, Arp2/3 complex exists in an inactivated state and must be activated before it can nucleate actin filaments. Arp2/3 complex is activated through multiple families of nucleation promoting factor (NPF) proteins which each allow for Arp2/3 complex activation in specific cellular processes [117, 110]. The most well-understood family of NPFs is the Wiskott-Aldritch Syndrome Protein (WASP) family [73]. Two non-

mutually exclusive mechanism have been proposed for how WASP family proteins are able to activate Arp2/3 complex branch formation. Using WASP as an example, the first mechanism proposes that WASP binds an actin monomer, then when WASP interacts with Arp2/3 complex it provides a third actin monomer, thus stabilizing the Arp2/Arp3 actin nucleus required for branch formation (Figure 1.2A) [35]. The second mechanism is that WASP family NPFs induce a conformational change upon binding to Arp2/3 complex that activates the Arp2/3 complex for nucleation [45]. Through both of these models, NPFs are able to efficiently activate Arp2/3 complex branch formation.

In some instances, Arp2/3 complex can be activated to nucleate linear F-actin by proteins from the WISH/DIP/SPIN90 family of proteins [154, 153]. While the *in vivo* phenotypes of Dip1 fission yeast cells are difficult to interpret [7], much has been elucidated about the mechanisms of this family of proteins *in vitro*. This family of NPFs binds Arp2/3 complex to form a dimer between the NPF and Arp2/3 complex [80]. This induces a conformational change in the Arp2/3 complex, allowing it to nucleate a linear actin filament, remaining bound at the pointed end of this filament [5, 80]. Further, recent work has shown that a ternary complex can be formed between SPIN90, Arp2/3 complex, and formins to promote enhanced actin nucleation via Arp2/3 complex with rapid filament elongation via the formin [21]. While the mechanisms for how these processes occur is newly developing research, it further demonstrates mechanism by which the cell can regulate and control network assembly and architecture using a subset of assembly factors and regulatory ABPs.

1.4 Actin binding proteins

We have discussed how actin assembly can be regulated in space and time through localization of actin assembly factors and their regulatory mechanisms, however, actin filaments do not exist as independent single filaments. F-actin must be assembled into highly ordered network structures to perform specific cellular functions. So how does a cell regulate this

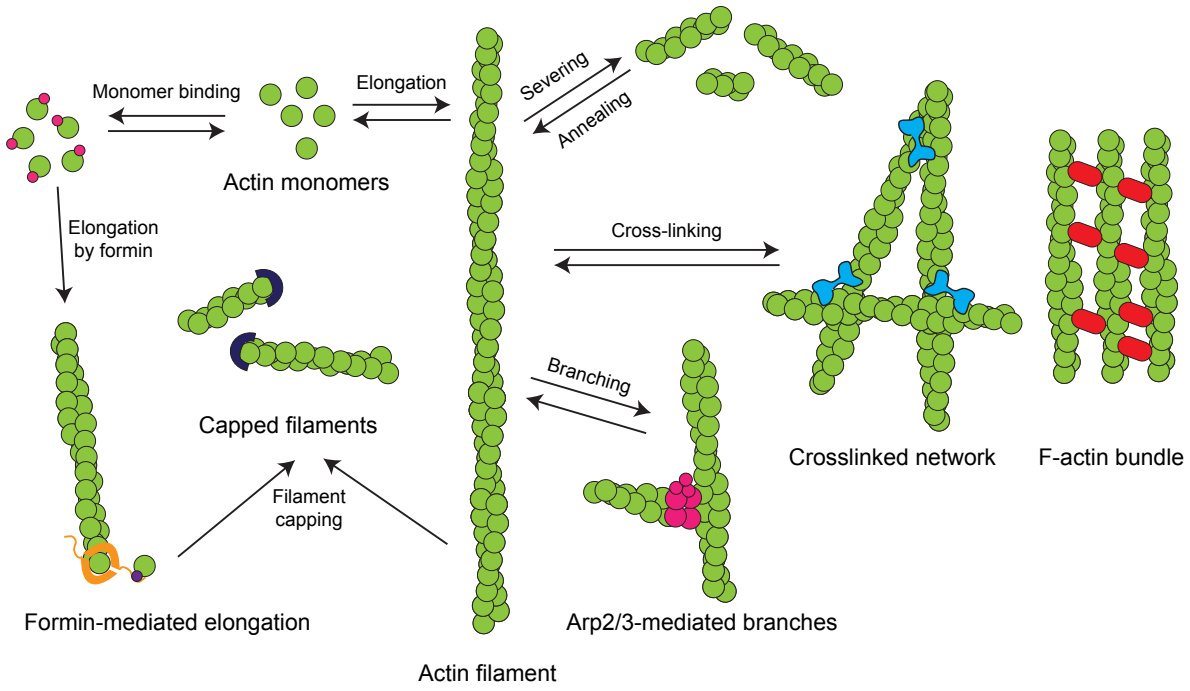

Figure 1.3: **Actin binding proteins regulate actin assembly and architecture.** Cartoon diagramming the various roles of actin binding proteins in the assembly, disassembly, and architecture of F-actin filaments and networks.

higher-ordered F-actin network in its structure, size, and timing?

Actin binding proteins (ABPs) work in concert to regulate these features of F-actin networks, tailoring an individual network for a specific cellular function, such as endocytosis or cytokinesis. ABPs control the size, structure, rigidity, and organization through depolymerizing, severing, capping, bundling, and crosslinking filaments in each network. Below, I will discuss the mechanisms of ABPs relevant to the work in the following chapters, with ABPs organized based on their specific functions.

1.4.1 Disassembly proteins

F-actin networks are dynamic structures that are undergoing cycles of assembly and disassembly. In order to maintain homeostasis and perform appropriate cellular functions, it is critical that the disassembly of actin filaments be properly regulated in space and time. Cells

disassemble actin through two major mechanisms: depolymerization of actin filaments from both ends and the severing of actin filaments (Figure 1.4). This role is primarily fulfilled by the gelsolin and actin depolymerizing factor (ADF)/cofilin families of proteins [110]. One chapter of this dissertation will focus closely on actin disassembly proteins in the ADF/cofilin family, as well as their cofactors.

The ADF/cofilin family of proteins plays a pivotal role in actin-severing in eukaryotic cell types with a unique mechanism that is enhanced by many cofactors. Cofilin binds to the sides of actin filaments in a cooperative manner, but if F-actin is saturated with cofilin the filament is stable. However, when cofilin is sparsely decorated on F-actin, the actin filament is severed at the boundary of cofilin-decorated and bare actin filament segments [143], which evidence suggests is caused by a change in the actin filament twist conformation [86, 147]. Additionally, cofilin has a preference for ADP-actin rather than ATP-actin [13, 22], helping it to promote the disassembly of "older" actin filaments, maintaining a cytoplasmic pool of G-actin for reuse in network assembly. In fission yeast, a single version of cofilin, ADF1, is expressed and is responsible for promoting actin disassembly and turnover at both actin patches and the contractile ring [74, 26, 149].

While cofilin has innate severing ability independently, in many systems cofilin's activity can be regulated by multiple cofactors. Two key cofactors of cofilin, which are found in fission yeast are Coronin (Crn1) and Actin Interacting Protein 1 (AIP1). This three component system works in concert to enhance actin-severing activity [59]. Briefly, coronin binds to actin filaments and rapidly recruits cofilin, which in turn recruits AIP1 to rapidly enhance cofilin-mediated severing and produce a behavior *in vitro* that recapitulates the process of actin treadmilling [59]. Most recently, cofilin-mediated actin turnover at the pointed end was shown to be enhanced through cyclase-associated protein (CAP), further extending the possible in vivo mechanism for cofilin regulation [127, 68].

Twinfilin (Twf1 in fission yeast) is another protein within the ADF/cofilin family, but

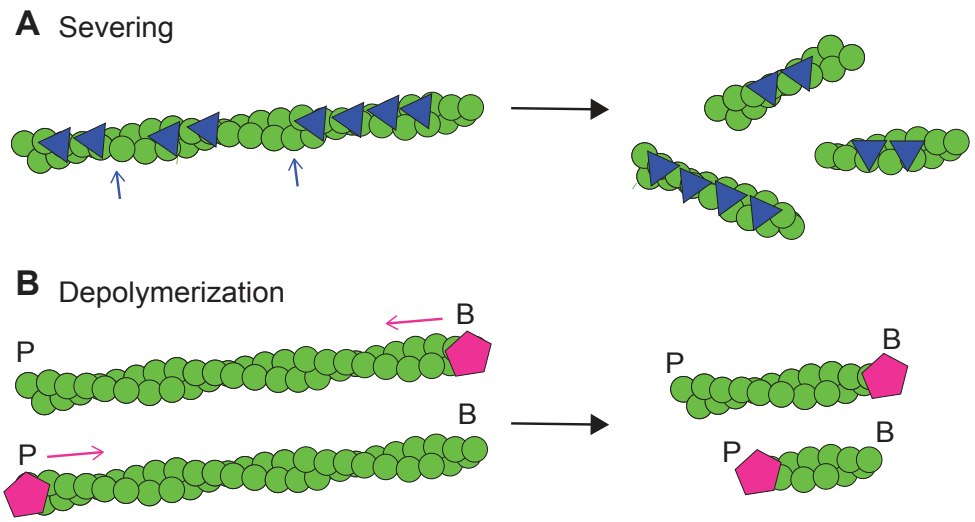

Figure 1.4: **Actin binding proteins disassemble F-actin through severing and depolymerization. A.** Severing proteins bind to the sides of F-actin in a cooperative manner and severing of F-actin occurs at the boundaries of decorated and undecorated filament (severing sites denoted by blue arrows). **B.** Actin binding proteins can bind to the barbed or pointed end of F-actin and promote depolymerization from that end (denoted by pink arrows).

promotes actin depolymerization rather than actin-severing as a mechanism for actin disassembly [47]. Twinfilin interacts with both the sides and barbed ends of actin filaments and is predicted to have conformational effects on F-actin that promote rapid pointed end depolymerization as well as slower, barbed end depolymerization in budding yeast. Twinfilin interacts with the Srv2/CAP (CAP1 in fission yeast) to further increase the depolymerization rate at both the barbed and pointed end [60, 119]. Interestingly, actin depolymerization by Twinfilin at the pointed end is a species-specific function as mouse twinfilin is unable to increase pointed end actin depolymerization rates, shown to be due to a divergence in the yeast C-terminal ADF-H domain [57]. However, Twinfilin's barbed end depolymerization function is evolutionarily conserved, marking its importance in F-actin network turnover across eukaryotes [57].

1.4.2 Capping proteins

In addition to regulating actin assembly and disassembly, cells must be able to maintain actin filaments at specific lengths to perform discrete functions. For example, Arp2/3 complex F-actin networks require dense, short, branched filaments in order to generate the forces needed to internalize vesicles or push the membrane forward during cell motility. To maintain short actin filaments, multiple types of ABPs are able to cap the ends of actin filaments to prevent further elongation and help maintain the desired filament length. One of the most important proteins which is expressed in a majority of eukaryotes, including fission yeast, is the appropriately named capping protein [110, 36]. Capping protein is a heterodimer of two structurally similar subunits, α- and β- capping protein, that binds to the barbed end of actin filaments preventing further elongation [67] (Figure 1.3). Within the cytoplasm, capping protein is found at high, local concentrations, such that F-actin is capped rapidly after assembly, limiting free barbed ends—thus excess F-actin assembly—and helping to maintain the cytoplasmic pool of G-actin monomers [72].

1.4.3 Crosslinking proteins

Actin crosslinking proteins provide the ability to impose stability and rigidity on virtually all F-actin networks within cells. Crosslinking proteins bind to multiple actin filaments simultaneously and provide a physical linkage between filaments, which can be accomplished in two ways (Figure 1.3) [84, 6]. In proteins such as fimbrin, crosslinking proteins contain multiple actin binding domains in a single protein [6]. This allows one molecule of fimbrin to simultaneously bind to multiple actin filaments. In contrast, proteins such as α-actinin contain only a single actin binding domain but dimerize two monomers to accomplish crosslinking [131, 152, 164]. Each crosslinking protein is localized to a specific F-actin network, tailored for the necessary function. How these proteins localize will be briefly discussed in Section

1.5 of this introduction on actin self-organization. In the case of fission yeast, there are two well-characterized and known bundling proteins: fimbrin and α-actinin. Fimbrin localizes to actin patches to crosslink branched filaments into dense F-actin networks for vesicle internalization [132]. α-actinin functions at the contractile ring to form dynamic F-actin bundles—a form of crosslinking in which two parallel filaments are linked at multiple points along each filament—that allow for F-actin sliding needed for cytokinetic constriction of the contractile ring [78].

1.4.4 Side-binding proteins

A varied class of ABPs comes in the forms of filament side-binding proteins. While their functions vary, side-binding proteins are often considered important for dictating how and when other ABPs can associate with specific actin networks, making them key regulators in actin self-organization [51]. One of the most well-studied side-binding protein that has been a key regulator of self-organization is the protein tropomyosin (Cdc8 in fission yeast). Tropomyosin is mainly known for its role in regulating skeletal muscle contraction [44, 137], but mammalian cells express over 40 different tropomyosin isoforms in other cells that are responsible for localization of actin binding proteins to specific F-actin networks, particularly the mediation of cofilin and myosins [98, 139]. In fission yeast, a single tropomyosin gene is found at actin cables and the contractile ring as an unacetylated and acetylated variant, respectively. Similar to mammalian tropomyosins, tropomyosin Cdc8 in fission yeast has been shown to be a major mediator in ABP sorting to particular F-actin networks [133, 28, 29]. Tropomyosin has been shown to inhibit cofilin Adf1 and myosin I activity (actin patch components) while promoting formin Cdc12 and myosin II activity (contractile ring components) [30, 132, 133].

1.5 Self-organization of the actin cytoskeleton

With actin networks able to perform such specific, discrete functions, a long-standing question is how actin is regulated in space and time for assembly and disassembly of dynamic structures with various architectures and a specified set of actin binding proteins. As Chapter 4 discuss how self-organization is initially established, in this section I will briefly discuss what we know about how assembly factors and actin monomer competition can influence the specific identity of individual actin networks. Actin network self-organization can also be influenced by actin binding protein sorting [28, 29, 12, 30, 70], which is discussed in Chapter 3.

1.5.1 Competition for actin monomers by actin assembly factors

While it is well known that signaling cascades localize and spatially regulate actin assembly factor function, it remains unclear how F-actin is assembled at the proper time, place, and with the proper size and architecture. Recent evidence shows that signaling cascades alone are insufficient and other mechanisms must be involved for proper self-organization.

Work in our lab argues for expanding the model of regulating actin network assembly—a limited pool of actin monomers regulates the size and density of different actin networks via monomer competition between actin assembly factors [17, 141, 142]. This model hypothesizes that if homeostatic actin networks compete for monomeric actin, then when one network is disrupted, the remaining F-actin networks will exhibit an increase in G-actin incorporation, leading to an increase in network size and/or density. While many studies have observed this phenomenon [17, 43], I will briefly discuss how this has been observed for fission yeast.

When fission yeast cells are treated with an Arp2/3 complex inhibitor, CK-666, the depletion of actin patches leads to an increase in formin-mediated actin structures throughout the cell [17]. The parallel is also true here: when fission yeast formins are genetically inhibited

or perturbed, Arp2/3 complex-mediated actin patches show an increased incorporation of actin monomers, leading to a greater number of actin patches [17]. Interestingly though, the increase in available actin monomers does not result in a change in actin patch size—only an increase in the number of patches present—suggesting that other factors help to regulate the distinct size of actin patches.

1.5.2 Profilin tunes actin monomer availability

As its been shown that F-actin networks will compete for actin monomers [17, 142], how does the cell spatially and temporally tune actin monomer distribution between specific actin networks? In fission yeast, there are 15-fold more Arp2/3 complex molecules than formin molecules, thus a mechanism must be in place for this small number of formins to be able to effectively compete with Arp2/3 complex [162, 129]. This mechanism comes from the monomer binding protein profilin. Profilin was previously discussed in this chapter as a monomer-binding protein which enhances formin-mediated actin assembly. Recent work has also demonstrated that profilin can inhibit Arp2/3 complex activity, likely through competition with Arp2/3 complex activators for actin monomers [141, 118]. Profilin therefore acts a mediator for internetwork competition by tuning actin monomer to favor formin-mediated assembly and is important for controlling this balance between actin networks in fission yeast.

1.6 Fission yeast actin networks

This dissertation focuses on investigating mechanisms of actin assembly, disassembly, and maintenance within the model organism, *Schizosaccharomyces pombe* (fission yeast). While fission yeast has four possible F-actin networks that can form, one F-actin network is only assembled during fission yeast mating processes. This dissertation does not investigate questions involving this process or its associated F-actin network. The three primary fission yeast

F-actin networks—actin patches, cables, and the contractile ring—are described below and are the focus of this dissertation.

1.6.1 Patches

Actin patches assemble at sites of endocytosis, and it is suggested their function in endocytosis accompanies cell wall remodeling and synthesis (Figure 6.1B) [41, 3]. In interphase cells, actin patches assemble at the tips of the cell for polarized cell growth (Figure 6.1A). In dividing cells, actin patches are found at the midzone. Work in budding yeast has shown that actin patch assembly occurs in a strict and ordered manner with specific timing for each individual actin patch component: proteins which promote membrane invagination are the first to arrive, followed by adaptor proteins and finally ABPs that mediate actin assembly [130]. As previously mentioned, actin patch assembly is dependent on Arp2/3 complex-mediated branched actin assembly, though the mechanism by which Arp2/3 complex-mediated actin assembly causes vesicle internalization is unclear. In order to promote Arp2/3 complex-mediated actin assembly, the Arp2/3 complex activators WASP homolog Wsp1 and type I myosin Myo1 are localized to cell tips and will localize at the base of the invaginating membrane [130, 75].

The structure and components of actin patches are fairly well understood. As stated previously, the actin patch is composed of a dense network of short branched actin filaments (Figure 6.1B). Mathematical modeling has predicted that a single actin patch is composed of approximately 150 actin filaments that are about 100-200 nm in length [11]. These are kept short through the rapid action of capping protein. Additionally, actin patches are crosslinked by fimbrin Fim1 to provide rigidity and disassembled primarily by the severing activity of cofilin Adf1 [130]. As there are many other ABPs that regulate vesicle internalization as well as patch assembly and turnover, the proteins relevant to each chapter will be discussed more thoroughly throughout this dissertation.

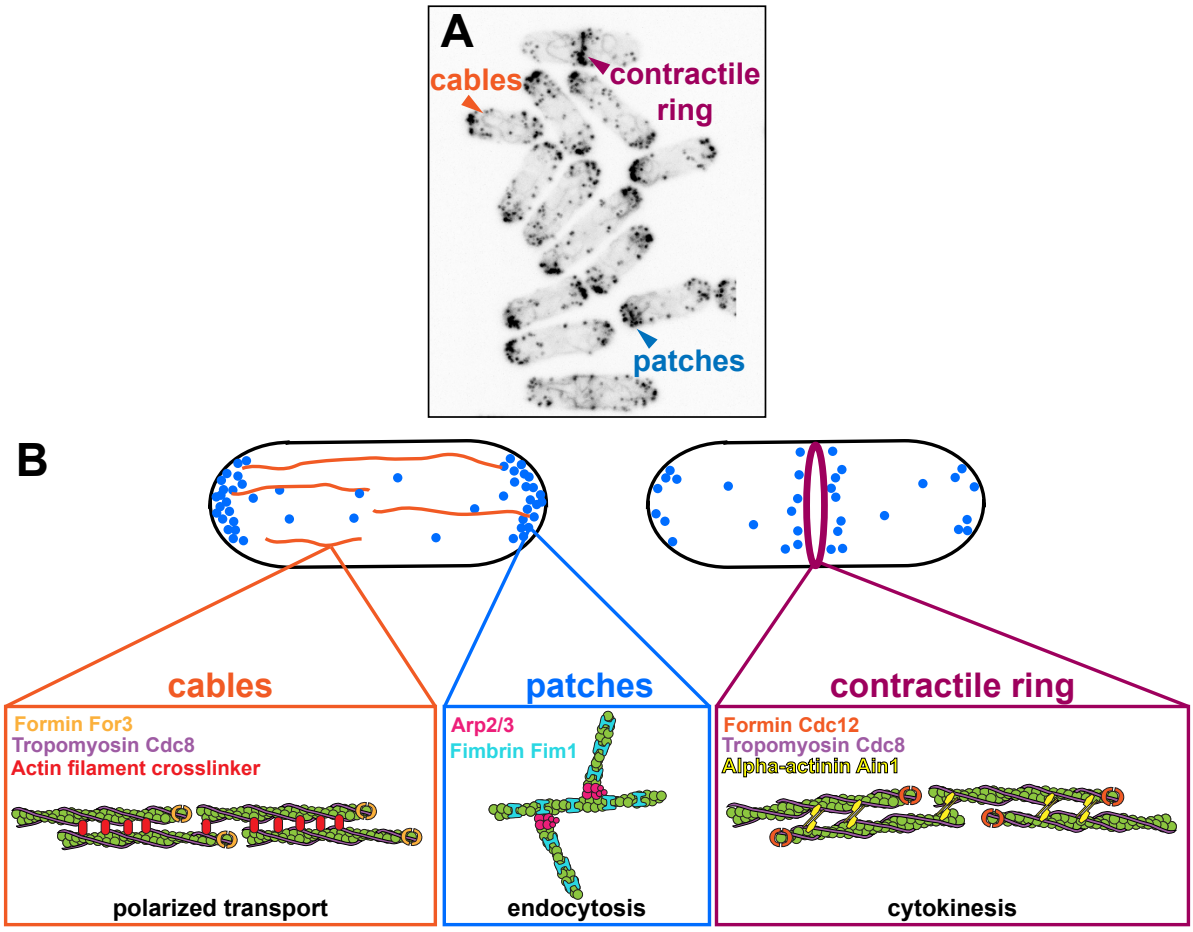

Figure 1.5: **Fission yeast primary F-actin networks. (A)** Confocal max Z-projection of fission yeast expressing Lifeact-GFP, which dynamically labels F-actin networks within the cells. Arrows and color denote the three primary F-actin networks present, which are diagrammed in B. **(B)** Cartoon of three primary F-actin networks in fission yeast in interphase (left) and dividing (right) cells. Key actin assembly factors and actin binding proteins are highlighted in cartoons.

1.6.2 Contractile ring

The actin contractile ring is responsible for the driving of cytokinesis in fission yeast (Figure 6.1). In fission yeast, this network is assembled by the formin Cdc12 at the midzone of the cell. Much of our current knowledge on the process of cytokinesis comes from genetic screens in both budding yeast and fission yeast that led to the identification and mechanistic information of many key players in this process. There are three major stages of the contractile ring which govern the process of cytokinesis: ring assembly, dwell, and constriction.

There are two distinct, but non-mutually exclusive models which have been proposed for contractile ring assembly: Search, Capture, Pull, and Release (SCPR) model and the leading cable model [150, 163]. As this dissertation does not focus on ring assembly, I will only briefly discuss the SCPR model, which is the currently prevailing model in the field. The SCPR model begins with the assembly of 65 pre-ring cytokinetic nodes around the nucleus, composed of the major proteins required for ring assembly (formin Cdc12, type-II myosin Myo2, and scaffolding and signaling proteins) [161]. Prior to mitosis onset, these nodes assemble at the cell midzone and Cdc12 nucleates F-actin [31]. These actin filaments then elongate and make contact with Myo2 in a neighboring node (Search and Capture), allowing Myo2 to pull which leads to node coalescence (Pull) [138]. Cofilin Adf1 will then release these node-node contacts via severing (Release) [95]. This cycle is repeated until ring compaction occurs and the constricting contractile ring is assembled. In addition to the SCPR cycle, the crosslinking protein α-actinin bundles the F-actin into short, anti-parallel bundles [64, 160].

1.6.3 Cables

Actin cables are difficult to image in live cells (Figure 6.1A), and thus are not well understood [71]. Actin cables are the essential tracks for polarized transport of cargo to the tips of

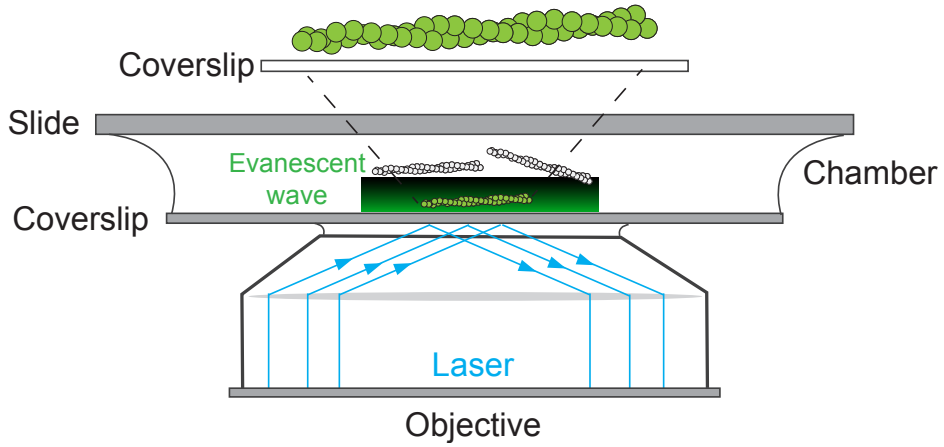

Figure 1.6: **Total Internal Reflection Fluorescence (TIRF) microscopy allows for high signal-to-noise visualization.** Cartoon diagram of TIRF microscopy set up. A through-the-objective laser illuminates at the critical angle. This allows for total internal reflection of the laser, but produces an evanescent wave, which illuminates 150-200nm above the coverslip surface rather than the whole sample.

fission yeast cells by type V myosins. Actin cables are assembled by the formin For3 and are bundles of short, parallel actin filaments (Figure 6.1B) [63, 39, 94]. For3 localizes and associates with the cell tips where it can nucleate and elongate F-actin for cables. By retrograde flow, For3 is moved inward into the cell with the elongating cable, and this inward motion partially inactivates For3, allowing the F-actin filaments in cables to remain short and polarized with barbed ends facing the cell tip [83]. Due to their difficulty to image as well as unclear phenotypes from mutants, identifying the actin binding proteins responsible for their assembly, disassembly, maintenance, and composition have been difficult to elucidate. The protein responsible for bundling F-actin cables has yet to be identified, though both tropomyosin Cdc8 and coronin Crn1 have been found to associate with this network.

1.7 TIRF microscopy

To understand mechanistic details of proteins and their interactions with the actin cytoskeleton, *in vitro* techniques are often required in combination with cell biological techniques.

Our lab and the studies presented in this thesis employ a specialized optical microscopy technique known as Total Internal Reflection Fluorescence (TIRF) microscopy (Figure 1.6) [40, 2]. Normally, fluorescence microscopy uses laser illumination to excite the entire sample on a microscope (EPI) or a small slice within a much larger sample (confocal). However, with commonly used fluorescence techniques, excitation of the whole sample leads to high background and therefore reduced resolution of single molecules or proteins. TIRF microscopy utilizes a specialized objective which allows for control of the laser's angle. The laser is instead shone at an incident angle at which the laser's emission is totally internally reflected back into the objective [40, 2]. This produces an exponentially decaying optical phenomena known as an evanescent wave, such that the evanescent wave illuminate 150-200 nm above the coverglass surface [2]. Since only a small field is being excited, this greatly increases the signal-to-noise ratio, allowing direct, clear visualization of single molecules. With this system, we can add purified proteins to a chamber and visualize the assembly of individual actin filaments and the binding of ABPs to these filaments in real-time with high resolution.

1.8 Summary

It is clear that the actin cytoskeleton is a pivotal player in many cellular functions, ranging from nutrient uptake, cellular transport, and cell division to higher order processes such as cell migration and muscle contraction. For all of these actions to occur properly, it is critical that we understand the mechanisms of existing component parts as well as how these component parts function together to allow for these higher order F-actin networks to self-organize for such diverse functions. Using a combination of *in vivo* cell biology, microfluidics, and *in vitro* reconstitution techniques, this work will address some of these underlying questions in the mechanisms of various fission yeast actin binding proteins as well as how self-organization of the actin cytoskeleton is initiated.

CHAPTER 2

AN OPTIMAL FLUORESCENTLY-LABELED FISSION YEAST ARP2/3 COMPLEX EFFICIENTLY NUCLEATES BRANCHED AND LINEAR ACTIN FILAMENTS IN VITRO.

Preface

The work in this chapter was performed in collaboration with Caitlin Anderson, a previous graduate student in our lab. Caitlin initiated the project and built, purified, and tested the many constructs before the successful Halo-tagged construct used throughout this work. She performed the pyrene assays in Figures 2.1 and 2.3, and performed the initial TIRF for the constructs in Figure 2.4. I conducted the cell biology work, TIRF microscopy, and analysis work in Figures 2.1C, 2.2, 2.5, 2.6, 2.7, 2.8, 2.9. Additionally, Michael James performed the patch dynamic analysis presented in Figures 2.5 and 2.6 and Vilmos Zsolnay performed the binding dynamics analysis presented in Figure 2.8. Both Caitlin and I contributed equally to figure construction, manuscript writing, and editing.

2.1 Abstract

Arp2/3 (actin-related protein 2/3) complex is a seven-component protein complex that binds to an actin filament ('mother') and nucleates a branched new filament ('daughter'). Arp2/3 complex must be activated by a nucleation promoting factor (e.g. WASp/Scar family proteins) The mechanism and pathway of Arp2/3 complex has been studied for years indirectly, yet there has been little direct visualization of this pathway. In this work, we have successfully engineered and purified multiple fluorescently-tagged fission yeast Arp2/3 complex constructs to identify the optimal construct that is active in vitro, exhibits no cellular defects, and can be visualized at the single molecule level. We have found that the fluorescently-tagged

ArpC5-Halo construct can be directly visualized using single molecule TIRF microscopy for investigations of Arp2/3 complex binding and activation. Arp2/3 complex F-actin binding is increased in the presence of VCA and it rapidly nucleates branch formation in 2.1 seconds post-binding. Further Halo-Arp2/3 complex is activated by both VCA containing and WDS family proteins, the classes of activators found in fission yeast. Through this tool, we make progress towards understanding fundamental biological questions about Arp2/3 complex and the actin cytoskeleton using proteins from a model organism for these studies.

2.2 Introduction

Cells must assemble and maintain diverse actin filament (F-actin) networks with unique architectures and dynamics that are best suited to facilitate their corresponding cellular processes [87, 14]. Cellular processes, such as motility and endocytosis, require short, branched networks that produce protrusive forces. Arp2/3 complex is essential for creating those branched F-actin networks, and Arp2/3 complex nucleates several force generating F-actin networks, including the lamellipodia in motile cells, endocytic actin patches in budding and fission yeast, and actin tail formation and propelling movement of pathogenic listeria [111, 155]. Arp2/3 complex binds to an existing mother filament and mediates daughter branch formation (Figure 2.1A), and in some cases, can assemble linear actin filaments without an existing mother filament [153]. It consists of two actin related proteins (Arp2 & Arp3) and five additional subunits (ArpC1-5), which together form the intrinsically inactive complex (Figure 2.1B) [145, 15]. Nucleation promoting factors (NPFs) are required to activate Arp2/3 complex. The most well studied NPFs are the Wiskott-Aldrich syndrome protein (WASp) and Scar/WAVE protein families. These NPFS contain a C-terminal VCA (Verpolin, Central, Acidic) region that is responsible for Arp2/3 complex activation [113, 101]. The different VCA (also known as WCA) domains have complimentary roles, as the V domain binds G-actin and the CA domain associates with Arp2/3 complex [82, 27].

Therefore, VCA initiates the interaction of the Arp2/3 complex and the first subunit of the daughter filament. . This creates a trimer structure that is more energetically stable than a trimer formed from three actin monomers. It has been proposed that two WASP proteins function as dimers and deliver two monomers to Arp2/3 complex [100]. In addition to VCA containing nucleation promoting factors (NPFs), the WISH/DIP/SPIN90 (WDS) family of NPFs utilize an armadillo repeat to activate Arp2/3 complex (Luan et al., 2018; Shabban et al., 2020). WDS proteins don't require a pre-existing mother filament and instead nucleate linear actin filaments (Wagner et al., 2013).

The formation of a ternary structure of Arp2/3 complex, VCA (one or more), and G-actin (one or more) is one step in the pathway leading to successful nucleation of an Arp2/3 complex-mediated branch. Arp2/3 complex must also bind ATP and change its conformation to bring Arp2 closer to Arp3 [8, 96]. The precise order and rates of the Arp2/3 complex-mediated branch formation pathway have been studied extensively over the years [9, 82]. While there is much known on how Arp2/3 complex branching occurs, there has been limited direct visualization of the branching pathway. Smith et al. (2013a,b) visualized the pathway with fluorescently labeled *Saccharomyces cerevisiae* (budding yeast) Arp2/3 complex and the VCA domain of WASP [134, 135]. However, *S. cerevisiae* Arp2/3 complex has a minimal basal level of activity in the absence of WASP (reviewed in [49]). In fission yeast and mammalian systems, Arp2/3 complex remains fully inactive in the absence of an activator NPF. Additionally, fission yeast is a long-standing model system for understanding the mechanisms and functions of the actin cytoskeleton and its associated actin regulatory proteins. Therefore, we engineered an optimal fluorescently labeled fission yeast Arp2/3 complex construct to further characterize the branching pathway with fission yeast proteins. This engineered tool can now be used for further investigation into understanding the formation and regulation of Arp2/3 complex-mediated F-actin networks in cells.

2.3 Results

2.3.1 Engineering the optimal labeled Arp2/3 complex for in vitro single molecule studies

To visualize Arp2/3 complex at the single molecule level in vitro, we initially needed to engineer and purify an optimally functional fluorescently-tagged Arp2/3 complex. We required three characteristics for an optimal construct sufficient for mechanistic studies: (1) the construct should not exhibit major growth and F-actin network defects in fission yeast cells, (2) the general F-actin branching activity should be as close to wild-type Arp2/3 complex as possible, and (3) single molecules of the fluorescently-labeled Arp2/3 complex should be visible by TIRF microscopy (TIRFM) imaging. As described in the following paragraphs, to determine the most optimal fluorescently-labeled fission yeast Arp2/3 complex construct, we (1) engineered a series of fission yeast strains in which various tags were integrated into the genome of the ArpC3 and ArpC5 subunits of Arp2/3 complex, (2) characterized their cell growth, general F-actin network organization, and endocytic actin patch dynamics, and (3) purified and fluorescently-labeled the Arp2/3 complexes and determined their actin assembly properties in 'bulk' pyrene and single filament/molecule TIRFM imaging actin assembly assays.

Since Arp2/3 complex has seven components, we wanted to engineer a fission yeast strain with an endogenously tagged component of the complex. Previous work in the field has demonstrated that the C3 and C5 subunits have little effect on fission yeast growth, and are historically used for examining Arp2/3 complex dynamics in vivo [130, 129, 106, 7, 144, 1]. Additionally, studies in budding yeast tagged the fission yeast ArpC3 ortholog with a SNAP-tag for in vitro mechanistic studies [134, 135]. Therefore, we engineered a series of fission yeast strains expressing different endogenously tagged Arp2/3 complex components: ArpC3-SNAP, ArpC3-mCherry, 2x-mCherry (ArpC3-mCh, ArpC5-mCh),

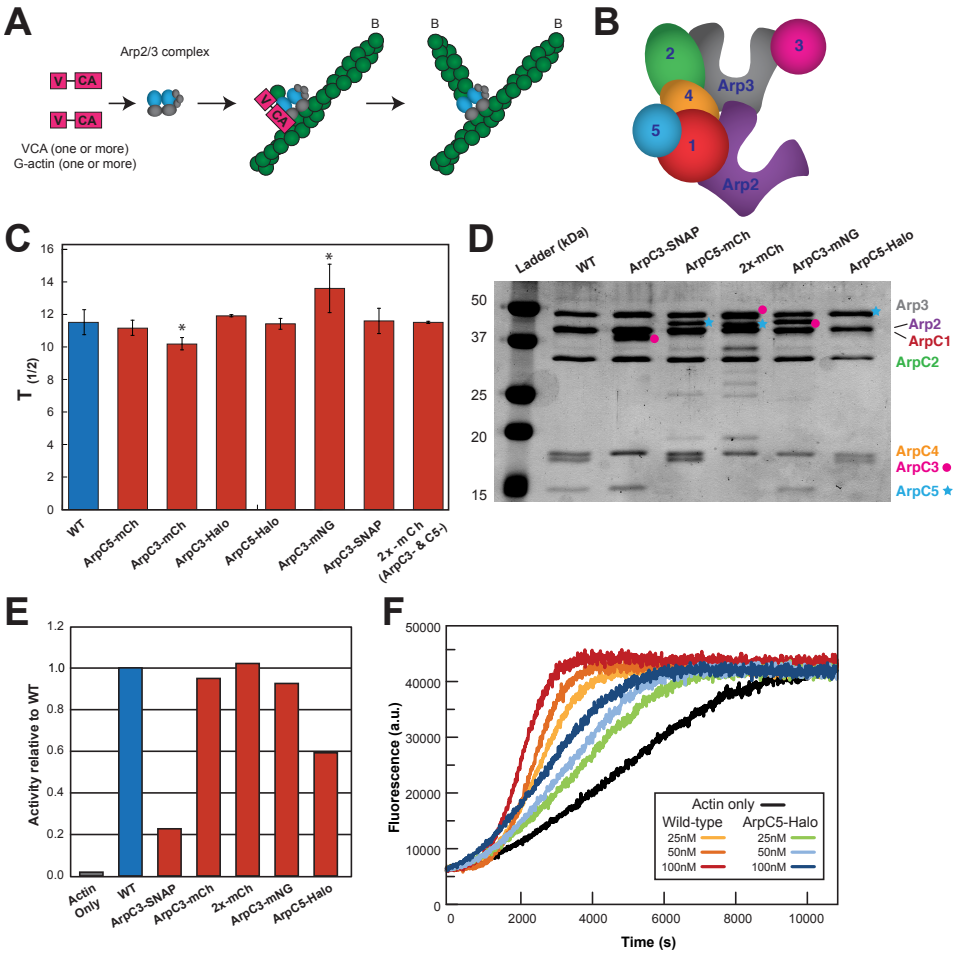

Figure 2.1: **Determining the optimal fluorescently tagged Arp2/3 complex.** A. Simplified schematic of the pathway of Arp2/3 complex-mediated branch formation. Typically, one or more VCA containing proteins brings one or more actin monomers to the Arp2/3 complex and initiates binding and branching. 'B' labels the barbed end of the filaments. **B.** Cartoon of the seven-component organization of Arp2/3 complex. **C.** Calculated $t_{1/2}$ for fission yeast growth assays of tagged Arp2/3 complex strains. n = 3 replicates for all strains except WT where n = 6, error bars = s.d. One-tailed t-test with unequal variance comparing each strain to WT yielded significantly different p-values for ArpC3-mCh (p = 0.0288) and ArpC3-mNG (p = 0.0235). (D) SDS-PAGE gel showing 0.6 μg of purified Arp2/3 complex for each construct. Pink circles and blue stars indicate shifts in ArpC3 and ArpC5 with fluorescent tags, respectively. **E.** Relative activity of each Arp2/3 complex construct normalized and compared to WT (1) and actin only (0), calculated from spontaneous pyrene assays containing 100 nM Arp2/3 complex and 100 nM VCA. **F.** Representative trial of spontaneous pyrene assays with 100 nM VCA and a range (25 nM, 50 nM, 100 nM) of WT or ArpC5-Halo.

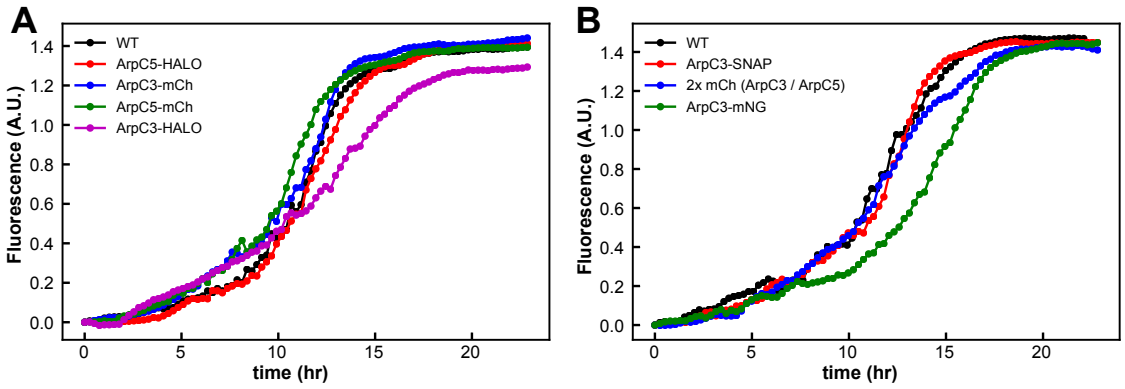

Figure 2.2: **Representative growth curves for fluorescent Arp2/3 complex fission yeast strains. A-B.** Representative curves showing OD_{600} for WT compared to multiple fission yeast strains with fluorescent Arp2/3 complex constructs.

ArpC3-mNeonGreen, ArpC3-Halo, and ArpC5-Halo, as well as a previously engineered strain (ArpC5-mCherry) 2.2. To determine whether endogenously tagged Arp2/3 complex components cause general cell growth defects, we first tested the tagged fission yeast strains in a bulk growth assay (Figures 2.1C, 2.2). By comparing the time to half-max ($t_{1/2}$) for each strain to reach plateau, most of the strains grow similar to WT (Figure 2.1C). However, both ArpC3-mCherry and ArpC3-mNeonGreen deviate from WT- ArpC3-mCherry has a significantly lower t1/2, while ArpC3-mNeonGreen has a significantly higher $t_{1/2}$ (Figure 2.1C). Furthermore, although the $t_{1/2}$ for the ArpC3-Halo strain is not significantly different, this strain was not considered further because it has general growth and stability issues and the growth curve plateaus much lower than WT (Figure 2.2A). Because of their normal general growth rates, we moved forward with further analysis of ArpC3-SNAP, ArpC5-mCherry, 2x-mCherry, ArpC3-mNeonGreen and ArpC5-Halo.

Next, we purified the remaining Arp2/3 complex constructs following previous purification methods to examine their actin assembly activities in vitro [129] (Figure 2.1D). To understand the activity levels of each Arp2/3 complex construct, we conducted 'bulk' spontaneous assembly pyrene assays comparing each construct to both actin alone and wild-type (WT) Arp2/3 complex (Figure 2.1E). The $t_{1/2}$ was calculated for each construct and com-

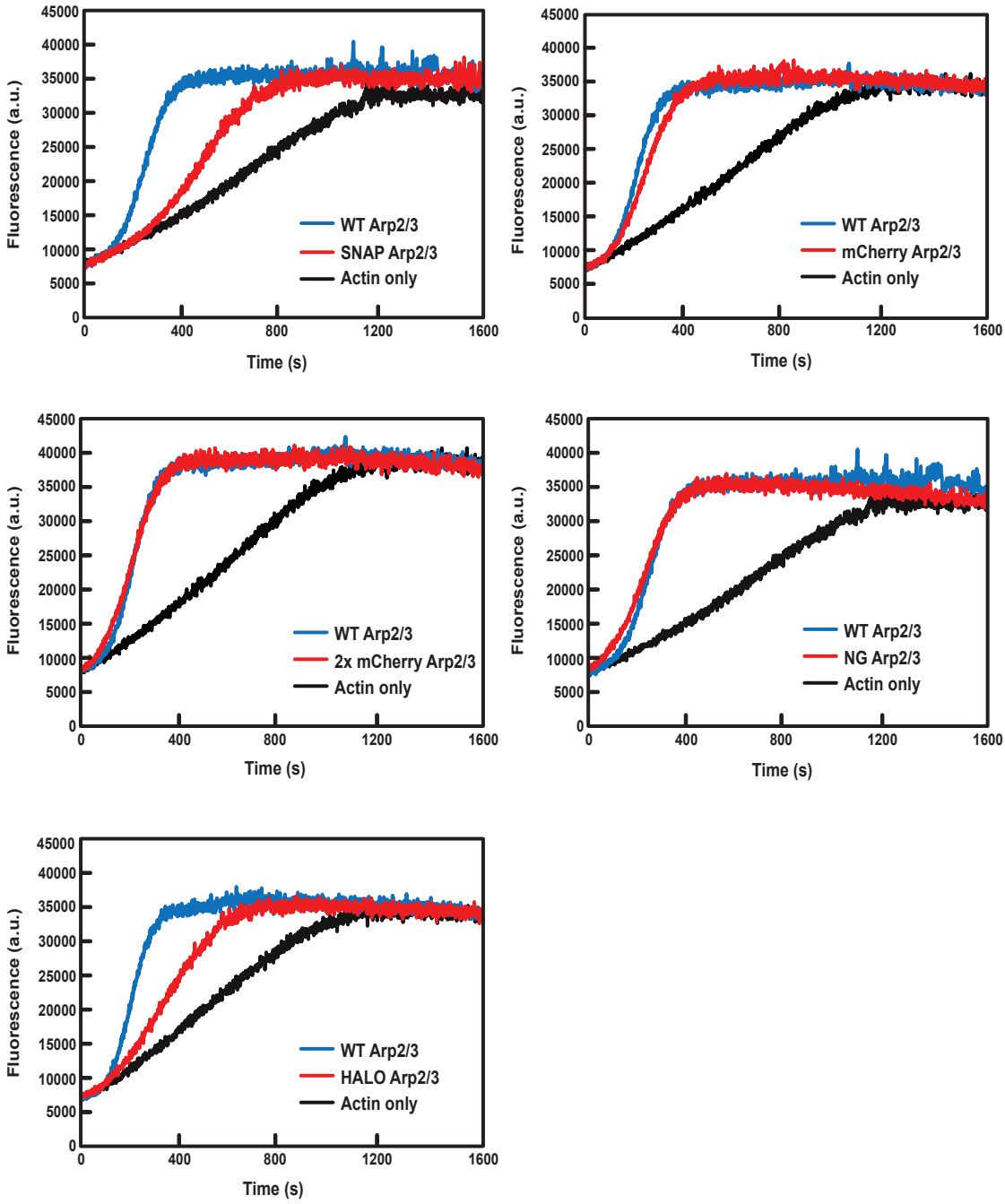

Figure 2.3: **Representative spontaneous pyrene F-actin assembly assays for fluorescent Arp2/3 complex construct.** Representative spontaneous pyrene curves for the different Arp2/3 complex constructs with their corresponding trials of WT Arp2/3 complex and actin only. Each reaction has 1 μM actin (10% pyrene labeled), 100 nM Arp2/3 complex, and 100 nM VCA.

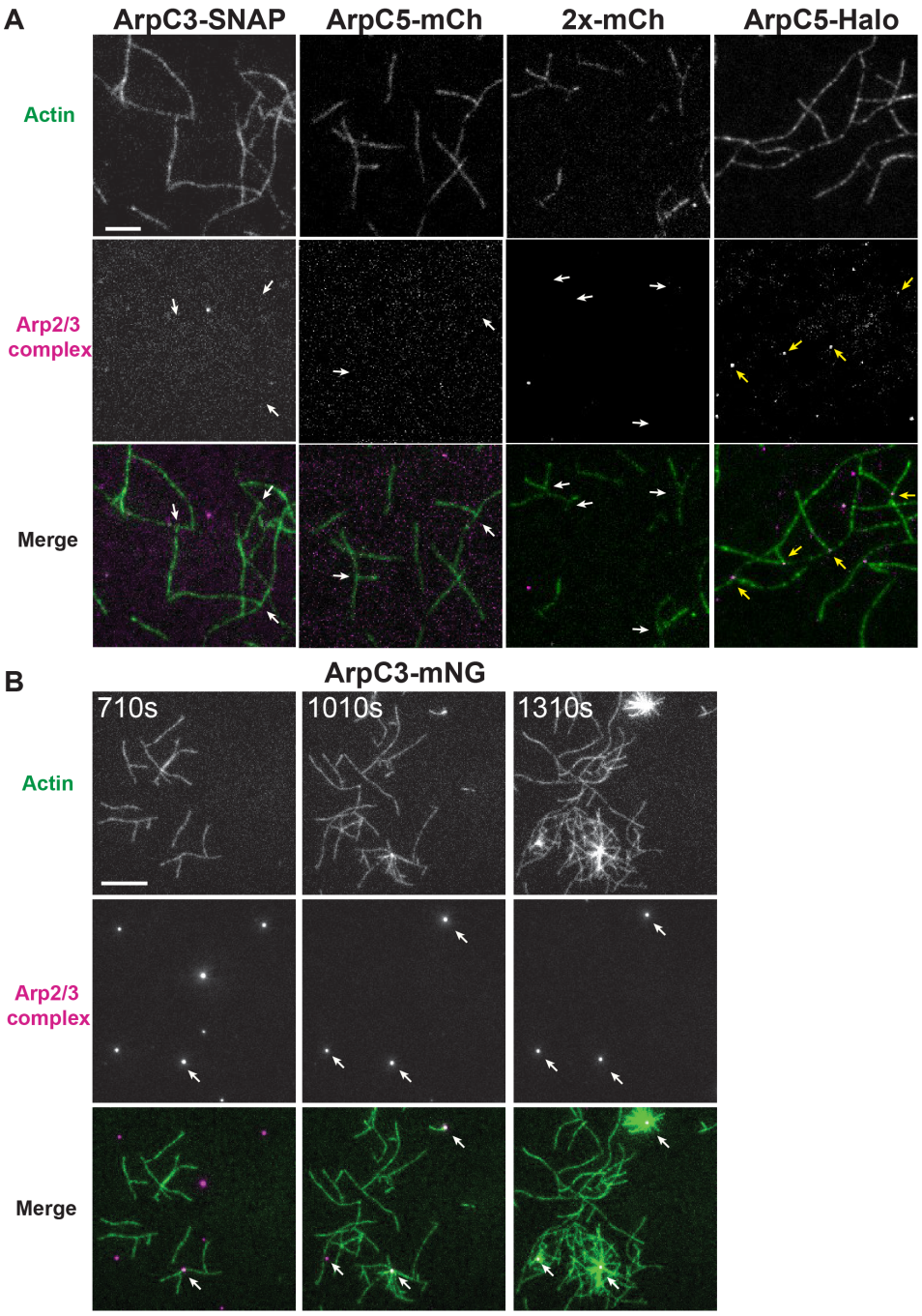

Figure 2.4: **Halo-Arp2/3 complex is the only fluorescently tagged Arp2/3 complex construct visible at singular branch sites at the single molecule level. A.** Representative TIRFM images of fluorescently tagged Arp2/3 complex branching events. White arrows denote branch sites with no visible Arp2/3 complex. Yellow arrows denote branch sites with visible Arp2/3 complex. **B.** Time-lapse TIRFM images of ArpC3-mNeonGreen showing aggregate branching events. White arrows denot branch sites with visible Arp2/3 complex, that then form aggregate branches.

pared and normalized to WT (1) and actin only (0) to determine relative activity level for each Arp2/3 complex construct (Figure 2.1E). The SNAP construct has the lowest relative activity level of 0.22, while the Halo construct has an activity level of 0.6 (Figure 2.1E). The mCherry, 2x-mCherry, and NG constructs are close to WT with 0.9-1 activity levels (Figure 2.1E). As our goal was to visualize Arp2/3 complex at the single molecule level, we also tested the constructs in single molecule total internal reflection fluorescence (TIRF) microscopy assays in the presence of the VCA portion of the fission yeast Wasp1, a well-studied Arp2/3 complex activator (Figure 2.4). In these assays, the ArpC3-mNG construct is visible but only in aggregates that cause large asters (Figure 2.4B). The ArpC3-SNAP, ArpC5-mCherry, and 2x-mCherry constructs do not aggregate, but the fluorescence signal at branch sites is not above background noise (Figure 2.4A). However, the Halo-Arp2/3 complex (ArpC5-Halo) does not aggregate and is visible at the single molecule level in these TIRF assays (Figure 2.4A). When combined with the lack of growth defect, we conclude that the Halo-Arp2/3 complex construct is the optimal tool for further mechanistic research. The decreased activity in pyrene is likely due to a fraction of inactive protein that was unable to be separated during purification. Additional spontaneous pyrene showed that Halo Arp2/3 complex increases with an increasing range of concentration (Figure 2.1F), and the decreased activity appears to scale with the concentration. The fraction of inactive protein should not affect the single molecule analysis of active Arp2/3 complexes.

2.3.2 Halo-Arp2/3 complex fission yeast cells exhibit no significant F-actin network deficiencies

As the ArpC5-Halo construct appears to be optimal for in vitro mechanistic studies, we further analyzed the effects of the endogenous HaloTag on fission yeast F-actin network morphology and function. When cells were stained with phallicidin, a marker for F-actin, we observed no major differences in F-actin network structures for *arpC5-Halo* cells when

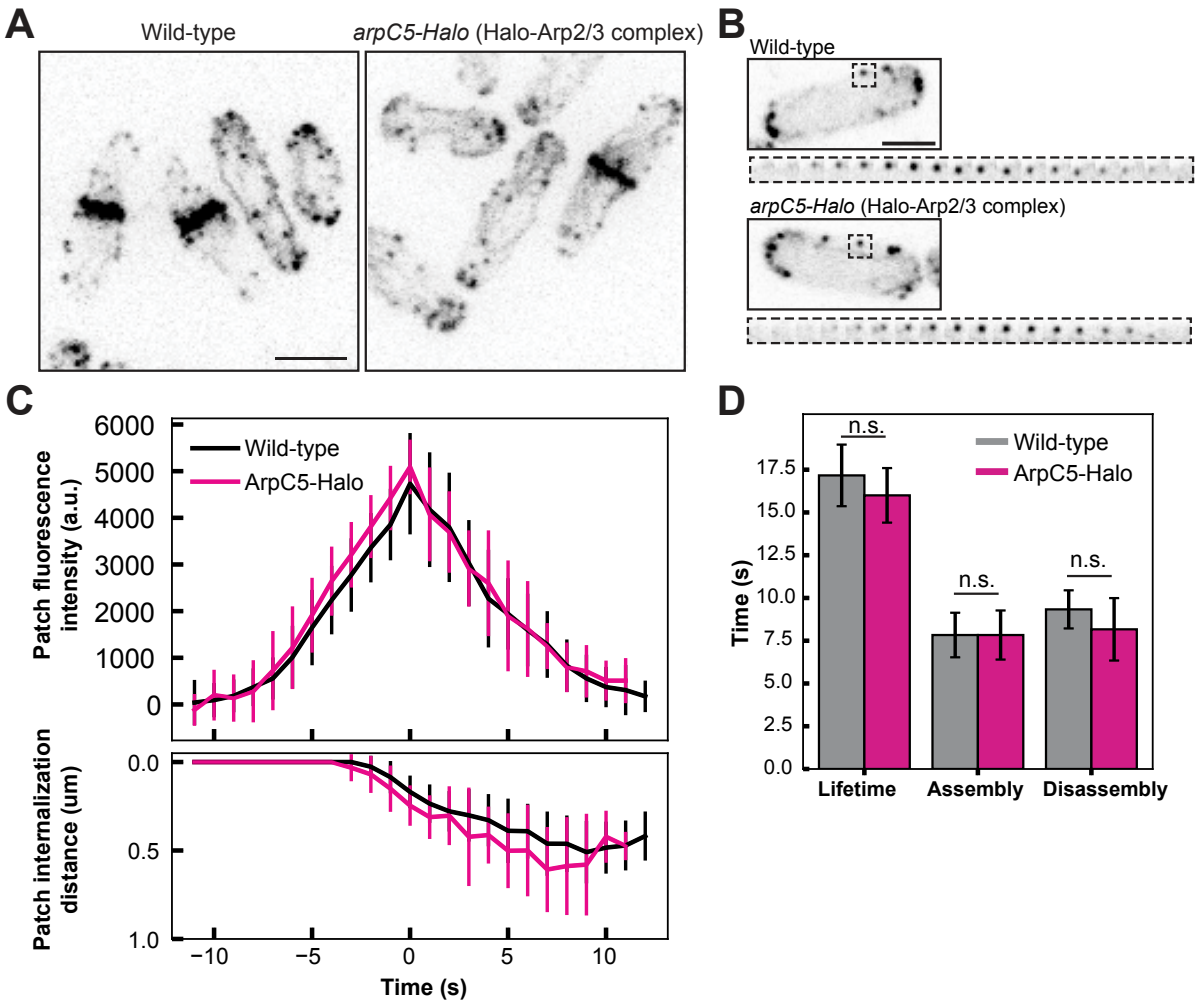

Figure 2.5: **Halo-Arp2/3 complex does not significantly affect fission yeast endocytic actin patches. A.** Representative fluorescent micrographs of fission yeast cells stained with phallicidin to mark F-actin networks. Scale bar = 5 μm. **B.** Representative time-lapse fluorescent micrographs showing fission yeast endocytic actin patches expressing Lifeact-eGFP. **C.** Lifeact-eGFP intensity and patch internalization distance in fission yeast endocytic patches over their lifetimes for cells with wild-type or *arpC5-Halo* genetics backgrounds. Traces represent the average of 10-12 endocytic patches, error bars = s.d. **D.** Lifetime, assembly time, and disassembly time of endocytic actin patches in wild-type or *arpC5-Halo* cells. n= 10-12 patches, one-tailed t-test with equal variance, error bars = s.d.

compared to wild-type fission yeast cells (Figure 2.5A). Since the primary role of Arp2/3 complex is the formation of endocytic patches, we investigated the effects of ArpC5-Halo on endocytic actin patch dynamics. Actin patch dynamics have been previously studied in immense detail and the assembly, disassembly, and lifetimes of them can be carefully quantified for multiple actin patch proteins [130]. We analyzed the dynamics of actin patches in wild-type and *arpC5-Halo* cells using the F-actin marker, Lifeact (Figure 2.5B-D). When compared to wild-type cells, we observed no significant difference in patch dynamics for lifetime (WT: 17.2 ± 1.8 s, *arpC5-Halo*: 16 ± 1.6 s), assembly (WT: 7.8 ± 1.8 s, *arpC5-Halo*: 7.8 ± 1.44 s), or disassembly (WT: 9.3 ± 1.11 s, *arpC5-Halo*: 8.2 ± 1.83 s) (Figure 2.5D). Further, the amount of protein per patch and the distance a patch is internalized also remained unchanged (Figure 2.5C).

While Lifeact is a commonly used F-actin network marker in vivo, it has been shown to sometimes negatively influence the dynamics of F-actin networks [10, 33, 91]. To address this possibility, we also examined the dynamics of actin patches using a fluoresecently tagged actin patch protein Fimbrin (Fim1). Similar to Lifeact, *arpC5-Halo* cells showed no significant difference in any of the actin patch dynamics analyzed. Compared to wild type, *arpC5-Halo* cells had similar rates for lifetime (WT: 16 ± 2.3 s, *arpC5-Halo*: 15.4 ± 1.88 s), assembly (WT: 5.9 ± 1.44 s, *arpC5-Halo*: 7 ± 1.38 s), and disassembly (WT: 10.1 ± 2.23 s, *arpC5-Halo*: 8.4 ± 2.15 s) (Figure 2.6B). Thus, the ArpC5-Halo construct does not cause any major defects to F-actin networks, and more specifically, endocytic actin patch function and dynamics in vivo.

2.3.3 Halo-Arp2/3 complex is active with multiple classes of nucleation promoting factors

The initial TIRF assays revealed that the Halo-Arp2/3 complex is active and visible with an unlabeled Wsp1(VCA) construct (Figure 2.4A). Since additional nucleation promoting

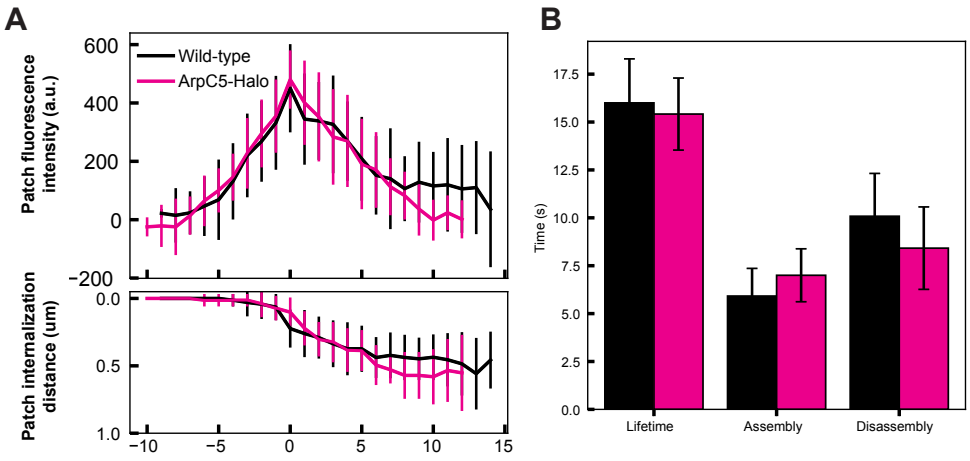

Figure 2.6: **Halo-Arp2/3 complex does not significantly affect fimbrin dynamics in fission yeast endocytic actin patches. A.** Fimbrin Fim1-mCh intensity and patch internalization distance in fission yeast endocytic patches over their lifetimes for cells with wild-type or *arpC5-Halo* genetic backgrounds. Traces represent the average of 10-12 endocytic patches, error bars = s.d. **B.** Lifetime, assembly time, and disassembly time of endocytic actin patches in wild-type or *arpC5-Halo* cells. n= 10-12 patches, one-tailed t-test with equal variance, error bars = s.d.

factors exist without VCA regions in fission yeast, we wanted to test the activation of Halo-Arp2/3 complex with the WDS family protein, Dip1. Unlike VCA-containing activators, Dip1 activates Arp2/3 complex to form linear actin filaments Thus, we expect Dip1 to increase nucleation of linear actin filaments in TIRF assays. In the presence of Dip1, the number of actin filaments nucleated increased 3.7-fold compared to reactions with Arp2/3 complex alone (Figure 2.7A-B). Additionally, labeled Halo-Arp2/3 complex could be observed at the pointed end of actin filaments, consistent with the mechanism that Arp2/3 complex and Dip1 remain at the pointed end for the filament lifetime[5] (Figure 2.7C). Thus, the engineered Halo-Arp2/3 complex construct can be activated by all major classes of canonical NPFs found in fission yeast, making it an optimal tool for further and future mechanistic investigations.

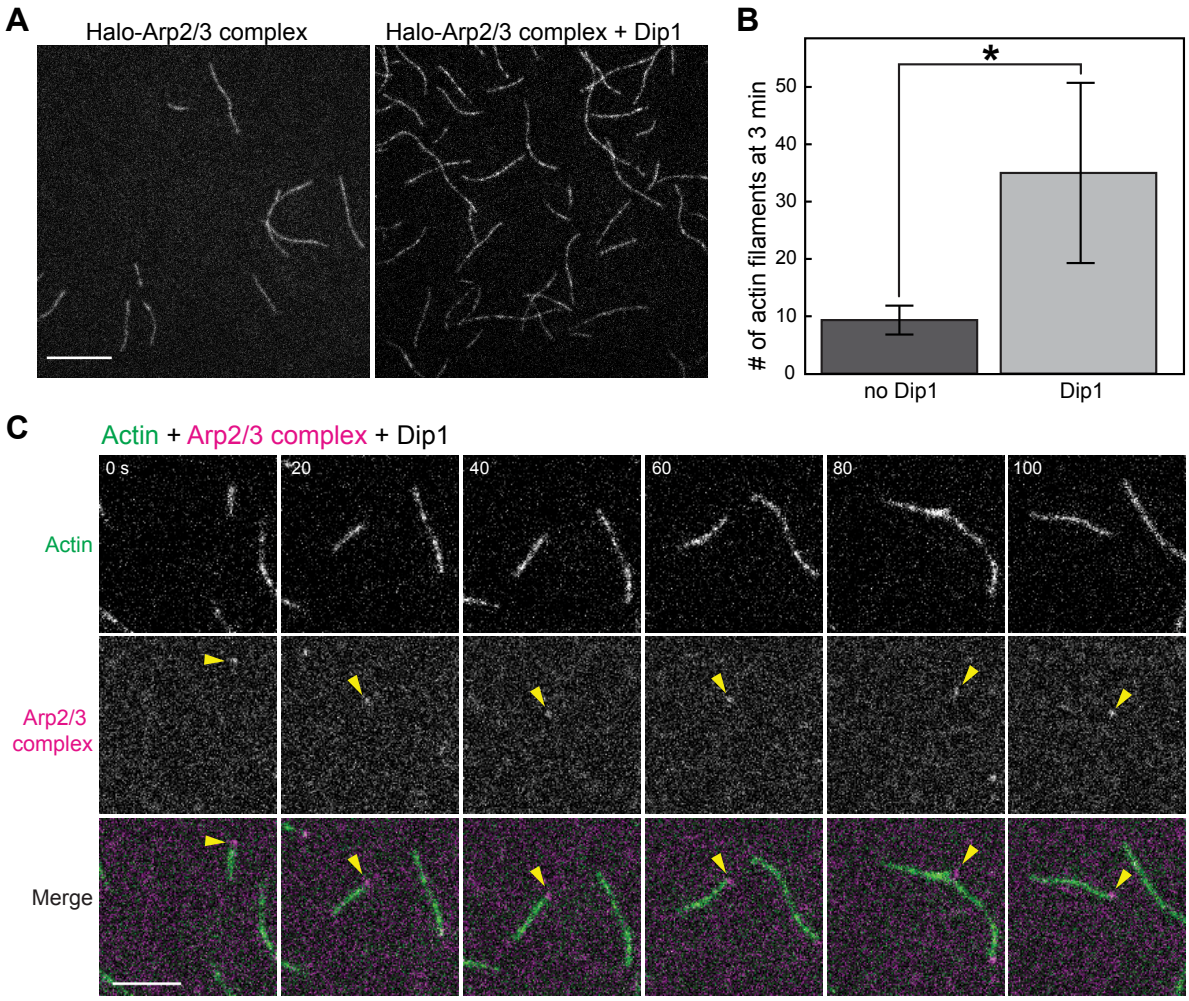

Figure 2.7: **Dip1 robustly activates Halo-Arp2/3 complex nucleation. A.** Single color TIRFM of 1.5 μM Mg-ATP actin (10% Alexa-488 labeled) with 25 nM ArpC5-Halo TMR, and either 0 or 50 nM fission yeast Dip1. Images at t = 3 min after initiation of actin assembly reaction. Scale bar, 10 μm. **B.** Quantification of the number of filaments nucleated by Arp2/3 complex. One tailed t-test with unequal variance yielded p-value *p=0.0492, error bars = s.d., n = 3 replicates. **C.** Representative time-lapse of Halo-Arp2/3 complex activated by Dip1 to form linear filaments. Scale bar, 5 μm.

2.3.4 F-actin binding of Arp2/3 complex increases in the presence of Wsp1(VCA).

In order to better understand how nucleation promoting factors influence Arp2/3 complex activity, we examined how Wsp1(VCA) affects Arp2/3 complex binding to actin filaments. Previous work has demonstrated that in the presence of VCA, Arp2/3 complex binds more frequently to actin filaments in vitro [134]. To examine Arp2/3 complex binding dynamics, we tethered actin filaments to the surface via biotin-actin and flowed in Halo-Arp2/3 complex and capping protein (to prevent new filament polymerization) with or without VCA present. In the absence of VCA, Arp2/3 complex very rarely binds to F-actin in vitro, and the addition of VCA significantly increases Arp2/3 complex binding events approximately 3-fold (Figure 2.8A-B).

Interestingly, in the presence of VCA, we observed a noticeable increase in total Halo-Arp2/3 complex in the field of view compared to movies without VCA. However, the fraction of bound Arp2/3 complex molecules is not significantly different between the two conditions (Figure 2.8C). When the same experiment was conducted in the absence of actin, we did not see this difference between the amount of total Arp2/3 complex molecules with or without VCA present (data not shown). Thus, we suspect that, as the presence of VCA increases Arp2/3 complex F-actin binding, the presence of more Arp2/3 complex molecules may be due to increased sampling. If the conformational change of VCA bound Arp2/3 complex increases filament binding events [38, 168], it would be likely that more Arp2/3 complex would be seen in the field of view. This result suggests that the conformational change of Arp2/3 complex when bound to VCA is better suited for filament binding than Arp2/3 complex alone.

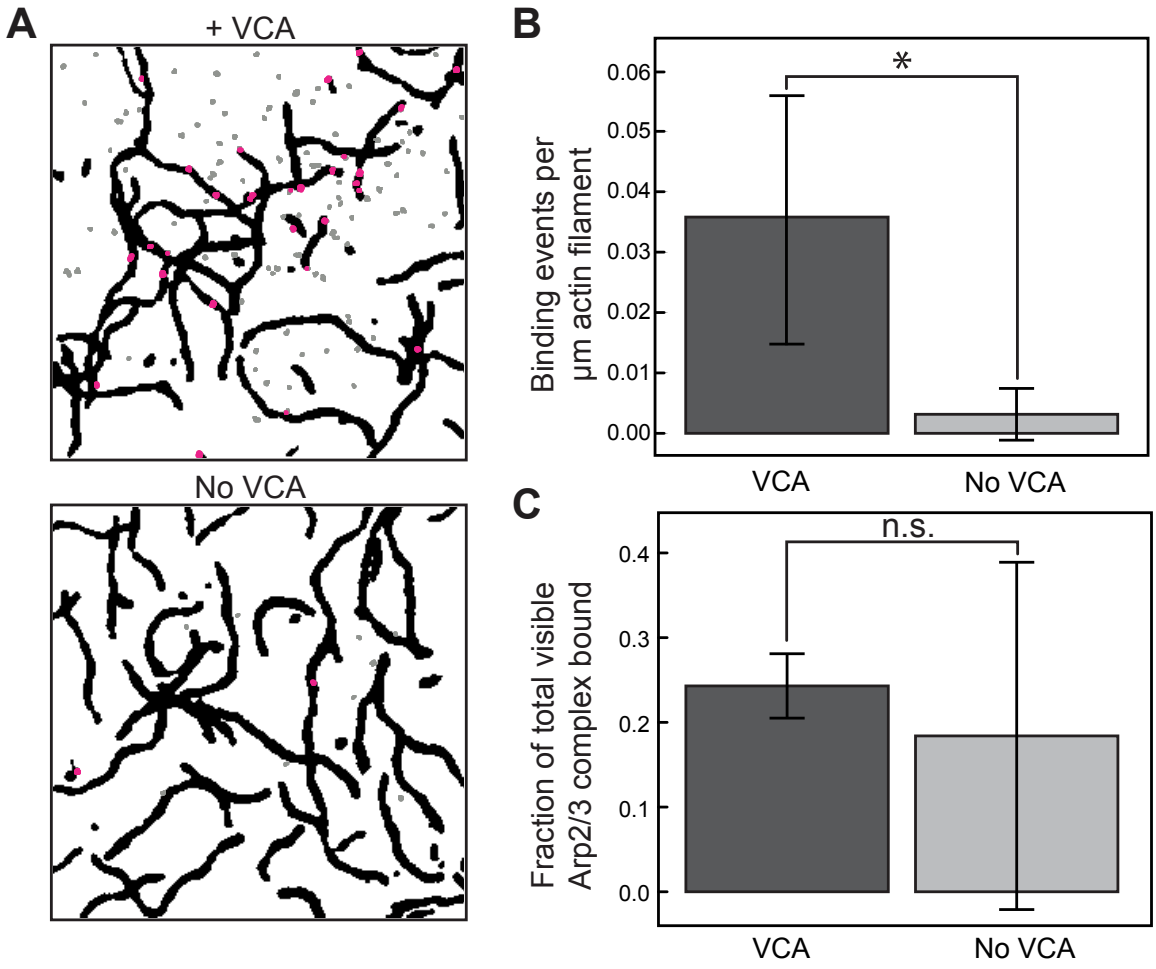

Figure 2.8: **Arp2/3 complex binding to F-actin increases in the presence of VCA. A.** Representative images showing the actin mask that was used to calculate whether the Arp2/3 complex is bound to actin filaments in the presence or absence of VCA. The magenta dots represent bound Arp2/3 complex molecules. Reactions contained 30 nM Halo-Arp2/3 complex TMR, 100 nM capping protein, and either 0 or 300 nM VCA. **B.** Binding events of Arp2/3 complex per μm of actin filament in the presence or absence of VCA. n = 3 movies, error bars = s.d., *p = 0.047. **C.** Fraction of Arp2/3 complex visible in the field bound to actin filaments, error bars = s.d.

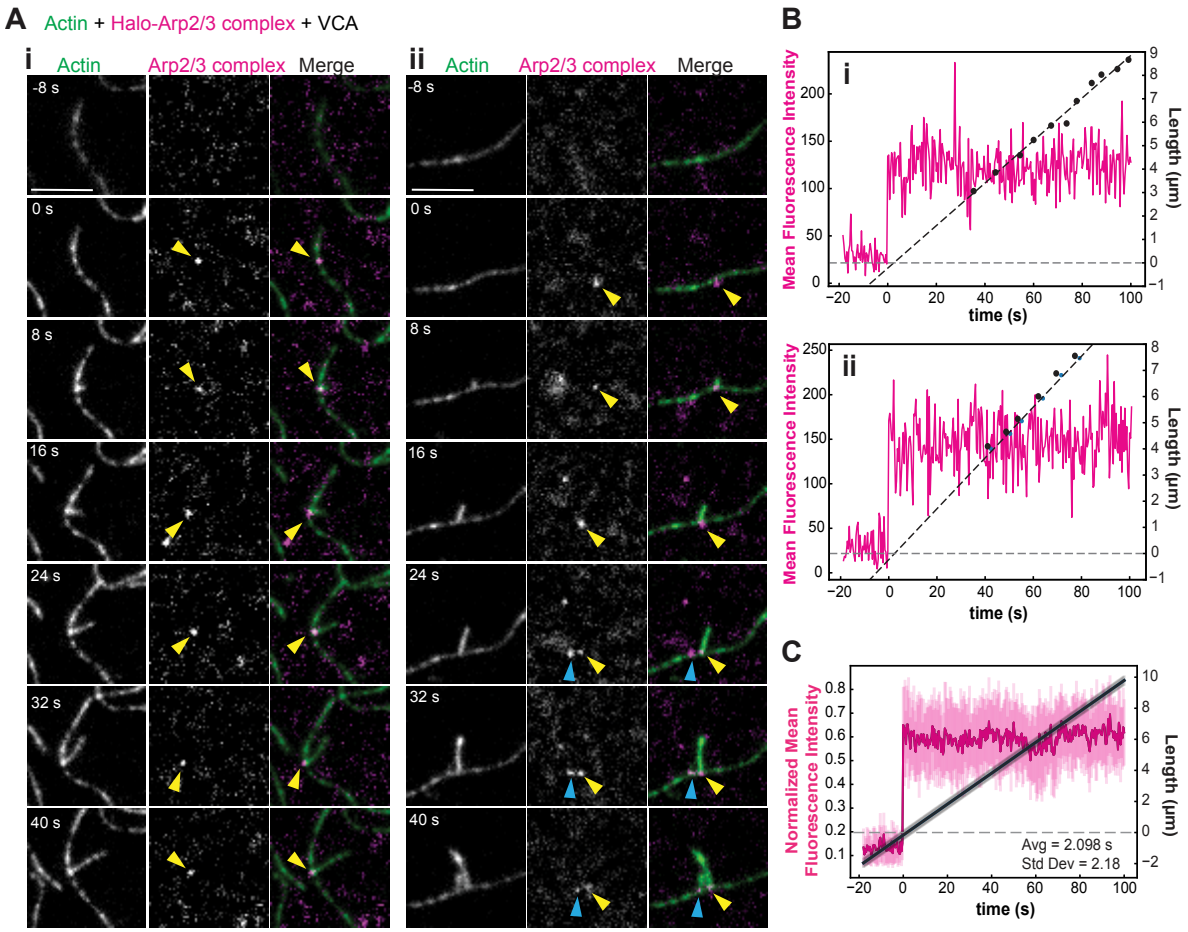

Figure 2.9: **Halo-Arp2/3 complex rapidly nucleates branch formation. A.** Representative time-lapse images of Halo-Arp2/3 complex binding to a mother filament and remaining through daughter branch formation. Yellow arrow denotes Halo-Arp2/3 complex binding. Scale bar = 3 μm. **B.** Representative nucleation graph. Pink line shows step-like increase of Arp2/3 complex fluorescence. The daughter filament length was traced at each data point, and the nucleation time can be calculated by using the elongation rate (slope) to determine when the daughter filament began to grow in relation to Arp2/3 complex binding. **C.** Average nucleation graph. Nucleation time = 2.098 $\pm$ 2.18 s, n = 18 events, error bars = s.d.

2.3.5 Arp2/3 complex rapidly nucleates branches after binding

Halo-Arp2/3 complex presents an optimal tool for understanding the mechanisms of Arp2/3 complex branch formation, including determining the time from Arp2/3 complex binding and daughter branch nucleation by tracking single molecule branching events (Figure 2.9A). Analysis of Halo-Arp2/3 complex photo-bleaching events and the amplitudes of Halo-Arp2/3 complex fluorescence confirmed that branching events with labeled Halo-Arp2/3 complex contain only a single molecule of Arp2/3 complex (Figure 2.10A-C). The time between Arp2/3 complex binding to the mother filament and daughter filament branch initiation was calculated by using the observed elongation rate of the daughter filament to retrospectively determine the time of branch nucleation (Figure 2.9B). When this process was iterated over multiple branch sites, we found that the average time delay to nucleation was 2.1 $\pm$ 2.2 seconds, consistent with previous rates found in budding yeast (Figure 2.9C) [134]. This demonstrates that Arp2/3 complex nucleates daughter filament branch formation rapidly after binding.

2.4 Discussion

In this work, we successfully engineer and initially characterize a fluorescently labeled Arp2/3 complex that is critical for further single molecule analysis of the Arp2/3 complex-mediated branch formation pathway. Arp2/3 complex branch formation involves three, multi-part steps (activation, binding, and branch formation), and the fluorescent Arp2/3 complex serves as an invaluable tool for analyzing each step in immense detail. By constructing and carefully analyzing multiple fluorescently-tagged Arp2/3 complex constructs, we found that ArpC5-Halo proves the optimal fluorescent tool for this work as it exhibits no cellular defects, is active in vitro, and be directly visualized at the single molecule level.

We discovered that fission yeast Arp2/3 complex is active with the Arp2/3 complex

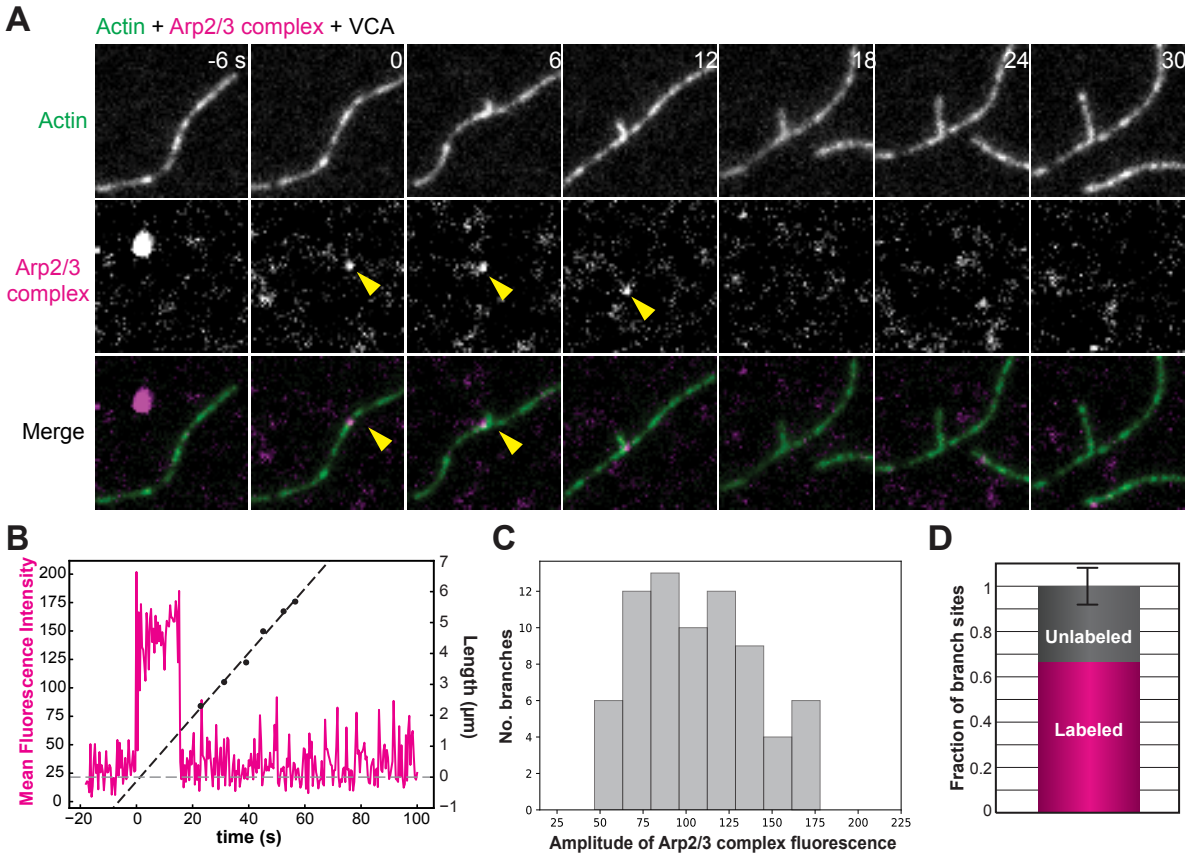

Figure 2.10: **Branch sites have a single molecule of Arp2/3 complex. A.** Time-lapse TIRFM images of Halo-Arp2/3 complex nucleating a branch and bleaching while branch elongation continues. **B.** Representative nucleation graph of the Halo-Arp2/3 complex single-step bleaching event shown in A. **C.** Fraction of branch sites with fluorescently labeled or unlabeled Halo-Arp2/3 complex. n = 3 independent movies with 111 events, error bars = s.d.

activator, Wsp1(VCA), and branch nucleation occurs rapidly after binding, averaging 2.1 seconds after binding. Additionally, Halo-Arp2/3 complex can be activated by Dip1, a WDS family protein that activates Arp2/3 complex to form linear actin filaments, demonstrating this fluorescent construct can be activated by all classes of nucleation promoting factors found in fission yeast. Further, Arp2/3 complex binding to F-actin increases in the presence of Wsp1(VCA). Interestingly, it also increases the total amount of Arp2/3 complex in the experimental field of view, in a manner that is dependent on the presence of actin. We hypothesize that Arp2/3 complex 'samples' actin filaments prior to choosing one site for binding and this process is increased with the presence of VCA, suggesting that the conformational change induced by VCA is better suited for mother filament binding [38, 168].

Future work will focus on utilizing Halo-Arp2/3 complex to examine how branch formation is regulated by other actin binding proteins. Previous studies have shown that different actin networks exist in homeostasis and must compete for available actin monomers (G-actin) to maintain their density and size [17]. The G-actin binding protein profilin favors formin-mediated actin filament (F-actin) elongation and directly inhibits Arp2/3 complex-mediated actin assembly [141, 69, 116, 37, 81, 56, 115]. However, the mechanism by which this inhibition occurs is still debated. Our lab has provided evidence that this inhibition occurs by profilin competition with Wsp1 for actin monomer binding [141], yet another possibility is that profilin directly prevents Arp2/3 complex from barbed end binding and subsequent branch formation [103]. With fluorescent Arp2/3 complex and VCA constructs, future studies will directly visualize the effects of profilin on Arp2/3 complex dynamics, including mother filament binding and profilin inhibition.

Further, recent work has demonstrated a critical link between the Wsp1 and Dip1 Arp2/3 complex activation pathways in endocytic patch formation, showing that these two proteins activate Arp2/3 complex in a synergistic manner for rapid patch assembly [4]. Direct visualization of Arp2/3 complex and both activators simultaneously will be crucial to mechanis-

tically understanding how these two pathways cooperate.

2.5 Materials and Methods

2.5.1 Cloning, strain construction, and cell growth

Table 2.2 lists the fission yeast strains used in this study. The SNAP pombe targeting vector SNAP-Kan-MX6, was engineered by inserting the SNAP-tag into pFa6a-KanMX6. The Halo targeting vector was obtained from Addgene (#87029), and other targeting vectors from previous work [136]. Inserts were amplified with corresponding primers (Table 2.1) and inserted at the locus via lithium acetate transformations into protease deficient strain KV480 (aka TP150). All strains were confirmed by sequencing of targeted regions. GST-VCA-linker-Halo-6xHis was cloned by restriction digest of a HaloTag vector (gift from Margaret Gardel) and insertion of an amplified VCA segment from the GST-Wsp1(VCA) construct used for unlabeled VCA experiments.

Fission yeast strains for patch dynamics imaging were obtained through genetic crosses on SPA5S plates followed by tetrad dissection on YE5S plates. Strains were screened for auxotrophic (leu, ura) or antibiotic (nat, kan) markers and maintained on YE5S plates. Glycerol stocks were created by re-suspending pelleted cells in 600 μL YE5S and 400 μL 50% sterile glycerol. For cell growth, standard growth medium (YE5S) was used. Table 2.2 lists the fission yeast strains used in this study.

2.5.2 Cell growth assay

Fission yeast cells were maintained on standard YE5S complete media and grown for 36 hr in a 25°C water bath shaker prior to any experimental procedures. Fission yeast cells were diluted from growing liquid YE5S cultures in 96 well plates (Corning Inc, Corning, NY) to an OD_{600} of 0.03 and 0.06 for each strain, with three technical replicates per assay. Cells were

Primer	Genome homology	Plasmid homology	Strains
ArpC3 forward #1	AACTGAAAAGGATCA TCCCAGCAAGTGGTG GACTTGCTTCAGCAA GAGACGTTTTATGAA CAAAGCTTTG	CGGATCCCCG GGTTAATTAA	KV984 KV996 KV1006
ArpC3 reverse #1	TGAAATAAAGGAAAC GGAAAAACATAAAGG CTTTGAAATACAGTA TGAGCCAAATTATTA ATTAATAGAC	GAATTCGAGC TCGTTTAAAC	KV984 KV996 KV1006
ArpC5 forward	GGTTTTGTAGGTGGT GGAAATATCCGGTAT AGGATGTATAGTTCG TGTTCTCAATAGTAG ACCCGATCTA	CGGATCCCCG GGTTAATTAA	KV984 KV997
ArpC5 reverse	AAACAGAATCATTGA TTCAGTTCCATAAGC GACAGAATAGTAGAT ACCAAAAAGTAAGAT AAAGCCATAT	GAATTCGAGC TCGTTTAAAC	KV984 KV997
ArpC3 forward #2	AAAGGATCATCCCAG CAAGTGGTGGACTTG CTTCAGCAAGAGACG TTTTATGAACAAAGC TTTG	GGAGGCAGTG GCGGTAGCGAA	KV981
ArpC3 reverse #2	GGAAACGGAAAAACA TAAAGGCTTTGAAAT ACAGTATGAGCCAAA TTATTAATTAATAGAC	CAGTATAGCG ACCAGCATTC AC	KV981

Table 2.1: **Cloning primers used in Chapter 2.**

monitored using an Infinite M200 Pro (Tecan Systems, Inc., San Jose, CA) fluorescent plate reader with constant shaking and temperature maintenance at 25-27°C. OD_{600} readings were recorded every 10 min for 23 hr. Growth assays were conducted three separate times for a

Strain name	Genotype	Reference
KV367	h-, ARPC5-mCherry-natMX6, ade6-M216, leu1-32, his3-D1, ura4-D18	V. Sirotkin, [129]
KV480	h?, protease deficient	T. Pollard
KV588	h+, pAct1 Lifeact-GFP::Leu+; ade6-m216; leu1-32; ura4-D18	[58]
KV678	h+, fim1-mCherry-natMX6, pAct1 Lifeact-GFP::Leu+, ade6-M216, leu1-32, his3-D1, ura4-D18	This study
KV981	h?, ARPC3-SNAP-KanMX6, protease deficient	This study
KV982	h?, ARPC3-mCherry-KanMX6, protease deficient	This study
KV984	h?, ARPC3-mCherry-KanMX6, ARPC5-mCherry-NatMX6, protease deficient	This study
KV996	h?, ARPC3-Halo-KanMX6, protease deficient	This study
KV997	h?, ARPC5-Halo-KanMX6, protease deficient	This study
KV1005	?, pAct1 Lifeact-GFP::Leu+, ARPC5-Halo-KanMX-6, **	This study
KV1006	h?, ARPC3-mNeonGreen-KanMX6, protease deficient	This study
KV1007	h?, ARPC5-Halo-KanMX-6, fim1-mCherry-natMX6, **	This study

Table 2.2: **Fission yeast strains used in Chapter 2.** Asterisks (**) denote strains where protease deficient background is unknown.

total of three biological replicates, each containing three technical replicates per strain. For analysis, initial reading of each assay was set to zero.

2.5.3 Phallicidin staining

BoDipy-phallicidin stocks were prepared by resuspending 300 units BoDipy-phallicidin (Thermo Fisher Scientific, Waltham, MA) in methanol (1.5 ml). This solution was aliquoted (10 μl), vacuum dried, and stored at -20°C until use. For staining, one dry BoDipy-phallicidin aliquot was resuspended in PEM buffer (10 μl) (0.1 M NA PIPES pH 6.8, 1 mM EGTA, 1 mM $MgCl_2$) immediately prior to use.

Cells were stained with BoDipy-phallicidin as adapted from [122]. Briefly, fission yeast cells (1 ml) at OD600= 0.4-0.5 were fixed with EM grade paraformaldehyde (16%, 333 μl) for 5 min. Cells were washed 3 times with PEM buffer with centrifuge spins between each

wash. Cells were permeabilized with PEM buffer + 1% Triton X-100 (1 ml) for 1 min, then centrifuged and washed 3 times with PEM buffer. Cells were resuspended in PEM buffer (10 μl) and 1 unit of BoDipy-phallicidin (Molecular Probes) was added and incubated in the dark for 30 min. Cells were washed once with PEM buffer and centrifuged, then resuspended in a small volume of PEM buffer. Stained cells were stored at 4°C and imaged within 24 hr.

2.5.4 Cell microscopy

Confocal images were acquired on an IX83-X1 (Olympus, Tokyo, Japan) equipped with a Yokogawa CSU-X1 Spinning Disk Confocal Unit fitted with an ImagEM X2 EM-CCD camera (Hamamatsu, Hamamatsu, Japan) controlled by CellSens software (Olympus, Tokyo, Japan). For phallicidin stained cells, images were acquired using Z-stacks of 10 slices with a 0.5 μm step-size every 2 minutes. For actin patch dynamics, a single plane confocal image was acquired every 1 s for 1 min.

2.5.5 Actin patch dynamics

Fission yeast cells were placed on glass coverslips and single plane confocal images were collected every second for 1 min. Actin patch dynamics were analyzed using ImageJ and the Fiji plugin TrackMate [123] as previously described [141]. Fluorescence intensity and distance traveled from the cell cortex over time were measured for at least 10 actin patches per strain. Time courses for individual patches were aligned to the initiation of patch movement (time 0) or peak intensity and averaged at each time point.

2.5.6 Protein purification and labeling

Actin was purified from chicken skeletal muscle acetone powder [137] and labeled on surface lysines with Alexa488-succinimidyl ester (Life Technologies, Carlsbad, CA) [65].

Fission yeast Arp2/3 complex was purified from *S. pombe* cells using Wsp1(VCA) affinity chromatography as described previously [141, 37, 129]. For Halo-Arp2/3 complex, size exclusion chromatography on a HiPrep 26/60 Sephacryl S-300 HR column (Cytiva) was performed following anion exchange chromatography. SNAP and Halo constructs were incubated with the corresponding SNAP-549 (New England Biolabs, Ipswich, MA) or Janelia Fluor 549 (Promega) overnight at 4°C following the manufacturers' protocols.

Bovine WASP (GST-WASP(VCA)), fission yeast WASP (GST-Wsp1(VCA)), and GST-Wsp1(VCA)-Halo constructs were expressed in *Escherichia coli* strain BL21-Codon Plus (DE3-RP) (Agilent Technologies, Santa Clara, CA) as described previously [141, 166]. Briefly, these constructs were purified using glutathione-Sepharose affinity chromatography (GE Healthcare Life Sciences, Pittsburgh, PA). Size exclusion chromatography on a Superose 6 Increase 10/300 GL (GE Healthcare, Little Chalfont, UK) was performed on the GST-VCA-Halo construct following affinitiy chromatography to remove aggregates.

The GST-TEV-Dip1 plasmid was obtained from the Nolen lab and purified similar to previous methods [5] with a glutathione sepharose column, TEV protease incubation, and anion exchange column (GE Healthcare, Little Chalfont, UK).

A Nanodrop 2000c Spectrophotometer (Thermo-Scientific, Waltham, MA) was used to obtain A280 measurements of purified proteins.

2.5.7 Spontaneous pyrene assembly assay

Pyrene assembly assays were conducted in 96-well plates in an Infinite M200 Pro (Tecan Systems, Inc., San Jose, CA) fluorescent plate reader to measure the fluorescence of pyrene-actin (excitation: 367 nm, emission: 407 nm) as described previously [167]. Briefly, for spontaneous assembly, a 10 μM mixture of 10% pyrene-labeled Mg-ATP-actin was mixed with 10x ME [500 μM $MgCl_2$, 2 mM ethylene glycol tetraacetic acid (EGTA)] and added to the upper wells of the plate followed by 100X anti-foam. The lower wells contained 10x

KMEI [500 mM KCl, 10 mM $MgCl_2$, 10 mM EGTA, 100 mM imidazole (pH 7.0)], Mg-Buffer G [2 mM Tris (pH 8.0), 0.2 mM ATP, 0.5 mM DTT, 1 mM sodium azide (NaN_3), 0.1 mM MgCl2], and the appropriate amounts of Arp2/3 complex and VCA. The contents of the lower wells were mixed with the actin monomers in the upper wells, which initiated the reaction and data collection.

2.5.8 Glass preparation for TIRF microscopy

Microscope slides (#1.5, Fisher Scientific) and coverslips were washed for 7 min in acetone, isopropanol, and water, followed by sonication in isopropanol for 30 min. Washed glass was then cleaned using piranha solution. For piranha solution, washed glass was incubated with piranha solution (66.6% H_2SO_4, 33.3% H_2O_2) for 2 hr, then washed with diH_2O and dried with air. Immediately following plasma or piranha cleaning, glass was passivated by incubation in 1 mg/mL PEG-Si (5000 MW) or a 1:1000 mixture PEG-Biotin-Si (1 μg/mL, 3400 MW):PEG-Si (1 mg/mL, 5000 MW) in 95% ethanol for 18 hr [157]. After glass was rinsed with ethanol and water, flow chambers were prepared as described previously [167].

2.5.9 TIRF microscopy (TIRFM)

TIRFM movies were collected using an Olympus IX-71 microscope with through-the-objective TIRF illumination and an iXon EMCCD camera (Andor Technology, Belfast, UK) equipped with a cellTIRF 4Line system (Olympus). 15% Alexa 488-labeled Mg-ATP-Actin was mixed with ABPs and polymerization buffer (10 mM imidazole (pH 7.0), 50 mM KCL, 1 mM $MgCl_2$, 1 mM EGTA, 50 mM DTT, 0.2 mM ATP, 50 μM $CaCl_2$, 15 mM glucose, 20 μg/mL catalase, 100 μg/mL glucose oxidase, and 0.5% 400 centipoise methylcellulose) to induce F-actin assembly [157, 28]. This mixture was flowed into a chamber on ultraclean glass and imaged at room temperature. For Arp2/3 complex nucleation rate with VCA, images were taken at 0.4 s intervals. For Arp2/3 complex and Dip1, images were taken at 5 s intervals.

For experiments where actin filaments were tethered to the coverglass, flow chambers were incubated with HEK-BSA for 3 min before adding 1 mg/mL neutravidin. After a 2 min incubation, the chamber was washed with HEK-BSA followed by 1X TIRF buffer. Following, Mg-ATP-actin (10% Alexa 488-labeled, 0.5% biotin-actin (Cytoskeleton)) was added to a polymerization mix (10 mM imidazole (pH 7.0), 50 mM KCl, 1 mM $MgCl_2$, 1 mM EGTA, 50 mM DTT, 0.2 mM ATP, 50 μM $CaCl_2$, 15 mM glucose, 20 μg/mL catalase, 100 μg/mL glucose oxidase, and 0.5% (400 centipoise) methylcellulose) to induce F-actin assembly.

For Arp2/3 complex binding dynamics, the mixture was added to the prepared flow chamber and allowed to polymerize for 5-10 min. Following, Arp2/3 complex and capping protein with or without VCA was added to a polymerization mix, flowed into the chamber. Reactions were imaged at room temperature continuously for Arp2/3 complex (100 ms interval) with an actin image acquired every 10 s interval.

In experiments with both labeled Arp2/3 complex and labeled VCA, a polymerization mixture of actin, Arp2/3 complex, and VCA was added and then imaged. The reaction was imaged at room temperature continuously for Arp2/3 complex and VCA (50 ms interval) with an actin image acquired every 10 s interval.

2.5.10 Arp2/3 complex nucleation rate analysis

The frame with the first appearance of Arp2/3 complex binding at the site of branch nucleation was manually identified. Then, a 2-px by 2-px square region of interest (ROI) was defined for each frame, overlapping with the fluorescence of Arp2/3 complex at the branch site for 100 s after initial binding, and 20 s prior to binding. The fluorescence of Arp2/3 complex was measured for each frame. The length of the actin branch was measured manually for a minimum of ten selected frames total, focusing on frames in which the branch did not overlap with other nearby filaments for clear measurement. Data was plotted in Python

and a line of best-fit was calculated. The time of nucleation was determined as the time where the actin filament length was equal to zero. This was compared to the time at which Arp2/3 complex first bound to the mother filament to discern the delay between binding time and nucleation time.

For experiments with labeled Arp2/3 complex and labeled VCA, analysis was done in a similar manner, measuring the Arp2/3 complex, VCA, and actin fluorescence for each time point.

2.5.11 Arp2/3 complex binding dynamics

Analysis was performed with custom Python code. To calculate the number of binding events in a given frame, we processed the actin filament and Arp2/3 complex channels separately, and then counted the number of "islands" in the overlapped composite image. To process the actin filament channel, we clipped pixel values at a maximum (maxpix= 60), applied a Gaussian filter (sigma= 2.5), normalized pixel values between 0 and 1, binarized (threshold= 0.2), and removed any collection of fewer than 20 bright pixels eliminate noise. Similarly, to process the Arp2/3 channel, we clipped pixel values at a maximum (maxpix=100), applied a Gaussian filter (sigma= 0.5), normalized pixel values by the order of magnitude of the maximum pixel value, binarized (threshold= 1.5), and removed collections of fewer than 6 pixels to denoise. The total number of Arp2/3 particles in the frame was calculated by counting the number of isolated clumps in the Arp2/3 channel. The number of Arp2/3 particles bound to actin was calculated by counting the number of regions of overlapping signal in both processed images. This number of bound particles was then divided by the total length of actin present in each frame, which was measured manually in FIJI. The images resulting from this analysis are illustrated in Figure 2.8.

2.5.12 Arp2/3 complex-Dip1 nucleation activity

The nucleation activity was determined by counting the total number of actin filaments for each TIRF movie at frame 36 (3 min), the same amount of time since each actin assembly reaction was initiated. Both conditions were counted in triplicate.

CHAPTER 3

ACTIN BINDING PROTEINS ARE TAILORED FOR THEIR SPECIFIC F-ACTIN NETWORKS

Preface

The work in this chapter was performed by me for two research articles from our lab by Jenna Christensen and Kaitlin Homa. The first article is titled "Cooperation between tropomyosin and α-actinin inhibits fimbrin association with actin filament networks in fission yeast" and was published in *eLife* in 2019. The other article is titled "Formin Cdc12's specific actin assembly properties are tailored for cytokinesis in fission yeast" and is in final review at *Biophysical Journal*. As this work is published and is not my own first-author work, I have only included the figures to which I contributed. Figure 3.1 is the initial cell work done by Jenna that led to work conducted by me for this project. In Figures 3.2-3.5, I performed the cell strain construction (Figures 3.4, 3.5), cell antibody staining (Figure 3.2), confocal microscopy (Figures 3.2-3.5), and preliminary analysis (Figures 3.2, 3.3). In Figures 3.6 and 3.7, I performed the confocal microscopy imaging (Figure 3.6A) and TIRF microscopy imaging (Figure 3.7B).

3.1 Introduction

Fission yeast assemble a diverse set of F-actin networks responsible for a multitude of functions ranging from endocytosis (actin patches), to polarization (actin cables), and cytokinesis (contractile ring). Each F-actin network possesses a distinct, yet overlapping, set of actin binding proteins (ABPs) that are responsible for the spatial, temporal, and functional identity of each individual network. In the following work, which is a combination of two research articles, we dissect how ABPs properly sort to their appropriate F-actin network and how

biochemical properties of specific ABPs tailor an ABP for optimal function compared to other ABPs from the same protein family.

In Christensen and Homa et al. [29], we hypothesized that competitive and cooperative interactions between actin binding proteins of different (competitive) or the same (cooperative) F-actin networks can drive their sorting and association to the appropriate F-actin network. We previously identified competitive binding interactions between three fission yeast ABPs with distinct network localizations—fimbrin Fim1 and ADF/cofilin Adf1 (endocytic actin patches) and tropomyosin Cdc8 (cytokinetic contractile ring) that help facilitate their sorting to the proper F-actin networks [28, 133]. Specifically, synergistic activities between Fim1 and Adf1 rapidly displace Cdc8 from F-actin networks such as actin patches [28, 133]. However, these interactions do not explain how Fim1 is prevented from strongly associating with other F-actin networks, such as the contractile ring. Therefore, we sought to determine whether other ABPs at the contractile ring prevent Fim1 association. In this study, we demonstrate that Fim1 competes with the contractile ring ABP α-actinin Ain1 (hereafter called Ain1) for association with F-actin, and that their ability to compete is dependent upon their residence time on F-actin.

In Homa et al. (in press), we wished to understand how multiple isoforms of the formin family can each be individually tailored for a specific F-actin network and function. Most organisms express multiple formin isoforms, from two in budding yeast, three in fission yeast, seven in nematode worms, fifteen in mammals, and more than twenty in plants [55, 114, 125]. Despite having well-conserved structural folds and general actin assembly mechanisms, distinct formin isoforms are required for different cellular processes in many cell types. For example, each of the three fission yeast formins assembles actin filaments for a specific F-actin network [71]: For3, polarizing actin cables [39, 94]; Cdc12, the contractile ring of dividing cells [25]; Fus1, the fusion focus during mating [108, 107]. While regulation via activation at the right time and place has been established to be critical for the functional specificity of formin

isoforms [16], it is also possible that a formin's particular actin assembly properties are also important [151]. In vitro measurements reveal that many formins have significantly different actin assembly properties, such as F-actin nucleation efficiency, barbed end elongation rate, and barbed end dissociation rate [48, 69]. Consistent with this possibility, we previously determined that the actin assembly properties of the three fission yeast formins (For3, Cdc12, and Fus1) vary widely [126], suggesting that a formin's specific properties might also be tailored for its cellular role. However, the extent to which each property contributes to the assembly of particular F-actin networks in vivo is less clear.

We first used a computational 3D search capture pull release (SCPR) model to characterize how formin-mediated actin filament nucleation efficiency and elongation rate affect cytokinetic ring formation. Our simulations predicted that changes in formin nucleation efficiency have the largest impact on the timing and probability of contractile ring formation. We then tested the physiological importance of formin's actin filament nucleation efficiency and elongation rate. We developed formin strains that express engineered formin chimeras in which the FH1FH2 domains of the cytokinesis formin Cdc12 were replaced with the FH1FH2 domains of functionally, evolutionarily, and biochemically diverse formins from different organisms. Quantitative imaging and analysis of the formin chimera cells reveals that formin-mediated cytokinesis in fission yeast is robust, but supports the modeling prediction that nucleation efficiency has the largest impact on contractile ring assembly rate.

3.2 Results

3.2.1 Fission yeast alpha-actinin Ain1 competes with Fimbrin Fim1 for association with F-actin networks

Previous work from our lab demonstrated that actin binding proteins (ABPs) can compete or cooperate to sort to their distinct F-actin networks. Specifically, our lab observed that

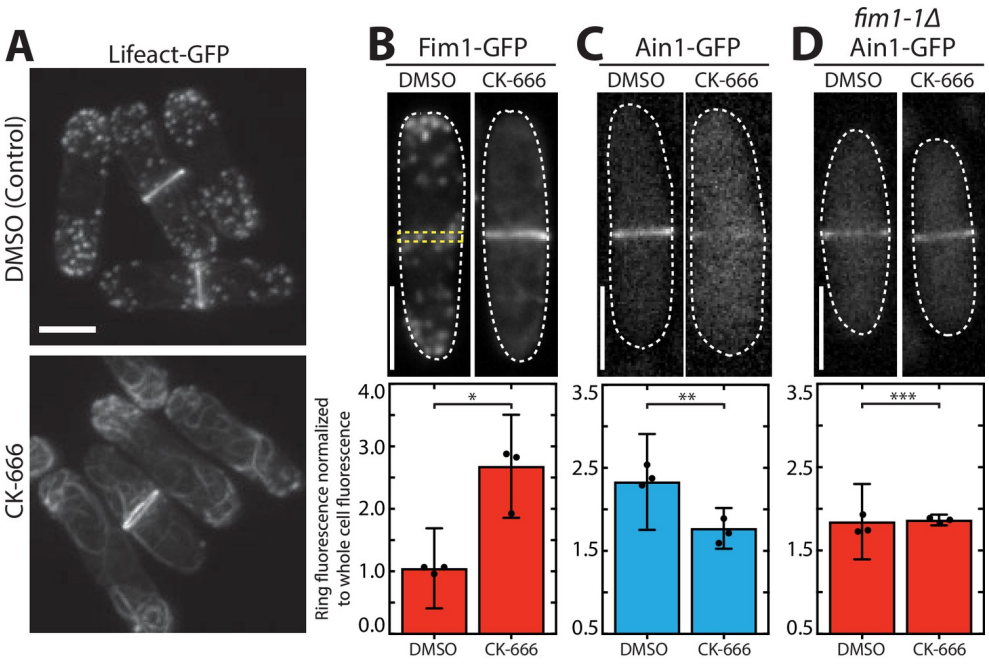

Figure 3.1: **Fimbrin Fim1 and a-actinin Ain1 compete for association with the contractile ring. A.** Fluorescence micrographs of fission yeast cells expressing Lifeact-GFP following treatment with DMSO (control, top) or 200 μM Arp2/3 complex inhibitor CK-666 (bottom). Scale bar, 5 μm. **B-D, top panels.** Fluorescence micrographs of fission yeast cells expressing Fim1-GFP (B), Ain1-GFP (C), or Ain1-GFP in a *fim1-1*Δ background (D), following treatment with DMSO (left) or 200 μM CK-666 (right). Dotted lines outline cells. Yellow dotted line denotes representative region used to quantify fluorescence value in cells lacking a visible contractile ring. Scale bars, 5 μm. **B-D, bottom panels.** Mean Fim1-GFP (B) or Ain1-GFP (C,D) fluorescence at the contractile ring normalized to whole cell fluorescence. Error bars = s.d. Filled circles indicate means of experimental replicates. n $\geq$ 18 cells from three independent experiments. Two-tailed t-tests for data sets with unequal variance yielded p-values *p=8.57x10^{-20}, $^{**}p = 1.75x10^{-6}$, $^{***}p = 0.81$.

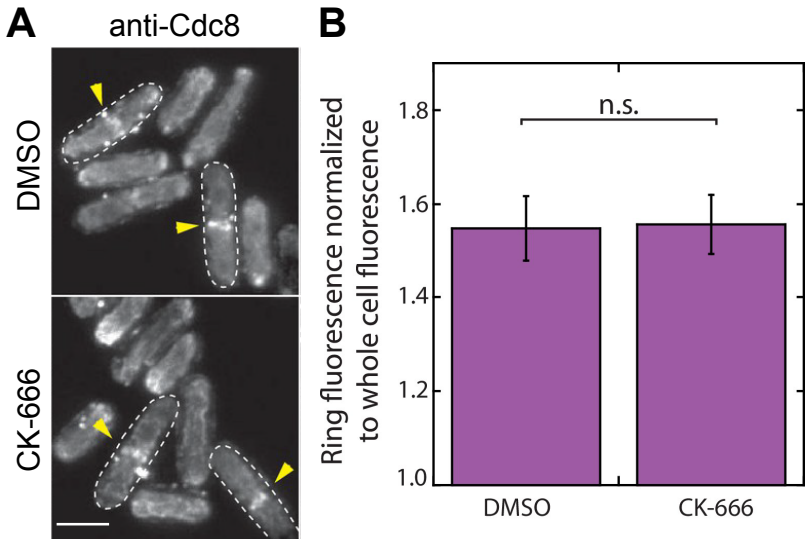

Figure 3.2: **Tropomyosin Cdc8 does not re-localize following CK-666 treatment. A.** Fluorescent micrographs of fission yeast cells immunostained for tropomyosin Cdc8. Cells were treated with DMSO (control) or 200 μM Arp2/3 complex inhibitor CK-666. Yellow arrowheads denote contractile rings. Dotted lines outline individual cells for clarity. Scale bar, 5 μm. **B.** Mean anti-Cdc8 contractile ring fluorescence normalized to total cell fluorescence. Error bars = s.e. Two-tailed t-test for data sets with unequal variance yielded p-value=0.9338. n $\geq$ 10 cells.

the actin patch protein fimbrin Fim1 can synergize with cofilin ADF1 to readily outcompete contractile protein tropomyosin Cdc8 on F-actin filaments [28, 133]. However, Fim1 is present in cells at much higher concentrations than Cdc8 and it is unclear how Fim1 is prevented from associating with the contractile ring. Our lab speculated that other contractile ring ABPs may compete with Fim1 to prevent contractile ring association.

When cells are treated with Arp2/3 complex inhibitor CK-666, F-actin patches are rapidly diassembled, releasing actin patch ABPs into the cytoplasm. Upon CK-666 treatment and patch disassembly, Fim1 relocalized to the contractile ring (Figure 3.1B). Interestingly, in this treatment the contractile ring bundling ABP α-actinin Ain1 was rapidly displaced into the cytoplasm (Figure 3.1C). This suggested that Fim1 and Ain1 may compete for binding to F-actin filaments at the contractile ring. In a *fim1-1*Δ background, upon CK-666 treatment, Ain1 was no longer displaced from the contractile ring, providing further evidence

that Fim1, rather than other patch ABPs is competing with Ain1 for binding to the contractile ring (Figure 3.1D). Additionally, upon CK-666 treatment, Fim1 fluorescence at the contractile ring was increased—and Ain1 decrased—for all stages of contractile ring lifetime (formation, dwell, and constriction) (Figure 3.3).

Previous work had demonstrated that fimbrin Fim1 can outcompete tropomyosin Cdc8 [28, 133], so we examined whether Fim1 re-localization to the contractile ring after patch disassembly also led to Cdc8 displacement into the cytoplasm. Immunostaining of Cdc8 revealed that tropomyosin was not displaced from the contractile ring in the presence of CK-666 (Figure 3.2). This suggests that other ABPs present at the contractile ring may help Cdc8 to remain bound to F-actin despite its competitor Fim1 localizing to this network, which we hope to explore in future work.

Interestingly, even in a fimbrin Fim1 deletion background (*fim1-1*Δ), α-actinin Ain1 was never observed at actin patches (Figure 3.4A, C). Ain1 is expressed at low concentrations within wild-type fission yeast cells, so we next examined whether in the presence of increased concentrations of Ain1 in a *fim1-1*Δ background, Ain1 was able to localize to actin patches. When Ain1 is overexpressed in a *fim1-1*Δ background, Ain1-GFP localizes to F-actin patches in more than 60% of cells (Figure 3.4B-C). This provides further evidence that Fim1 and Ain1 compete for localization to F-actin networks in cells.

We next wished to determine what mechanisms allow for fimbrin Fim1 and α-actinin Ain1 to properly sort to their appropriate F-actin networks. Previous studies have demonstrated that Ain1 has a rapidly short residence time on actin filaments, whereas, Fim1 exhibits longer residence times [78]. This difference in residence times could account for how Fim1, and potentially other actin patch ABPs, are able to keep Ain1 from associating with patches. Previous work from our lab found that a key arginine residue, R216, affects the residence time of Ain1 on F-actin filaments [78]. By mutating this residue to a glutamic acid Ain1(R216E), Ain1's residence time increases, causing slower dissociation from F-actin filaments. When

Ain1(R216E) is overexpressed in fission yeast, Ain1 is observed at acitn patches in nearly all cells, even when Fim1 is expressed (Figure 3.5A-C). Taken together, this work suggests that Fim1 and Ain1 compete with one another and this competition is driven by differing residence times on F-actin.

3.2.2 Formin Cdc12 is specifically tailored for fission yeast cytokinesis

To understand the role that nucleation and elongation play in fission yeast cytokinesis, our lab simulated the SCPR model of cyotkinetic ring formation and found that nucleation was the primary factor that influenced if a cytokinetic ring would form. Further, we engineered and transformed formin chimera constructs, where the FH1 and FH2 domains of fission yeast Cdc12 were replaced by formins with different nucleation and elongation properties: mDia2, Bni1, and For3.

When formin chimeras were introduced into fission yeast cells, we observed that mDia2 chimeras showed ring assembly times similar to wild-type, but Bni1 and For3 had significant lag times in ring assembly. Additionally, all formin chimeras, other than mDia2, exhibited a distinct contractile ring assembly pathway. In wild-type cells and those with the mDia2 chimera construct, cells assembled by the traditional node coalescence mechanism that has been observed previously (Figure 3.6A-B). However, for the For3, Bni1, and CYK-1 chimeras—those with nucleation rates lower than Cdc12 or mDia2—less than 50% of cells followed the traditional node mechanism of assembly (Figure 3.6B). Instead, we observed that ring formation occurred from a single spot density at the cell's mid zone (Figure 3.6A). This suggests that, while all formins with their individual biochemical properties can assemble contractile rings, the mechanisms of this ring assembly can occur through different, distinct pathways, that lead to delays in contractile ring assembly times.

To confirm that the chimera constructs transformed into fission yeast exhibited nucleation and elongation properties similar to their non-chimeric counterparts, we engineered and

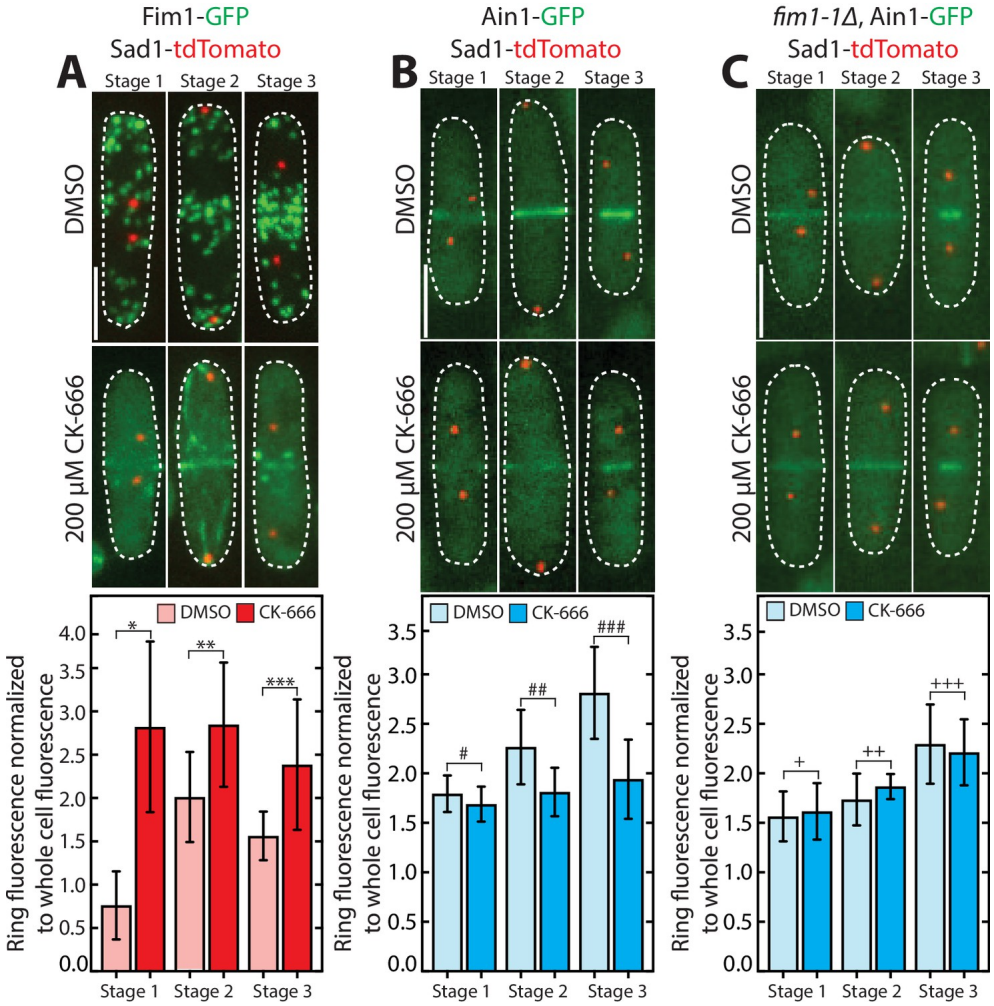

Figure 3.3: **Fimbrin Fim1 displaces α-actinin Ain1 from the contractile ring following CK-666 treatment. A-C, top.** Fluorescent micrographs of fission yeast cells expressing spindle pole body marker Sad1-tdTomato and Fim1-GFP (A), Ain1-GFP (B), or Ain1-GFP in a *fim1-1*Δ background (C), following treatment with DMSO (control, top) or 200 μM Arp2/3 complex inhibitor CK-666 (bottom). Lines outline cells. Scale bar, 5 μm. **A-C, bottom.** Mean Fim1-GFP (A) or Ain1-GFP (B–C) contractile ring fluorescence normalized to whole cell fluorescence for cells in stage 1 (contractile ring formation), stage 2 (contractile ring dwell), or stage 3 (contractile ring constriction) of cytokinesis following treatment with DMSO (control) or 200 μM CK-666. Error bars = s.d. Two-tailed t-test for data sets with unequal variance yielded p-values *p=0.024, **p=0.034, ***p=0.13, $^{\#}$p=0.38, $^{\#\#}$p=0.094, $^{\#\#\#}$p=0.061, $^{+}$p=0.53, $^{++}$p=0.87, $^{+++}$p=0.55.

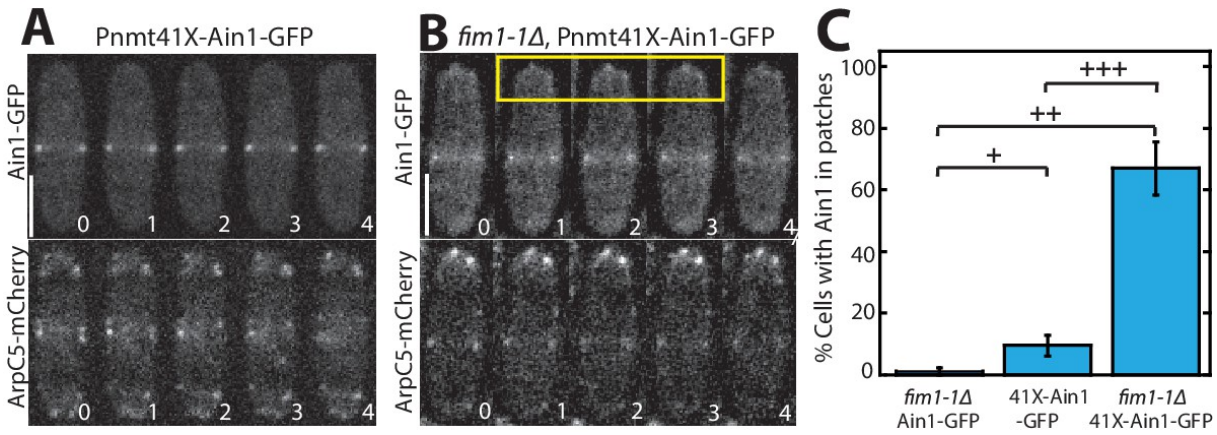

Figure 3.4: **Fimbrin Fim1 and α-actinin Ain1 compete for association with actin patches. A-B.** Time-lapse fluorescent micrographs of fission yeast cells expressing ArpC5-mCherry (bottom) and overexpressing GFP-tagged α-actinin Ain1 from the 41Xnmt promoter (top) for 20 hr in a wild-type (A) or *fim1-1*Δ background (B). Yellow box highlights Ain1-GFP localization at actin patches. Scale bars, 5 μm. Time in s. **C.** Percentage of cells in which Ain1-GFP is observed in actin patches. Error bars = s.e. Two-tailed t-tests for data sets with unequal variance yielded p-values $^{+}p = 0.113$, $^{++}p = 0.002$, $^{+++}p = 0.012$. n = 3 experimental replicates.

purified the chimeras for biochemical analysis (Figure 3.7A). Spontaneous F-actin assembly revealed that all formin chimeras had nucleation and elongation similar to their non-chimeric versions (Figure 3.7B-D).

In vivo evidence reveals that different rates of contractile ring assembly are primarily responsible for major differences between the formin chimera strains in the overall time course of cytokinesis. This is consistent with formin-mediated actin assembly having a major role in generation of the contractile ring [25, 113], and because mDia2 has the most similar nucleation properties to Cdc12 (Figure 3.7C), this supports the conclusion from the quantitative modeling, that efficient formin-mediated nucleation of actin filaments is critical for contractile ring assembly in fission yeast.

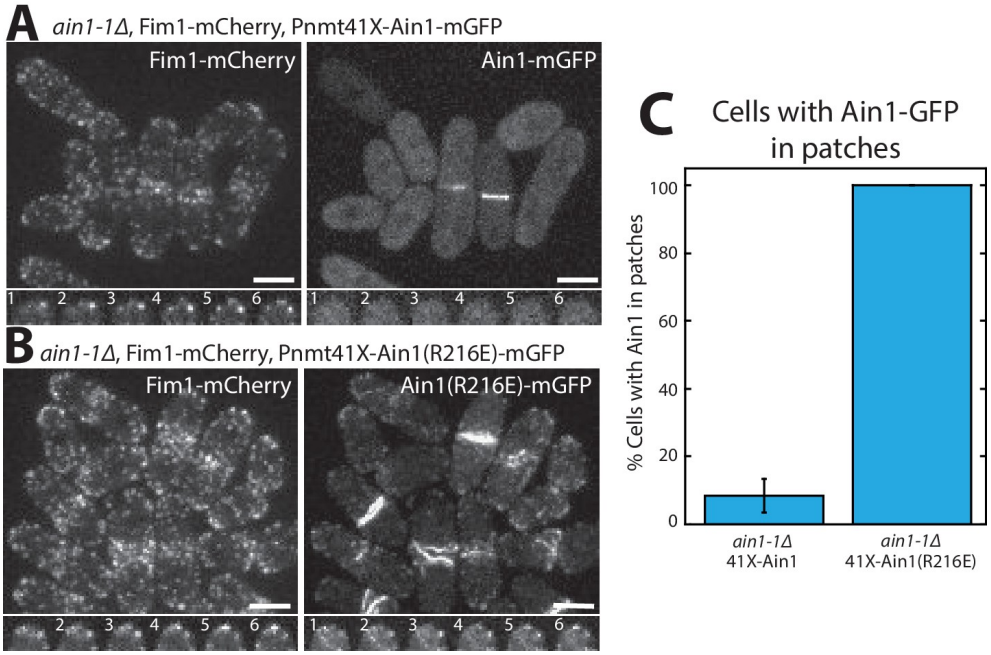

Figure 3.5: **Fimbrin Fim1 and α-actinin Ain1 competition at actin patches is driven by their residence time on F- actin. A-B, top.** Fluorescence micrographs of fission yeast in an *ain1-1*Δ background overexpressing GFP-tagged wild-type Ain1 (A) or mutant Ain1(R216E) (B) from the 41Xnmt1 promoter. Scale bars, 5 μm. **A-B, bottom.** Timelapse (in s) of cell taken from a single Z-plane. **C.** Percentage of cells in which Ain1-GFP is observed in actin patches. Error bar, s.e. Two-tailed t-test for data sets with unequal variance yielded p-value=0.0029.

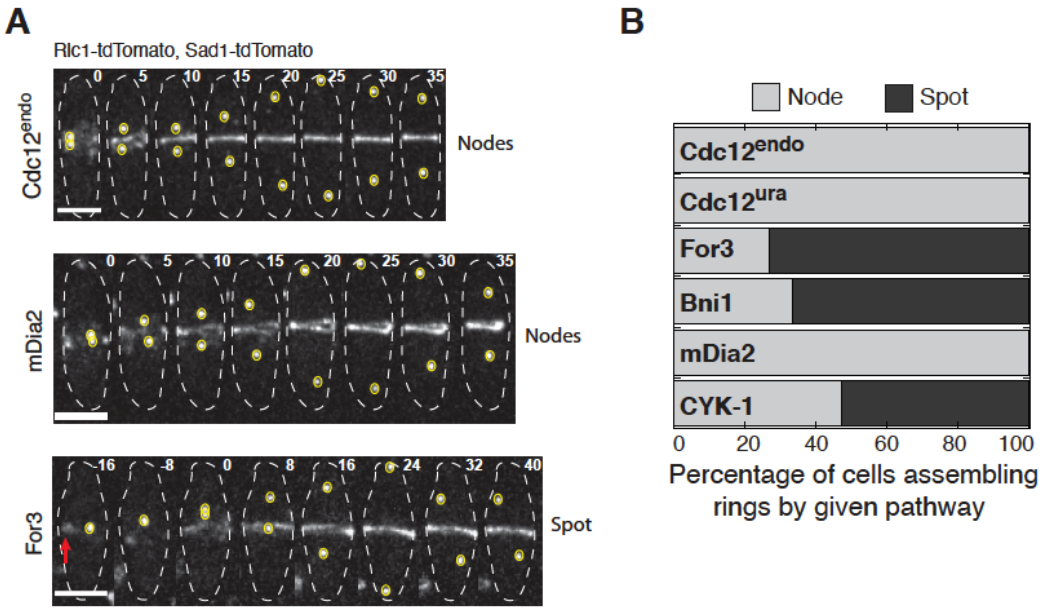

Figure 3.6: **Formin chimera strains assemble contractile rings through different pathways. A.** Representative confocal time-lapse images of the indicated strains showing assembly of the contractile ring (Rlc1-tdTomato). Red arrow indicates Rlc1-tdTomato spot (bottom panel). Spindle pole bodies are labeled with Sad1-tdTomato. Time 0: spindle pole body (yellow circles) separation. Time is indicated in minutes. Scale bar, 5 μm. **B.** Percentage of cells that build contractile rings through the precursor cytokinesis node or spot pathways.

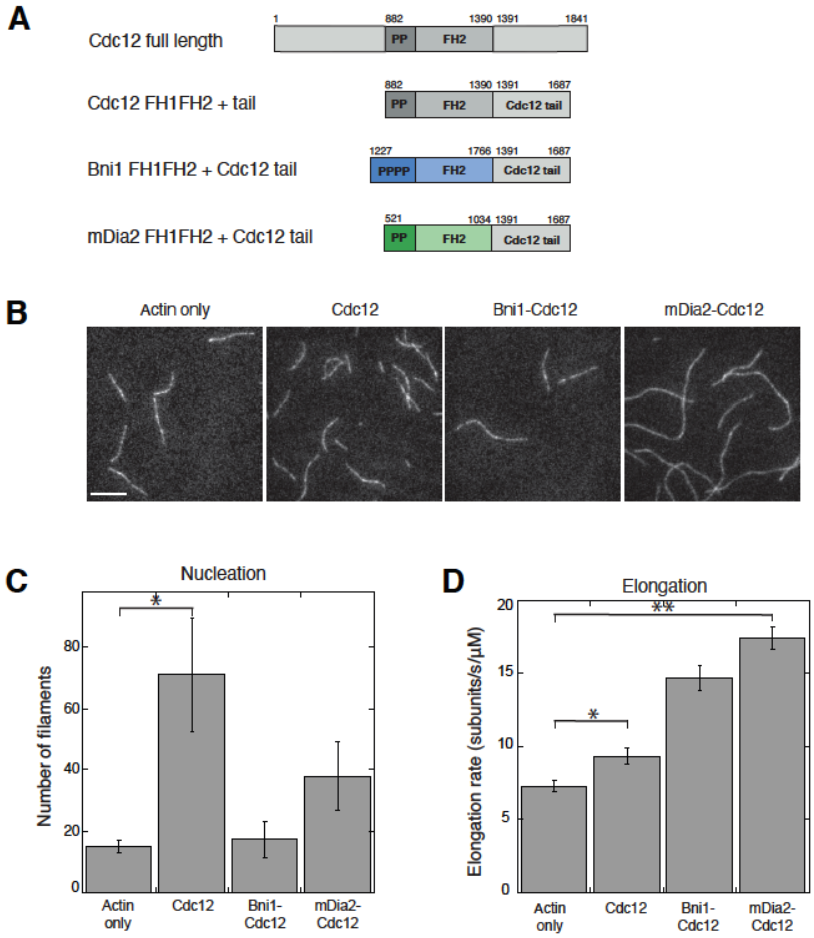

Figure 3.7: **The biochemical properties of formin chimeras with a Cdc12 tail are similar to previously measured biochemical properties of isolated FH1FH2 domains. A.** Schematic of full length Cdc12 compared to formin chimera constructs tested for biochemical activity. **B.** Single color TIRFM of 1.5 μM Mg-ATP actin (10% Alexa-488 labeled) with 2.5 μM fission yeast profilin Cdc3, and either no formin (actin only) or 1 nM Cdc12, Bni1-Cdc12, or mDia2-Cdc12 formin chimeras. Scale bar, 8 μm. **C.** Quantification of the number of filaments nucleated by formin chimera constructs. Two tailed t-tests for data sets with unequal variance yielded p-value *p=0.047. Error bars indicate standard error of three independent biological replicates of 10 actin filaments for actin only, Cdc12, and mDia2-Cdc12, and two independent biological replicates of 10 actin filaments for Bni1-Cdc12 due to a lack of Bni1-Cdc12-associated filaments in the third replicate. **D.** Quantification of formin chimera elongation rates. Two tailed t-tests for data sets with unequal variance yielded p-values *p=0.038, **p=0.0013. Error bars indicate standard error of three independent biological replicates of 10 actin filaments for actin only, Cdc12, and mDia2- Cdc12, and two independent biological replicates of 10 actin filaments for Bni1-Cdc12 due to a lack of Bni1-Cdc12-associated filaments in the third replicate.

3.3 Materials and Methods

3.3.1 Strain construction and growth

Fission yeast strains were created by genetic crossing on SPA5S plates followed by tetrad dissection on YE5S plates. Strains were screened for auxotrophic (leu, ura) or antibiotic (nat, kan) markers and maintained on YE5S plates. Glycerol stocks were created by pelleting cells and resuspending in 750 μL media and 250 μL of 50% sterile glycerol. Tables 3.1-3.2 list the fission yeast strains used in this study.

Strain name	**Genotype**	**Reference**
KV459	h+, rlc1-tdTomato-natMX6 ade6-M210 leu1-32 ura4-D18	This study
KV579	h-, ain1-GFP-KanMX6, URA+	[160]
KV588	h+, pAct1 Lifeact-GFP::Leu+; ade6-m216; leu1-32; ura4-D18	[58]
KV707	h-, leu1-32, his3-D1, ura4-D18, ade6-M216, Pnmt41-SpAin1-mGFP::Leu+	This study
KV804	h?, fim1-mCherry-natMX6, ain1-Δ1::kanMX6, Pnmt41-SpAin1-mGFP::Leu+	This study
KV856	h?, h?, ain1-Δ1:: kanMX6, Pnmt41-SpAin1(R216E)-mGFP::Leu+, fim1-mCherry-natMX6, ade6, leu1-32, ura4-D18	This study
KV861	h?, ain1-GFP-kanMX6, sad1-tdTomato-natMX6, ade6-m21?, leu1-32, ura4-D18	This study
KV878	h+, fim1-mGFP-kanMX6, sad1-tdTomato-natMX6	This study
KV908	h? fim1-1Δ-kanMX6, ain1-GFP-kanMX6, sad1-tdTomato::natMX6	This study
KV963	h?, fim1-1Δ::kanMX6, Pnmt41-SpAin1-mGFP::Leu+	This study
KV968	h? Pnmt41-SpAin1-mGFP::Leu+, ARPC5-mCherry-natMX6	This study

Table 3.1: **Fission yeast strains used in Chapter 3 from [29].**

3.3.2 Cell imaging and treatment with CK-666

For live cell imaging, cells were grown in YE5S media overnight at 25°C, subcultured into EMM5S media without thiamine, and kept in log phase for 20–22 hr at 25°C. Cells were imaged directly on glass slides. Z-stacks of 10 slices, 0.5 μm apart were acquired with a 100x, 1.4 NA objective on a Zeiss Axiovert 200M equipped with a Yokogawa CSU-10 spinning-disk unit (McBain, Simi Valley, CA) illuminated with a 50-milliwatt 473 nm DPSS laser, and a Cascade 512B EM-CCD camera (Photometrics, Tucson, AZ) controlled by MetaMorph software (Molecular Devices, Sunnyvale, CA). For CK-666 treatments, CK-666 powder stock (Sigma, St. Louis, MO) was diluted to 10 mM in DMSO. Cells were grown as stated above, and incubated with CK-666 or an equivalent volume of DMSO (control) in a rotator at 25°C for 30 min prior to imaging. Cells were then immediately imaged as above.

3.3.3 Contractile ring fluorescence quantification

Contractile ring maturation was divided into three stages by measuring the distance between spindle pole bodies (SPBs, visualized by Sad1-tdTomato) and noting constriction of the contractile ring. Stage 1 cells had SPBs less than 6 μm apart, with no observable ring constriction. Stage 2 cells had SPBs greater than 6 μm apart, with no observable ring constriction. Stage 3 cells had SPBs less than 9 μm apart, with evident ring constriction. The contractile ring region was determined by visually examining the z-stack for the ring site. Normalized contractile ring fluorescence was taken by drawing a region of interest (ROI) around the observed ring and around the whole cell using ImageJ. To obtain fluorescence values for cells without a visible contractile ring (for example, DMSO-treated Fim1-GFP cells), mitotic cells were determined by the presence of two spindle pole body markers. These fission yeast cells were measured along their length and a 4-pixel width line was drawn across the exact center of the fission yeast cell (denoted as a yellow dotted-line in Figure 3.1). The

mean fluorescence of the ring divided by the whole cell was then determined. A value of 1.00 indicates no increased fluorescence at the site of the contractile ring, while values > 1 indicate increased fluorescence at the ring. Maximum projections were used for images in figures and sum projections were used for quantification.

3.3.4 Tropomyosin Cdc8 antibody staining

Following standard growth and culturing protocols for live cell imaging, fission yeast cells were stained with anti-Cdc8p [34]. Cells were fixed in 16% formaldehyde for 5 min at 20°C. Cells were then washed in cold 1X PBS and resuspended in 140 μL 1.2 M sorbitol. 60 μL fresh protoplasting solution (3 mg/ml zymolase 100T in 1.2 M sorbitol) was added and cells were incubated for 7 min on a rotator at room temperature. 1 mL of 1% Triton-X was then added to the cells and incubation continued for 2 min. Cells were then pelleted and resuspended in 0.5 mL PBAL (10% BSA, 100 mM lysine monohydrochloride, 1 mM NaN3, 50 ng/ml ampicillin in PBS) and incubated for 2.5 hr on a rotator at room temperature. Cells were resuspended in 100 μL of anti-Cdc8p 1:10 in PBAL (gift of Sarah Hitchcock-DeGregori) and incubated overnight at 4°C on a rotator. Following incubation with primary antibody, cells were washed three times with 0.5 mL PBAL and resuspended in 50 μL Alexa-Flour 555 goat anti-rabbit secondary antibody (Thermo-Fisher Scientific, Carlsbad, CA) (1:100 in PBAL) and incubated for 90 min at room temperature on a shaker in the dark. Cells were then washed five times with 0.5 mL PBAL and resuspended in 20–30 μL PBAL for imaging. Cells were stored at 4°C and imaged within 48 hr of staining.

3.3.5 Quantifying number of cells with Ain1 in actin patches

To quantify the number of cells containing Ain1-GFP in actin patches, 1 min timelapse movies of 1 frame per second were taken, imaging both Ain1-GFP and an actin patch marker (ArpC5-mCherry or Fim1-mCherry). Movie files for independent experiments and replicates

were blinded and independently analyzed for number of cells containing Ain1-GFP in actin patches using FIJI [123, 124]. For a single cell to count as positively containing Ain1-GFP in actin patches, three criteria had to be met: 1) at least one distinguishable actin patch containing Ain1-GFP was observed, 2) the observed actin patch(es) contained Ain1-GFP for at least three frames and 3) the Ain1-GFP signal trajectory matched the channel expressing either ArpC5-mCherry or Fim1-mCherry. Total number of cells and cells with actin patches containing Ain1-GFP were then calculated to obtain percent of cells containing Ain1-GFP in actin patches.

3.3.6 Protein purification

The Cdc12 fragment [Cdc12(882-1687)] and the Bni1-Cdc12 and mDia2-Cdc12 chimeras were expressed in E. coli strain BL21-Codon Plus (DE3)-RP (Agilent Technologies, Santa Clara, CA) with 0.5 mM isopropyl ß-D-1-thiogalactopyranoside for 16 h at 16°C. Cells were lysed by sonication in extraction buffer (50 mM NaH2PO (anhydrous), 500 mM NaCl, 10% glycerol, 10 mM imidazole, 10 mM BME pH 8) with EDTA-free Protease Inhibitor Cocktail (Roche, Basel, Switzerland) and were clarified. The extract was incubated for 1 h at 4°C with Talon Resin (Clontech), loaded onto a column, washed with extraction buffer, and protein was eluted with 250 mM imidazole. The formin chimeras were dialyzed into buffer [50 mM HEPES (pH 7.0), 50 mM NaCl, 5% glycerol, 0.01% NaN3, 1 mM DTT] for cation exchange chromatography (GE Healthcare, Little Chalfont, UK). The cleanest fractions were pooled and dialyzed into SNAP buffer [20 mM HEPES (pH 7.4), 200 mM KCl, 0.01% NaN3, 10% glycerol, and 1 mM DTT]. The mDia2-Cdc12 chimera required additional size exclusion chromatography and was filtered on a Superdex 200 10/300 GL column (GE Healthcare). Aliquots of all formin proteins were flash frozen in liquid nitrogen and stored at -80°C. Chicken skeletal muscle actin was purified as described in [137]. Fission yeast profilin Cdc3 was overexpressed and purified from E. coli using poly-L-proline affinity chromatography as

described in [79].

3.3.7 TIRF microscopy (TIRFM) and analysis

TIRFM was conducted with the formin chimeras as described previously (40). Briefly, timelapse TIRFM movies were obtained with through-the-objective TIRF illumination on an Olympus IX-71 microscope with an iXon EMCCD camera (Andor Technology) and a cellTIRF 4-line system (Olympus). 1 nM of either Cdc12, Bni1-Cdc12, or mDia2-Cdc12 formin chimeras was added to a polymerization mix (see [29]) along with 2.5 μM fission yeast profilin Cdc3, which was then added to Mg-ATP-actin (10% Alexa-488 labeled) to induce actin assembly. This mixture was added to a flow chamber and imaged at 5 s intervals at room temperature.

The nucleation activity was determined by counting the total number of actin filaments for each TIRFM movie at frame 48, the same amount of time since the initiation of each actin assembly reaction. Each construct (actin only, Cdc12, Bni1-Cdc12, or mDia2-Cdc12) was counted in triplicate. To determine the actin filament elongation rate, 10 individual actin filaments from each TIRFM movie were tracked over time, with their lengths measured every fifth frame for 7-9 total measurements. An average elongation rate was calculated for each filament, and then those were averaged to obtain an average for each movie. Each construct (actin only, Cdc12, or mDia2-Cdc12) was measured in triplicate with the exception of Bni1-Cdc12, which was only measured in duplicate due to a low number of Bni1-Cdc12-associated filaments in the third TIRFM movie due to Bni1-Cdc12's low nucleation activity.

Strain name	Genotype	Reference
KV343	h?, cdc12-mGFP::KanR	This study
KV405	h-, cdc12Δ::KanR, cdc12(Nterm)-cdc12(FH1FH2)-cdc12(Cterm)-GFP::ura4+	This study
KV407	h-, cdc12Δ::KanR, cdc12(Nterm)-for3(FH1FH2)-cdc12(Cterm)-GFP::ura4+	This study
KV408	h-, cdc12Δ::KanR, cdc12(Nterm)-bni1(FH1FH2)-cdc12(Cterm)-GFP::ura4+	This study
KV437	h-, cdc12Δ::KanR, cdc12(Nterm)-mdia1(FH1FH2)-cdc12(Cterm)-GFP::ura4+	This study
KV445	h-, cdc12Δ::KanR, cdc12(Nterm)-mdia2(FH1FH2)-cdc12(Cterm)-GFP::ura4+	This study
KV451	h-, cdc12Δ::KanR, cdc12(Nterm)-cyk-1(FH1FH2)-cdc12(Cterm)-GFP::ura4+	This study
KV489	h?, rlc1-tdTomato::natMX6; FY527 cdc12-mGFP::KanR	This study
KV552	h?, sad1-mCherry-NatMX6, cdc12Δ::KanR, cdc12(Nterm)-cyk-1(FH1FH2)-cdc12(Cterm)-GFP::ura4+	This study
KV778	h? rlc1-tdTomato-natMX6, cdc12Δ::KanR, cdc12(Nterm)-cdc12(FH1FH2)-cdc12(Cterm)-GFP::ura4+	This study
KV779	h? rlc1-tdTomato-natMX6, cdc12Δ::KanR, cdc12(Nterm)-bni1(FH1FH2)-cdc12(Cterm)-GFP::ura4+	This study
KV790	h? rlc1-tdTomato-natMX6, cdc12Δ::KanR, cdc12(Nterm)-for3(FH1FH2)-cdc12(Cterm)-GFP::ura4+	This study
KV791	h? rlc1-tdTomato-natMX6, cdc12Δ::KanR, cdc12(Nterm)-mDia1(FH1FH2)-cdc12(Cterm)-GFP::ura4+	This study
KV793	h? rlc1-tdTomato-natMX6, cdc12Δ::KanR, cdc12(Nterm)-mDia2(FH1FH2)-cdc12(Cterm)-GFP::ura4+	This study
KV794	h? rlc1-tdTomato-natMX6, cdc12Δ::KanR, cdc12(Nterm)-CYK1(FH1FH2)-cdc12(Cterm)-GFP::ura4+	This study
KV942	h?, cdc12Δ::KanR, cdc12(Nterm)-bni1(FH1FH2)-cdc12(Cterm)-GFP::ura4+, sad1-tdTomato-natMX6	This study
KV944	h? cdc12Δ::KanR, cdc12(Nterm)-mdia1(FH1FH2)-cdc12(Cterm)-GFP::ura4+, sad1-tdTomato-natMX6	This study
KV948	h? cdc12-mGFP::KanR, sad1-tdTomato-natMX6	This study
KV949	h? cdc12Δ::KanR, cdc12(Nterm)-cdc12(FH1FH2)-cdc12(Cterm)-GFP::ura4+, sad1-tdTomato-natMX68	This study
KV950	h? cdc12Δ::KanR, cdc12(Nterm)-for3(FH1FH2)-cdc12(Cterm)-GFP::ura4+, sad1-tdTomato-natMX6	This study
KV951	h- cdc12Δ::KanR, cdc12(Nterm)-mdia2(FH1FH2)-cdc12(Cterm)-GFP::ura4+, sad1-tdTomato-natMX6	This study

Table 3.2: **Fission yeast strains used in Chapter 3 from Homa et al. (in press).**

CHAPTER 4

INITIATION OF ACTIN CYTOSKELETON NETWORK FORMATION AND SELF-ORGANIZATION

Preface

The work presented in the following chapter was performed by me, with guidance on cell biology techniques by other lab members.

4.1 Abstract

Cells facilitate many fundamental processes such as division, polarization, endocytosis and motility by controlling the assembly of specific actin filament (F-actin) networks with defined properties such as F-actin architecture/organization, size and density, and dynamics, which are tailored to perform their specific functions. As F-actin networks simultaneously assemble in a common cytoplasm from a shared pool of actin monomers, cells must be able to self-organize these actin networks for their necessary functions. While much work has been done to understand this self-organization in steady state F-actin networks, I do not yet understand how this self-organization is initiated. In this work, I investigated the spatial and temporal pathway of the initiation of F-actin network assembly in vivo using microfluidics. While this work proved too complex for currently available techniques to have continued, it provides significant preliminary insight into how cells initiate self-organization.

4.2 Introduction

The ability of complex cellular structures to temporally and spatially self-organize within a common cytoplasm is a fundamental biological question. The actin cytoskeleton is an important self-organization model because it assembles into a range of networks to execute diverse

cellular processes, such as cytokinesis, polarization and endocytosis. How diverse F-actin networks are self-organized and maintained from a shared actin monomer pool is poorly understood. Fission yeast is an ideal system to dissect the underlying molecular mechanisms that facilitate complex actin cytoskeleton self-organization because it simultaneously assembles three functionally diverse F-actin networks—actin patches (endocytosis), actin cables (polarized growth), and the contractile ring (cytokinesis). Each network is assembled by a specific actin assembly factor—Arp2/3 complex (patches), formin For3 (cables), and formin Cdc12 (ring)—and contains a unique set of actin binding proteins (ABPs) that collectively define the organization and dynamics of each network. Although multiple studies have investigated how self-organization is maintained, how self-organization of these distinct networks is initially established, and how the presence or absence of each network affects this, is currently unknown. While an "initial" state may not exist in nature, since cells will divide from mother cells which contain F-actin networks already, dynamic transitions from homeostasis constantly occur during cellular processes. Additionally, in any drug treatment or genetic alterations performed during laboratory experiments, dynamic transitions are induced and it is critical to understand how these homeostatic steady states of self-organization are initially established to truly understand what possible pathways and systems are being affected by these experiments.

In this work, I begin to investigate the spatial and temporal pathways of F-actin network assembly and self-organization using a combination of novel microfluidic techniques and confocal microscopy that allows us to monitor real-time network assembly in vivo. I determined both (1) the timing and order of network formation and (2) present evidence to support a long-standing hypothesis that actin cable network formation relies on actin patch network formation, though the direct mechanism which links these is not yet clear.

4.3 Results

4.3.1 Adaptation and optimization of microfluidic drug delivery system for fission yeast

In order to mimic the initial disassembled state where there are no steady-state F-actin networks, I wished to continuously monitor fission yeast cells during treatment and washout of the actin depolymerizing drug Latrunculin A (LatA), which sequesters actin monomers from the cytoplasm. This approach allows the (1) global depolymerization of all F-actin in fission yeast cells, and then (2) washout of LatA initiates the acute, rapid reassembly of F-actin network self-organization. The reassembly and self-organization of diverse F-actin networks can thereby be directly observed using quantitative multi-color time lapse fluorescence microscopy.

Using a microfluidic system, cells are "trapped" in a chamber via a stepwise ceiling, allowing for long term imaging of the same cells while rapidly changing media and treatment conditions (Figure 4.1A). Upon an initial trial of LatA treatment of fission yeast cells, I did not observe rapid actin network disassembly when cells were in the microfluidic chamber, but could see this rapid disassembly if cells were bulk treated with LatA in a culture tube prior to imaging on a standard glass slide. As the microfluidic chambers are made of polydimethylsiloxane, which small molecules can stick to, this suggested that the drug was sticking to the microfluidic chamber. To address this, I added the surfactant, Pluronic F-127, to the cell media and pre-coated microfluidic chambers prior to cell addition. While slightly higher concentrations were still needed, the addition of Pluronic F-127 allowed the use of workable concentrations where LatA could rapidly disassemble all F-actin within the cell (Figure 4.1B). Using a cell growth assay, I confirmed that the addition of Pluronic F-127 to the media did not impair fission yeast cell growth (Figure 4.2).

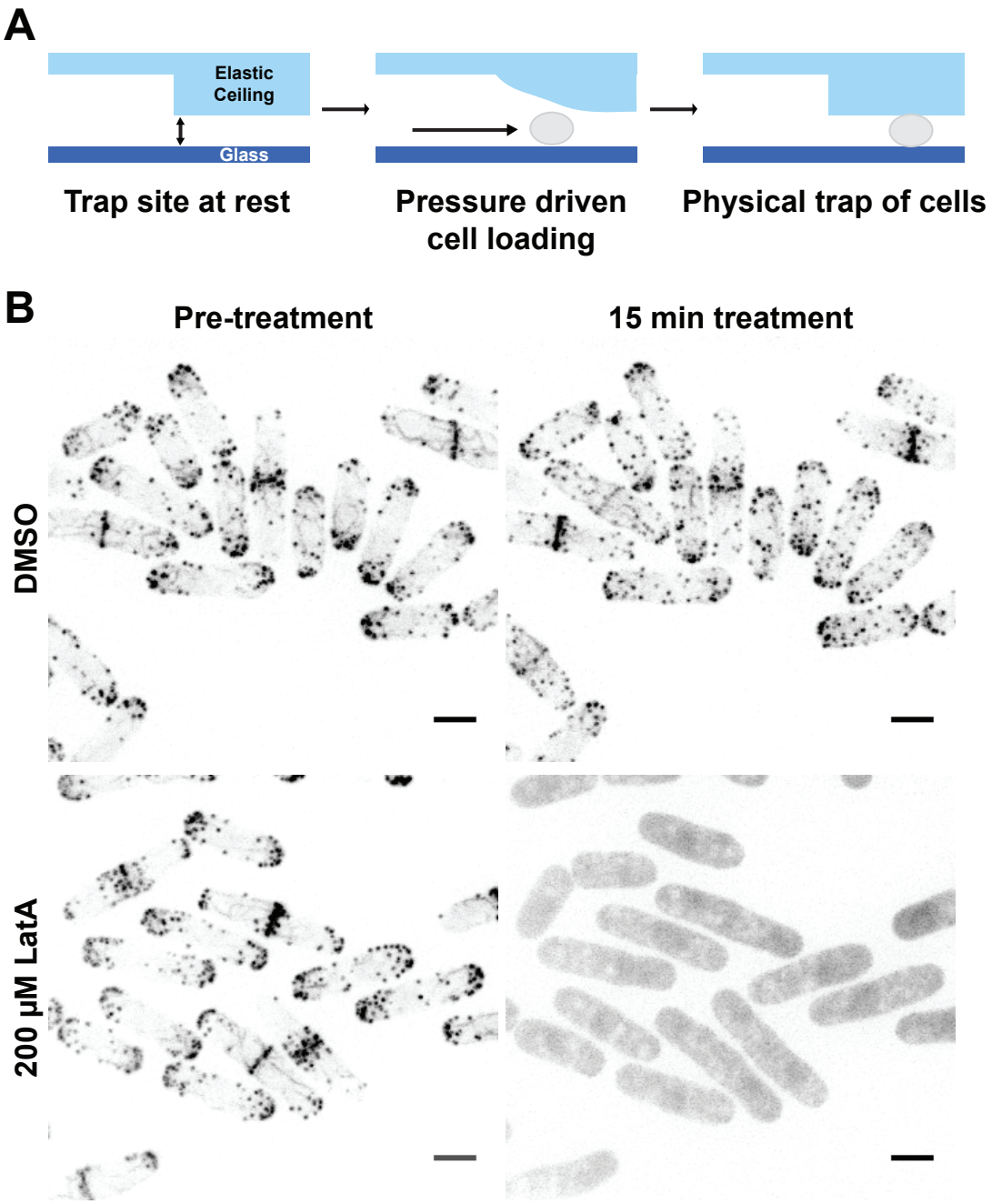

Figure 4.1: **Drug treatment of fission yeast via a microfluidic system. A.** Cartoon of CellASIC ONIX microfluidic system, in which pressure driven loading physically traps fission yeast cells between an elastic ceiling and the imaging surface. **B.** Fission yeast cells expressing Lifeact-eGFP either pre- (left) or post- (right) treatment with DMSO or 200 μM Latrunculin A.

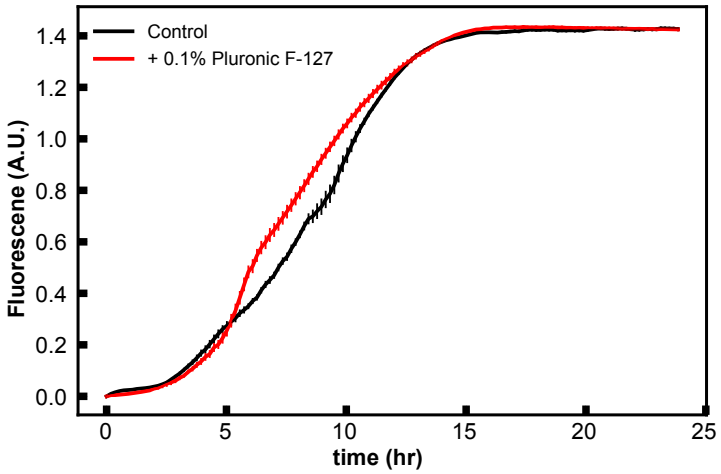

Figure 4.2: **Pluronic F-127 does not affect fission yeast growth.** Fission yeast cell growth in YE5S alone or with 0.1% Pluronic F-127. Curves are averages of three technical replicates, error bars = s.e.m.

4.3.2 Temporal pathway of fission yeast actin reassembly

To investigate the temporal pathway of F-actin network assembly, I (1) treated cells with LatA to fully disassemble all steady-state F-actin networks and then (2) rapidly washed out the LatA to monitor initial F-actin network assembly. This strategy allows us the ability to watch F-actin network disassembly and assembly initiation in real time in vivo, which was not previously possible in fission yeast. Upon LatA treatment, I observed that actin cables and contractile rings are rapidly disassembled within the first few minutes of treatment and actin patches are the last network to be fully disassembled. As actin patches are the most dynamic network with high turnover, I expected that these would be the first network that is disassembled, as monomers would become rapidly available for LatA binding and then be removed from the available monomer pool. To confirm this, I varied the concentration of LatA. Even at low LatA concentrations (50 μM), I observed rapid disassembly of contractile rings and cables, but actin patches remained persistent (Figure 4.3). While this result was unexpected, this suggests that mechanisms other than actin turnover can influence the action of LatA on disassembly. This suggests that one or more actin binding proteins at

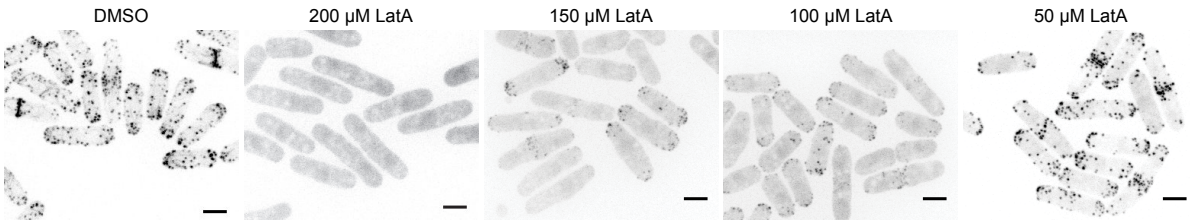

Figure 4.3: **Endocytic actin patches are the last F-actin network to be disassembled.** Fluorescent micrographs fission yeast cells expressing Lifeact-eGFP after 15 min treatment with DMSO (left) or varying concentrations of Latrunculin A. Scale bar = 5 μm.

actin patches might compete with LatA for an actin monomer binding site and thus, it could be critical to understand which proteins overlap with this actin binding site to better understand how LatA can function on F-actin network disassembly.

Next, I determined the temporal order of F-actin network assembly from the mimicked "initial" state. To do this, LatA was washed out and fission yeast cell F-actin networks were observed over time. When LatA was washed out, actin patches rapidly reassembled within the first two minutes of wash out (Figure 4.4). Interestingly, I observed that while actin patch assembly is initially polarized to the cell poles (the normal cellular localization for these networks) they then depolarize throughout the cell (Figure 4.4B). Patches remain depolarized until rings and cables are re-assembled, at which time they are re-polarized to cell tips (Figure 4.4B). This result provides further evidence for the role of actin cables in the polarization of cellular F-actin networks, and suggests that the spatial self-organization of F-actin patches to the cell poles is at least partially initialized and maintained through the presence of F-actin cable networks.

Interestingly, when examining F-actin network reassembly, I found that cells that had contractile ring networks prior to treatment were not able to immediately begin re-assembling these networks. Instead, I observed a time delay of contractile ring assembly ranging from 25-45 minutes, timing that is consistent with cells that are just beginning cell division, rather than continuing progress from where they were pre-treatment.

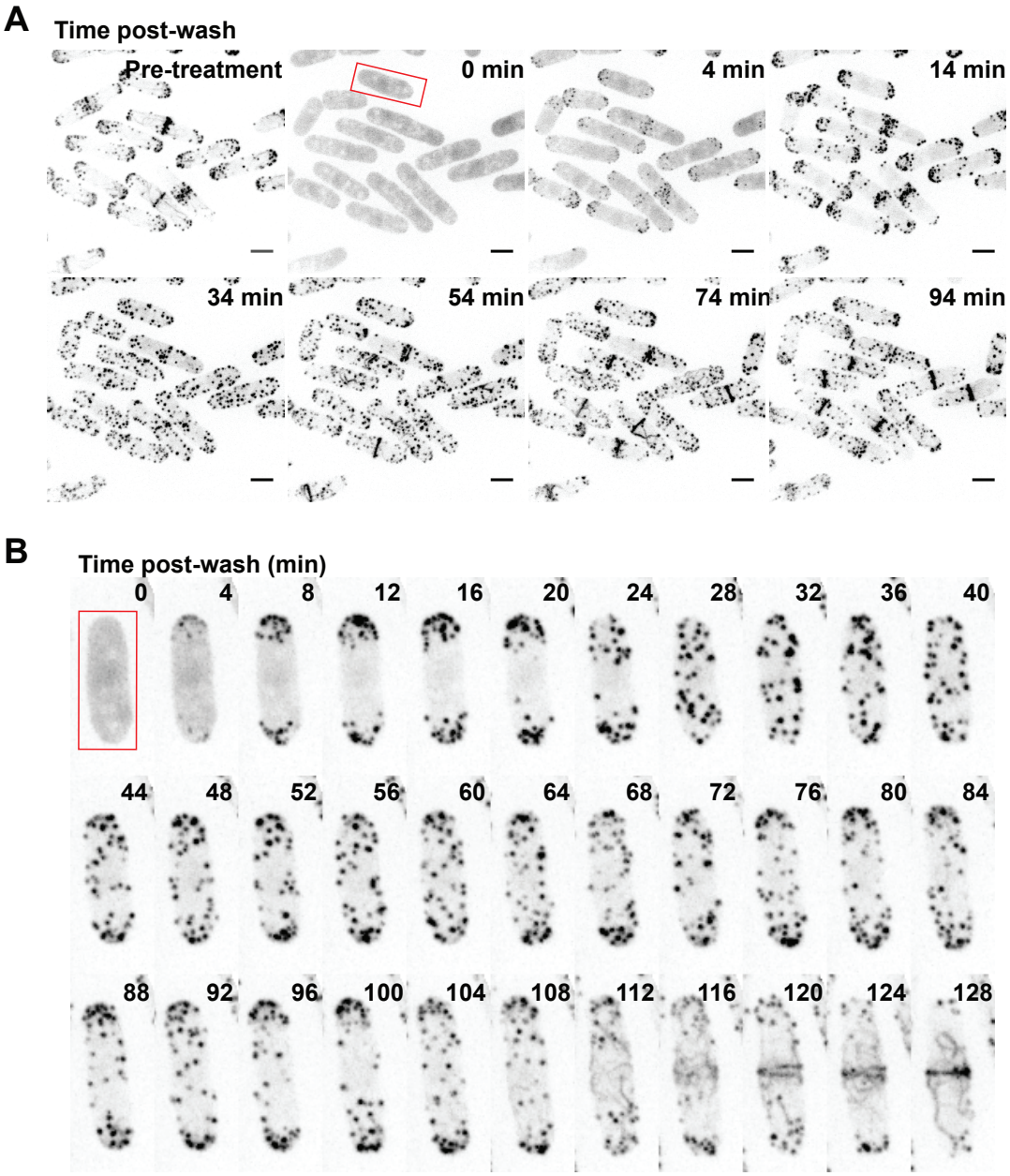

Figure 4.4: **Endocytic actin patches rapidly assemble and depolarize after Latrunculin A treatment wash out. A.** Time-lapse fluorescent micrographs of fission yeast cells expressing Lifeact-eGFP treated with 200 μM Latrunculin A for 15 min (post-wash time 0 min) and then removal of drug treatment (top left, second panel). Red box denotes the cell selected for (B). Scale bar = 5 μm. **B.** Single cell time-lapse fluorescent micrograph from representative experiment in (A).

4.3.3 Inhibition of actin patch assembly does not accelerate assembly of other F-actin networks

As previous work has shown that by inhibiting assembly of one F-actin network, it drives increased F-actin assembly by other nucleation factors, I sought to determine if this held true for the initial assembly of F-actin networks. As actin patches are the first F-actin network to rapidly form after Latrunculin A (LatA) washout, I predicted that by inhibiting actin patch assembly, I might see an acceleration of F-actin assembly in actin cables, rings, or ectopic F-actin, similar to what has been seen in homeostatic fission yeast cells [17, 141, 142].

To inhibit actin patch assembly, I used the Arp2/3 complex inhibitor, CK-666. Briefly, cells were treated with LatA to completely disassemble all F-actin. Then, cells were co-treated with LatA and CK-666 (or DMSO) before LatA was washed out and cells were monitored in the presence of CK-666 or DMSO (Figure 4.5B). In control cells treated with DMSO, F-actin networks assembled in similar timing to previous experiments in media alone. Unexpectedly, when LatA was washed out in the presence of CK-666, I saw no F-actin assembly within cells until CK-666 was washed out, upon which re-assembly began with actin patches followed by other F-actin networks (Figure 4.5B). This suggests that the initial assembly of other F-actin networks is contingent on the presence of actin patches or its endocytic function.

Why other F-actin networks are not initially assembled when F-actin patches are inhibited could be due to a few different possibilities. It has been hypothesized that because the actin cable nucleator, formin For3, is a poor nucleator, that actin patches may contribute to actin cable formation. However, no direct evidence for this theory has yet been provided. Many issues arise when trying to address this theory further in fission yeast though. First, I would need to inhibit endocytosis or Arp2/3 complex in a way other than drug treatment in order to show this is not an off-target effect of CK-666 in initial assembly.

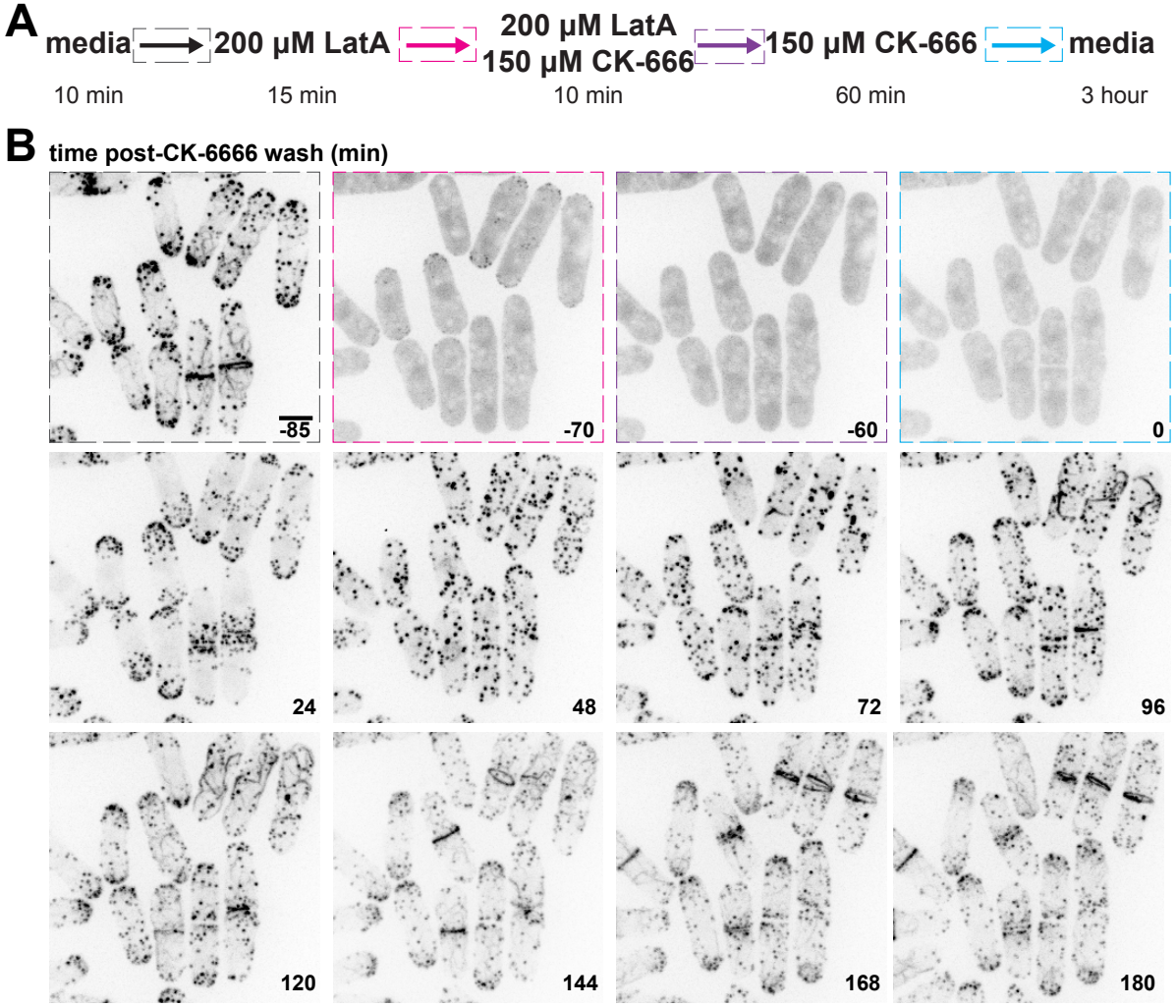

Figure 4.5: **F-actin networks do not re-assemble in the absence of endocytic actin patches. A.** Diagram of microfluidic treatment time course. **B.** Time-lapse fluorescent micrographs of fission yeast cells expressing Lifeact-eGFP. Time denotes the time relative to the wash-out of CK-666 (A, blue arrow). Each colored dashed box corresponds to the frame directly before the microfluidic treatment change denoted by the colored arrows in (A). Scale bar = 5 μm.

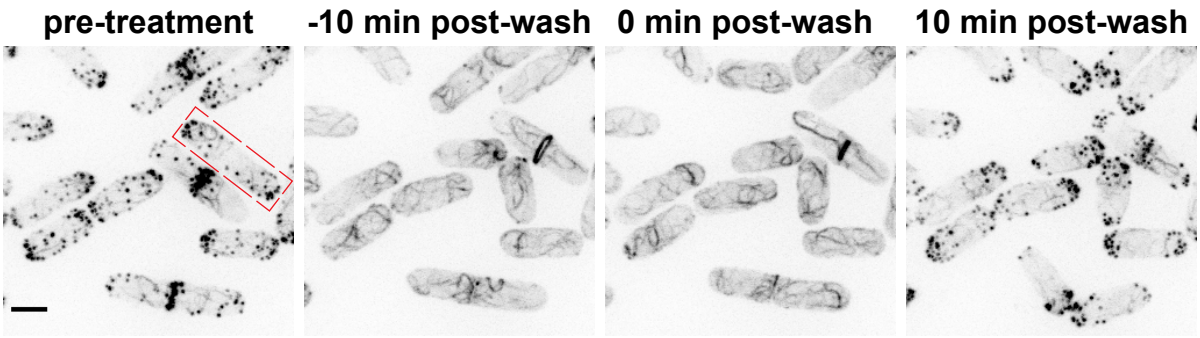

Figure 4.6: **Actin cables and contractile rings function normally in the presence of CK-666.** Time-lapse fluorescent micrographs of fission yeast cells expressing Lifeact-eGFP before, during, and after treatment with 200 μM CK-666.Red box denotes cell that undergoes normal contractile ring formation and contraction while under CK-666 treatment. Scale bar = 5 μm.

While previous work has shown CK-666 specifically inhibits Arp2/3 complex, these studies were done in homeostatic conditions, thus, re-confirmation of the drug not having off-target effects is required. However, in fission yeast, as Arp2/3 complex is essential, a cold-sensitive, temperature-sensitive mutant exists (*arp3-c1*) and only partially inhibits Arp2/3 complex and endocytic activity [85]. While a thiamine-repressible Arp2/3 complex has been used previously, this strain also will not fully suppress Arp2/3 complex activity or actin patch formation [17]. In trials where CK-666 was used at lower concentrations, such that some actin patches were present, I observed other F-actin network re-assembly as well. Thus, neither the cold-sensitive or thiamine repressible Arp2/3 complex strains will provide a possible mechanism for addressing this question.

Further, no endocytic mutants exist to fully inhibit endocytosis and, unlike most cell types, fission yeast do not use dynamin for internalization of endocytic vesicles. Due to this, drugs such as Dynasore, which are typically used to inhibit endocytosis in other cell types, are ineffective. Thus, there exists no mechanism for full, temporally controlled inhibition of endocytosis. Thus, I do not have a currently available method for dissecting this hypothesis.

The second possibility for why all F-actin network assembly is initially inhibited if actin patch formation is prevented is through profilin-actin monomer ratios, which are critical for

proper F-actin network assembly and maintenance under steady state conditions [17, 141, 142]. By inhibiting actin patches, the ratio of actin monomer to the actin monomer binding protein profilin, Cdc3, is disrupted, causing disruptions to formin activity, thus inhibiting the initial assembly of both actin cables and the contractile ring.

4.3.4 The inhibition of initial F-actin network re-assembly does not seem to be fully influenced by the profilin to actin monomer ratio.

In order to determine if the ratio of actin monomer and profilin Cdc3 influences why other F-actin networks do not initially reassemble in the absence of endocytic actin patches, I overexpressed Cdc3 under the Pnmt81X promoter, a weak overexpression promoter, in addition to endogenous Cdc3 expression. Interestingly, when cells were treated to the same Latrunculin A and CK-666 microfluidic treatment, I saw only minimal F-actin assembly before CK-666 washout. In the presence of CK-666 and absence of endocytic actin patches, Cdc3 overexpression cells ectopically assembled small amounts of F-actin in the center of the cell, seeming to be localized near the nucleus (Figure 4.7B). Further, upon CK-666 washout, this F-actin was rapidly disassembled and actin patches reappeared, leading cells to follow the same previous order of initial F-actin assembly observed in wild-type cells (Figure 4.7B).

As the Pnmt81X promoter is a weak expression promoter, I next examined Cdc3 overexpression where Cdc3 was overexpressed from a strong promoter (Pnmt3X) in addition to endogenous Cdc3 levels. By doing this, I hoped to confirm if the ectopic F-actin observed could be increased by further increasing the profilin to actin monomer ratio. When cells strongly overexpressed Cdc3, I saw now F-actin assembly during CK-666 treatment, similar to wild type cells (Figure 4.7B). Upon washout, I observed actin patches rapidly reassembling, but there were fewer and had a higher actin density, a phenomenon consistent with Cdc3 overexpression (Figure 4.7B).

It was unexpected that, while a weak Cdc3 overexpression (Figure 4.8B) resulted in ec-

topic F-actin assembly, I saw no F-actin assembly under strong Cdc3 overexpression (Figure 4.7B). I speculated this could be due to increasing the profilin to actin monomer ratio too far. While having too little profilin to actin monomer can result in decreased formin activity, I see a similar phenomenon when profilin is in excess. This occurs as profilin alone can bind to the FH1 domains of formin, preventing profilin-actin monomers from binding.

To address this possibility, I performed the same experiment at different time points after overexpression is induced. Typically, for overexpression studies, I perform experiments at 18-22hr to ensure that cells have had ample time for full overexpression. In this case, I hoped to observe if I saw a "switch" from ectopic F-actin assembly (similar to using the weak promoter for 20hr) to an overexpression point at which no F-actin assembly occurs (similar to the strong promoter at 20hr). This would indicate that the profilin to actin monomer ratio is crucial for the reassembly of initial formin-mediated actin assembly when actin patches are absent.

I took strong promoter Cdc3 overexpression cells at four time points (4, 8, 12, 16h) and treated them with Latrunculin A followed by CK-666. Unexpectedly, I did not observe any ectopic or formin-mediated F-actin network assembly at any of these induced time points (Figure 4.7C). As I consistently saw ectopic F-actin assembly when Cdc3 was overexpressed from a weak promoter, this result was puzzling. Initially, this suggests that there is some inherent difference between these two strains, though they are cloned from the same background strain. Potentially, this suggests that while the profilin to actin monomer ratio may play a small role in F-actin network initiation, there are other mechanisms controlling why cables and contractile rings will not assemble in the absence of actin patches.

4.4 Discussion

The question of how F-actin networks are initially established and self-organized remains an open and interesting question. While current techniques were not able to fully elucidate the

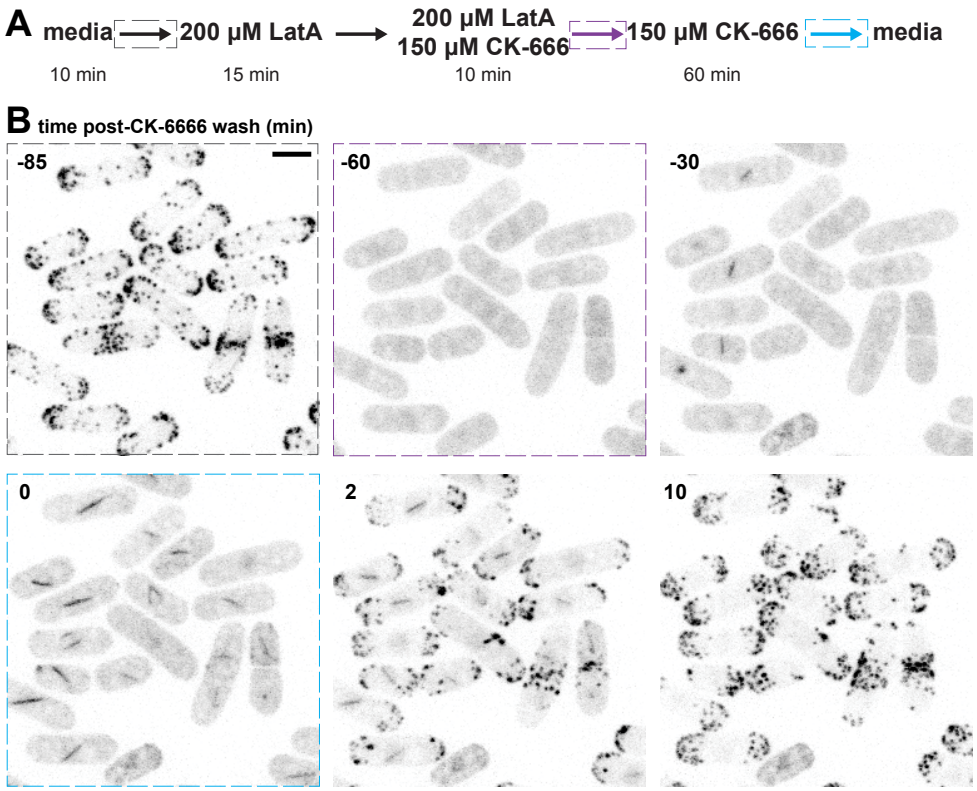

Figure 4.7: **Profilin overexpression only partially restores F-actin assembly in the presence of CK-666. A.** Diagram of microfluidic treatment time course. **B.** Time-lapse fluorescent micrographs of fission yeast cells overexpressing profilin (Pnmt81X) and expressing Lifeact-mCherry. Time denotes the time relative to the wash-out of CK-666 (A, blue arrow). Each colored dashed box corresponds to the frame directly before the microfluidic treatment change denoted by the colored arrows in (A). Scale bar = 5 μm.

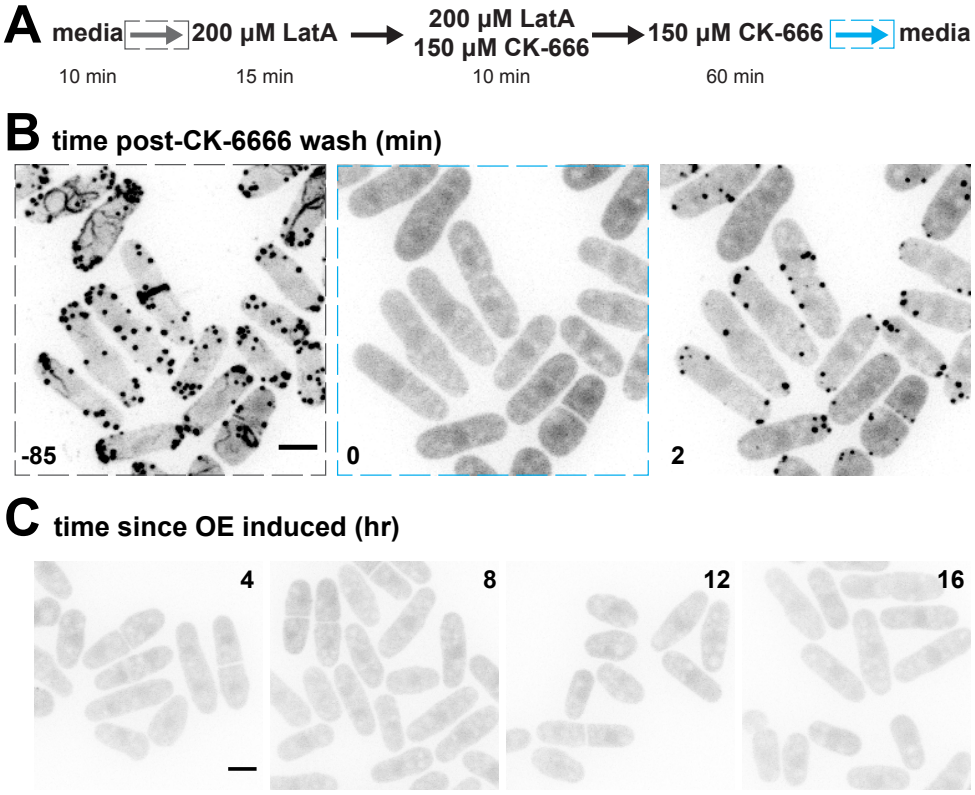

Figure 4.8: **Higher profilin overexpression inhibits initials F-actin assembly in the presence of CK-666. A.** Diagram of microfluidic treatment time course. **B.** Time-lapse fluorescent micrographs of fission yeast cells overexpressing profilin (Pnmt3X, strong promoter) and expressing Lifeact-eGFP. Time denotes the time relative to the wash-out of CK-666 (A, blue arrow). Each colored dashed box corresponds to the frame directly before the microfluidic treatment change denoted by the colored arrows in (A). **C.** Fluorescent micrographs of fission yeast cells overexpressing Cdc3 (Pnmt3X promoter) at different time intervals since overexpression induction. Cells underwent individual microfluidic treatments at different times post-induction, but were collected from the same fission yeast culture. Each micrograph shows the time point directly before CK-666 wash out (blue arrow in A). Scale bar = 5 μm.

mechanisms behind these processes, I have gained some insights that will allow future work as new mutants and techniques are developed to address this question in the future.

4.4.1 Endocytic actin patches are rapidly assembled during initial F-actin network assembly

In this work I found that upon full disassembly of F-actin networks, to mimic the initial state, formin-mediated actin networks (cables, contractile rings) are more rapidly disassembled than Arp2/3 complex-mediated actin networks (endocytic actin patches). Further, upon initiation of assembly by Latrunculin A washout, actin patches are rapidly reformed while formin-mediated F-actin networks required upwards of 30 minutes to assemble. Unexpectedly, when actin patches assembled in the absence of these formin-mediated networks, I saw actin patches assemble at the polarized cell tips, but then de-polarize until the formation of these formin-mediated networks. This further confirms that actin cables are required for actin patch polarization, a known function for this network.

However, another non-mutually exclusive possibility is that it is not the presence of the F-actin cables and actin monomer competition which helps to limit actin patches to the cell poles, but could be an indirect effect of mis-targeting of biosynthetic cargoes from the lack of actin cables [89, 156]. It is well known that in fission yeast that cargo transport by myo4 is required for secretory vesicle localization and, as endocytosis is often recycling the cellular components needed for vesicle secretion, endocytic patches may be forming elsewhere in the cell solely because secretory vesicles are now mis-localized. It will be interesting for future work to look at the localization of myo4 and secretory vesicle components under this initial wash-out state where patches are depolarized to address this question. Further, to separate the role of secretory vesicle cargo from the presence of actin cables on patch polarization in this initial reassembly state, future work to build recombinant cargo proteins that are targeted to specific cell areas, such as the poles, and seeing if this loss of polarization still

occurs will be critical for clear distinction of these processes.

4.4.2 Formin-mediated F-actin networks do not assemble in the absence of F-actin patches

Interestingly, if actin patch assembly was inhibited, formin-mediated F-actin networks were unable to assemble at all. As previous work has speculated that cables may arise from actin patches since For3 is a poor nucleator [126], this poses an interesting possible hypothesis. I then hypothesized from these early results that either (1) actin patches or (2) the profilin to actin monomer ratio may be required for the initial formation of these actin networks.

I both weakly and strongly overexpressed profilin Cdc3 to test if the profilin to actin monomer ratio was causing the inability of formin-mediated F-actin networks to not assemble in the absence of actin patches. However, while in the weak overexpression case I observed mild ectopic F-actin assembly, even in short induction times for the strong overexpression, I were unable to repeat this observation. The reason for this puzzling result is still unclear. While it may indicate that the profilin to actin monomer ratio plays a minor role in the initial assembly of formin-mediated F-actin networks, it does not appear to be the driving force.

While these results suggest that actin patches may be required for the initial formation of formin-mediated F-actin networks. If actin patches are required for this, there are a few possible mechanisms as to why: (1) Arp2/3-mediated F-actin assembly is required; (2) endocytic function is required; (3) both processes are required; or (4) formin activators mis-localize from their normal locations in the cell. However, the ability to address these possible mechanisms on how this could be occurring is extremely limited by current biological techniques. First, no mutants exist for either Arp2/3 complex or endocytic proteins that can completely eliminate their individual functions. While CK-666 was used here, I cannot confirm that, in an initial state with no F-actin networks, the drug does not have

off-target effects. Without another mechanism that can inhibit either Arp2/3 complex or endocytosis separately, I cannot distinguish between these two possible mechanisms. Additionally, the exact upstream components for cable formation, cytokinesis, and contractile ring formation are still unknown in fision yeast. Identification of these upstream activators and their pathways will be critical to understanding their role in actin cytoskeleton initiation and self-organization.

A currently evolving technique in fission yeast is the auxin inducible degron (AID) system, which acutely degrades a protein of interest by the addition of auxin to the media. While this system has been widely used in budding yeast [128], no system for AID has been developed yet for fission yeast, except for nuclear proteins [66]. Future work to engineer an AID system for Arp2/3 complex or endocytic proteins would allow continuation of this study as well as addressing many other questions about Arp2/3 complex and actin patch function within cells without the use of CK-666. As not much work has been done with this system in fission yeast, it will be critical to understand the timing to full degradation and recovery of protein concentration post-wash out. Additionally, drug or substrate induced degradation and inhibition systems are not always fully penetrative. Thus, in some instances, it may be necessary to combine AID systems with temperature sensitive mutants for full effect.

4.5 Materials and Methods

4.5.1 Strain construction and growth conditions

Fission yeast strains were created by genetic crossing on SPA5S plates followed by tetrad dissection on YE5S plates. Strains were screened for auxotrophic (leu, ura) or antibiotic (nat, kan) markers and maintained on YE5S plates. Glycerol stocks were created by pelleting cells and resuspending in 750 μL media and 250 μL of 50% sterile glycerol. Table 4.1 lists the fission yeast strains used in this study.

Prior to assays, fission yeast cells were maintained on standard YE5S plates and grown for 36 hours in a 25° C water bath shaker prior to any experimental procedures. For live cell imaging of genes of interest under inducible promoters, cells were grown in YE5S media overnight at 25° C, subcultured into EMM5S media without thiamine, and kept in log phase for 20-22 hours at 25° C.

4.5.2 Cell growth assay

Strains were grown for 24-36 hr in YE5S and then seeded in triplicate in a 96-well plate at initial OD_{600} readings of 0.03 and 0.06 and the presence or absence of Pluronic F-127. OD_{600} readings were measured every 10 min for 24 hr at 26° C in a Tecan Inifinite M200Pro (Tecan Systems, Inc., San Jose, CA) plate reader with an orbital shaking amplitude of 4 mm. Technical replicates were averaged for final reporting.

4.5.3 Cell imaging and microfluidic drug treatment

Confocal images were acquired on an IX83-X1 (Olympus, Tokyo, Japan) equipped with a Yokogawa CSU-X1 Spinning Disk Confocal Unit fitted with an ImagEM X2 EM-CCD camera (Hamamatsu, Hamamatsu, Japan) controlled by CellSens software (Olympus, Tokyo, Japan). Images were acquired using Z-stacks of 11 slices with a 0.5 μm step-size every 2 minutes.

Microfluidic assays were performed in an ONIX microfluidic perfusion chamber (CellASIC Corporation, Hayward, CA). Since the microfluidic plate (Y04C) is polydimethylsiloxane (PDMS), small molecules will often stick to the surface. To avoid this, YE5S or EMM5S media with the surfactant 1% Pluronic F-127 was flowed into the chamber at 3 psi for 1 hour to pre-coat the surface. Cells (OD_{600} of 0.5.-0.7) were then loaded into the chamber at 8psi for 3 seconds. Chambers were manually checked for effective cell density and trapping and this loading process was repeated if necessary to capture more cells. Cycles of drug treatments

and media exchanges are outlined in the relevant figures. Briefly, for each treatment change, media with 0.1% Pluronic F-127 alone or with appropriate control or drugs was flowed in at 6 psi for 10 min. The pressure was then lowered to 3 psi for the rest of the treatment or wash time. Cells were imaged consistently throughout all washes and treatment steps

For CK-666 treatments, CK-666 powder stock (Sigma, St. Louis, MO) was diluted to 10 mM in DMSO, aliquoted, and stored at 4° C until use. For Latrunculin A (LatA) treatments, LatA powder stocks (Sigma, St. Louis, MO) were resuspended to 5 mM in DMSO, aliquoted, and stored at -20° C until use.

Strain name	**Genotype**	**Reference**
KV648	h?, Pnmt81-SpPRF::Ura4+, Lifeact-mCherry::Leu1+	[141]
KV696	h+, pAct1 Lifeact-GFP::Leu+; Sad1-mCherry::Nat	[17]
KV781	h-, natMX4-3xPnmt1-cdc3, leu1-32::Pact1-Lifeact-GFP-leu1+	[141]

Table 4.1: **Fission yeast strains used in Chapter 4.**

CHAPTER 5

MECHANISMS OF FISSION YEAST ACTIN DISASSEMBLY PROTEINS

Preface

The work in the following chapter was performed by me. While this work will not form a completed manuscript, it is fundamental work towards our ability to purify and mechanistically understand actin disassembly processes in fission yeast. My hope is this work will lay the foundation for a future thesis project on how actin disassembly mechanisms influence F-actin network self-organization.

5.1 Introduction

F-actin networks are complex, dynamic cellular structures that must undergo dynamic rearrangements for a multitude of functions. In addition to actin assembly, F-actin networks must also be disassembled in rapid, highly regulated manners. Cells control the disassembly and turnover of F-actin networks through a variety of disassembly and depolymerization proteins and their cofactors, such as cofilin (with cofactors coronin and actin interacting protein 1 (AIP1)) and twinfilin (with cofactor cyclase associated protein 1 (CAP1)). While these proteins have been studied in other systems, the exact mechanisms and dynamics of how these proteins function and are regulated in fission yeast is not fully understood. Additionally, much of how F-actin disassembly contributes to actin self-organization is unknown, despite this process being a fundamental component of every F-actin network.

Fission yeast contain one isoform of each major disassembly protein and cofactors. Previous work has demonstrated that cofilin severing mechanisms in fission yeast are similar to budding yeast and that cofilin plays an important role in the sorting of the actin binding

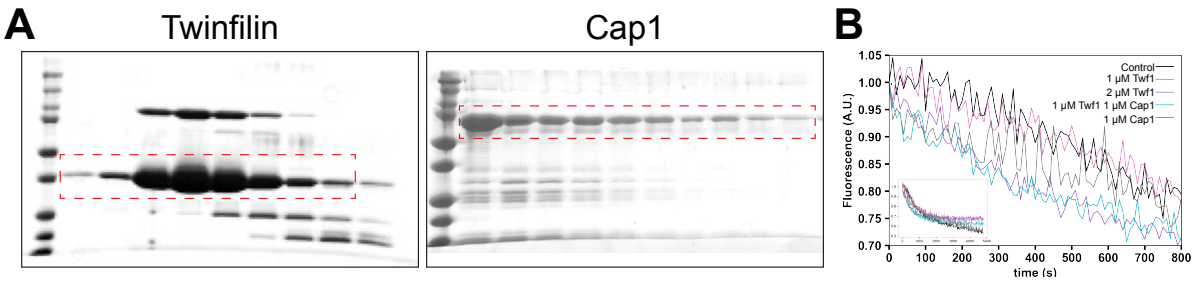

Figure 5.1: **Twinfilin and Cap1 work together to increase bulk F-actin disassembly. A.** SDS-PAGE protein gel of purified Twinfilin and Cap1. Red dotted box denotes the band containing the protein. **B.** Bulk pyrene actin disassembly assay in the presence or absence of Twinfilin and/or Cap1. Actin filament seeds (5 μM, 30% labeled) were diluted to 0.1 μM actin at time zero to induce disassembly. In-set graph is the full bulk assay run.

proteins fimbrin and tropomyosin to their appropriate networks [28]. In this work, I aimed to (1) engineer, purify, and characterize the fission yeast actin disassembly proteins Coronin, AIP1, twinfilin, and CAP1 in order to understand their roles in the F-actin disassembly and to (2) elucidate the role disassembly proteins play in actin network self-organization.

5.2 Results

5.2.1 Twinfilin and CAP1 increase bulk F-actin disassembly.

Twinfilin (Twf1) and cyclase associated protein 1 (CAP1) have been shown in budding yeast and mice to work together to accelerate actin depolymerization at both the barbed and pointed ends, though the dynamics of these processes are species and isoform specific [57]. Despite this knowledge, the mechanisms of these two proteins in fission yeast has not been studied.

In order to understand how disassembly proteins can influence F-actin network self-organization, I must first understand their distinct mechanisms. Thus, I began by engineering and purifying constructs of both Twf1 and its cofactor CAP1 (Figure 5.1A). After successful purification, I asked whether these proteins accelerated bulk F-actin disassembly

both alone and in concert. I pre-assembled and diluted F-actin seeds to concentrations at which actin will depolymerize in the presence or absence of Twf1 and CAP1. In the presence of low concentrations of Twf1 or CAP1, I saw no change in F-actin disassembly from control conditions (Figure 5.1B). However at higher concentrations of Twf1, I observed an increased rate of F-actin disassembly (Figure 5.1B). Interestingly, when Twf1 and CAP1 were combined in concentrations at which neither induces increased F-actin disassembly on its own, I observed disassembly rates equivalent to higher concentrations of Twf1 alone (Figure 5.1B), consistent with work seen in budding yeast.

5.2.2 Twifilin accelerates F-actin depolymerization at the barbed and pointed ends.

I next wanted to determine the mechanism of Twf1- and CAP1-induced F-actin disassembly. Previous work has shown that Twf1 induces increased depolymerization at either the barbed end, pointed end, or both, dependent on the species and isoform [57]. To do this, I adapted a previous experiment for visualization of F-actin disassembly of individuals actin filaments (Figure 5.2). Briefly, I preformed actin filaments in a flow chamber and sparsely tethered them to the surface via a low concentration of biotin-actin. Upon polymerization, monomers are flowed out—inducing depolymerizing conditions—and buffer or the proteins of interest are flowed in (Figure 5.2). I are then able to observed F-actin disassembly at each end at a single filament level, with barbed ends identified by faster assembly kinetics prioir to actin monomer washout (Figure 5.3A).

When Twf1 was present, I consistently observed more F-actin disassembly events from both the pointed and barbed end (Figure 5.3A). In the presence of Twf1, actin filament depolymerization rates at the barbed end increased 1.5-fold over control condtions (Figure 5.3B), consistent with budding yeast and mouse Twf1 observations. While it is clear from kymographs that Twf1 also increases pointed end depolymerization, I observed many events

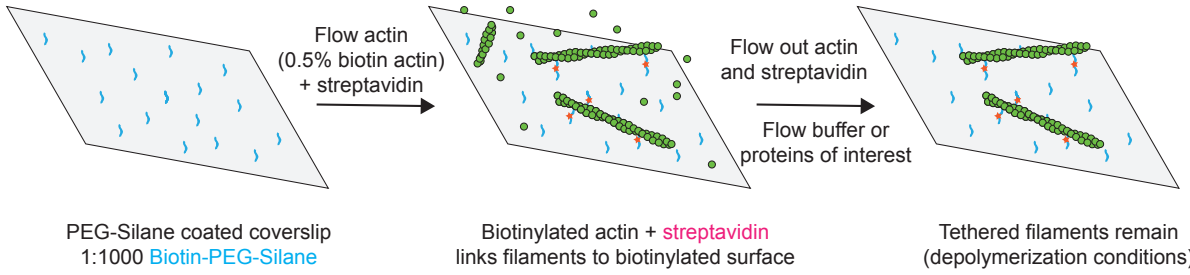

Figure 5.2: **Cartoon of depolymerization assay workflow.** Coverslip is cleaned and pre-coated with 1:1000 PEG-Silane:Biotin-PEG-Silane. Following washing and blocking steps, actin (0.5% biotin actin) and streptavidin are flowed in. After time for filament assembly, actin and streptavidin are washed out—creating depolymerization conditions—and proteins of interest are flowed into chamber.

which were either (a) actin severing/breakage or (b) depolymerization at rates faster than our imaging conditions (Figure 5.3A). Future work will investigate how Twf1 and CAP1 work in concert at the single filament level for F-actin depolymerization as current attempts for fluorescently tagged versions of these constructs were unsuccessful in TIRF microscopy (data not shown). Additionally, as cofilin is the prominent disassembly protein within fission yeast (as it is the only essential F-actin disassembly gene during gene mutation studies) it will be interesting to understand how these separate mechanisms may act in concert and provide a regulated F-actin disassembly network to control and regulate actin patch size and density.

5.2.3 Coronin requires insect cell purification for high expression levels and minimal degradation.

As cofilin is the essential F-actin disassembly protein in fission yeast, I wished to understand how its cofactors coronin (Crn1) and actin interacting protein 1 (AIP1) influence (1) cofilin's F-actin disassembly properties and (2) cofilin's role in actin binding protein sorting. I first focused on Crn1 as previous work in budding yeast has demonstrated that Crn1 alone enhances cofilin-mediated F-actin severing [88].

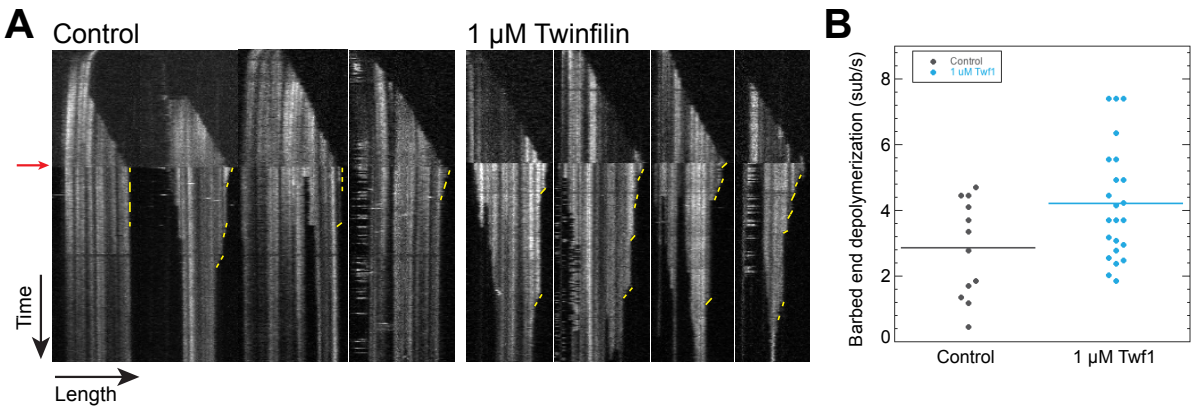

Figure 5.3: **Twinfilin increases depolymerization of F-actin at the barbed end. A.** Representative kymographs of actin filament growth and depolymerization. Reactions contained 1.5 μM actin (10% labeled). Red arrow denotes flow out of actin monomers and addition of either buffer (control) or twinfilin (1 μM). Yellow dashed lines highlight barbed end depolymerization events. **B.** Barbed end depolymerization rates of F-actin under depolymerization conditions in the presence of 0 or 1 μM Twinfilin.

I first engineered a His-tagged Crn1 construct similar to that used in previous work [97], but saw low amounts of Crn1 collected during elution (Figure 5.4A). I saw a similar issue with a Crn1-ΔCC construct, as previous studies have used this construct in mechanistic studies due to its increased ability to enhance cofilin binding (Figure 5.4B) [18, 19, 42]. To determine if Crn1 was binding to the beads with low affinity initially, I next incubated the cell lysate on TALON resin beads overnight to attempt to increase yield. However, for both Crn1 and Crn1-ΔCC an overnight incubation did not improve protein yield efficiency (Figure 5.4C-D). From this, however, I did see that Crn1 and Crn1-ΔCC appeared to be binding to the beads (Figure 5.4C-D, beads), suggesting that the issue was occurring during the elution step rather than column binding.

Knowing that Crn1 was binding but not eluting from the column, I next attempted a two-step elution process: 1) a "wash" elution of our previous elution buffer, which contains 250 mM imidazole, followed by 2) protein elution with a higher imidazole concentration (600 mM). By doing this in a two-part process, I hoped to be able to get the Crn1 to elute from the resin, while potentially getting a cleaner product as non-specific proteins and

degradation products should elute at the lower imidazole concentration. Yet, even at high imidazole concentrations, Crn1 remained bound to the beads (Figure 5.4E-F). This suggests the protein was binding non-specifically to the affinity column, meaning it was interacting with the resin itself and not the metal ion. While some protein would elute from the column, it seemed to not be correlated with imidazole concentration, was low concentration, and was accompanied by many contaminants and potential degradation products.

I next attempted ammonium sulfate precipitation prior to affinity chromatography to determine whether this could increase purity of Crn1, thus reducing the amount of contaminant present in what is able to be retrieved after affinity chromatography. However, most contaminants remained in the same ammonium sulfate cut as Crn1, demonstrating that this method would not improve our yield any further (Figure 5.4G). Last, I engineered a N-terminal GST-tagged Crn1 variant, similar to those done in previous studies [88, 59]. However, I saw low expression and no major improvement in purification methods (data not shown). Similar issues have been observed with *C. elegans* coronin (POD-1) (Rachel Kadzik, personal communication).

From multiple construct design and methodology attempts, I concluded that fission yeast Crn1 is a low expressing and low stability construct when expressed in bacterial protein expression systems. Therefore, future work and studies will focus on engineering and purification of Crn1 from insect cell expression systems.

5.3 Discussion

While there is still much work to be done for understanding the mechanisms of disassembly proteins in fission yeast, there are many interesting open questions to be addressed further once these mechanistic investigations are complete. While these will be discussed in greater detail in Chapter 6, I will briefly touch on them here.

As a key component of F-actin networks is their dynamic nature, F-actin disassembly is

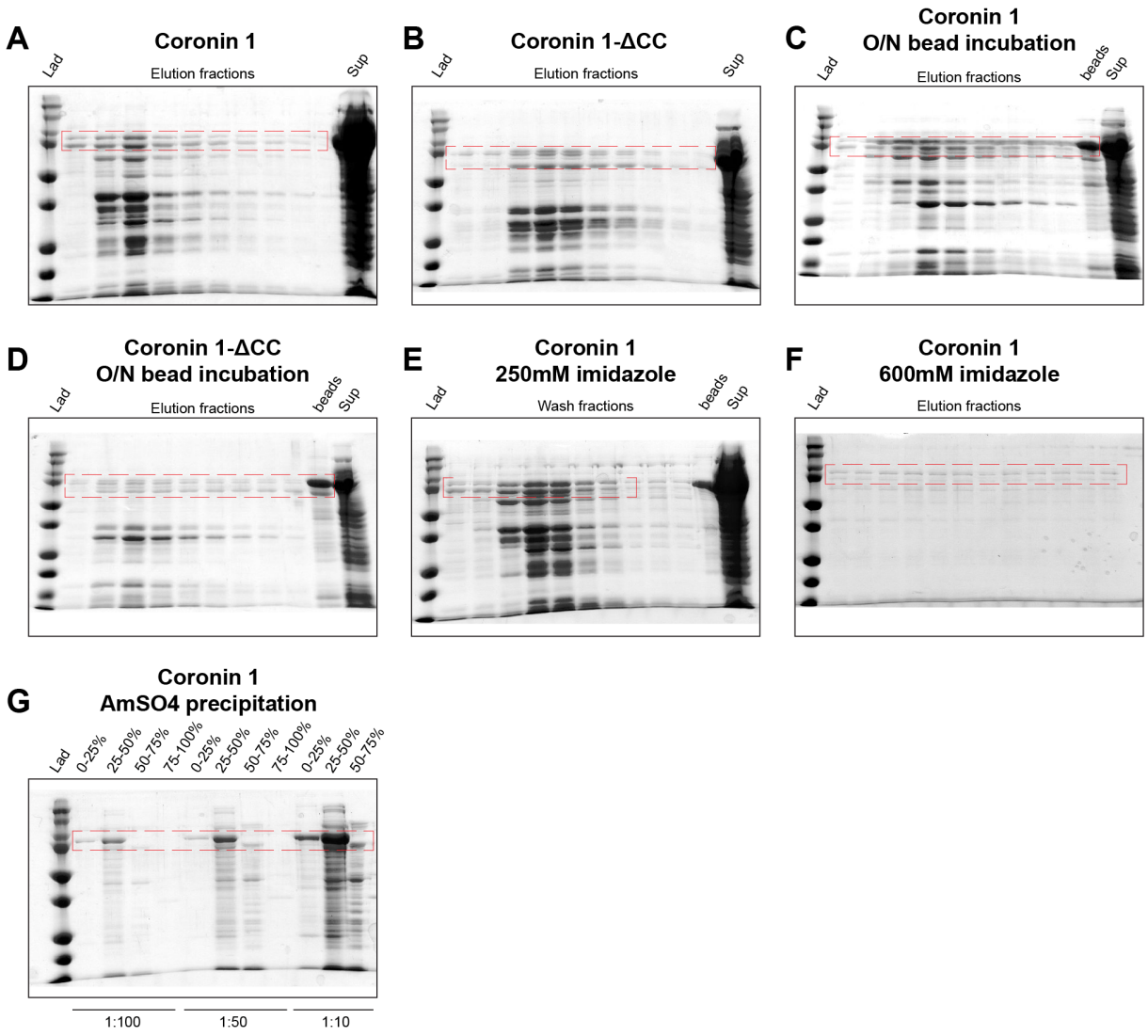

Figure 5.4: **Coronin 1 (Crn1) expression and purification is not robust with His-tag or ammonium sulfate methods.** Red dashed boxes denote Coronin 1 (Crn1) doublet. **A.** Purification of Crn1 via TALON affinity chromatography with 250 mM imidazole. **B.** Crn1-ΔCC purification via TALON affinity chromatography with 250 mM imidazole. **C.** Crn1 purification via TALON affinity chromatography after an overnight incubation of cell lysate with TALON beads. **D.** Crn1-ΔCC purification via TALON affinity chromatography after an overnight incubation of cell lysate with TALON beads. **E-F.** Crn1 purification via TALON affinity chromatography - washing with 250 mM imidazole (E) and then eluting with 600 mM imidazole (F). **G.** Ammonimum sulfate precipitation of Crn1 cell lysate, showing different dilutions of resulting precipitants.

as critical to each network's function as assembly. While knowing each disassembly protein's individual mechanisms is a key component to our broader understanding, knowing how these disassembly proteins interact, cooperate, and compete with other actin binding proteins (ABPs) is key to fully understanding each F-actin network and actin self-organization as a whole.

Previous work has demonstrated that fission yeast cofilin cooperates with fimbrin to prevent tropomyosin's association with endocytic actin patches [28], but the role of other disassembly proteins in this system remains to be explored. Recent in vitro work with mouse proteins has demonstrated a competition between twinfilin and capping protein, in which twinfilin is able to uncap filaments [61]. Additionally, cyclase associate protein (CAP) has been shown to cooperate with both twinfilin and cofilin to regulate pointed end F-actin disassembly [68]. Moving forward, it will be interesting to understand how these disassembly proteins cooperate or compete with one another to drive rapid, yet regulated disassembly of F-actin networks in cells and to further understand their interactions with other ABPs.

5.4 Materials and Methods

5.4.1 Protein purification

Chicken skeletal muscle actin was purified as described previously [137]. Twinfilin (Twf1), Cyclase Associated Protein 1 (Cap1), and Coronin (Crn1) purifications were adapted from previous work in other systems [50, 97, 57]. Briefly, proteins were expressed in BL21-Codon Plus (DE3)-RP (Agilent Technologies, Santa Clara, CA). His-tagged versions of these proteins were purified using Talon Metal Affinity Resin (Clontech, Mountain View, CA) and dialyzed overnight into buffer for either anion exchange or size exclusion chromatography (see Table 5.1 for buffer recipes). Coronin was subjected to anion exchange chromatography while twinfilin was subjected to size exclusion chromatography on a Superose 6 column.

The A280 of purified proteins was taken with a Nanodrop 2000c Spectrophotometer (Thermo-Scientific, Waltham, MA). Protein concentration was calculated using extinction coefficients Crn1: 84,590 M^{-1} cm^{-1}, Twf1: 15,025 M^{-1} cm^{-1}, CAP1: 41,285 M^{-1} cm^{-1}. Proteins were flash-frozen in liquid nitrogen and stored at -80° C.

5.4.2 Pyrene Disassembly Assay

Disassembly was monitored via pyrene fluorescence as previously described [120]. Briefly, actin seeds (5 μM, 30% pyrene iodacetamide-labeled) were polymerized for 2 hr. Pre-assembled actin seeds were diluted to 0.1 μM in buffer alone or buffers containing indicated proteins of interest. Fluorescence was monitored by a Tecan Inifinite M200Pro (Tecan Systems, Inc., San Jose, CA) plate reader at 25° C with an orbital shaking amplitude of 4 mm.

5.4.3 Glass preparation for TIRF microscopy

Microscope slides (#1.5, Fisher Scientific) and coverslips were washed for 7 min in acetone, isopropanol, and water, followed by sonication in isopropanol for 30 min. Washed glass was incubated with piranha solution (66.6% H2SO4, 33.3% H_2O_2) for 30 min, then washed with diH_2O and dried with air. Immediately following, glass was passivated by incubation in a PEG-Si mixture (1 mg/mL PEG-Si (5000 MW), 1 μg/mL Biotin-PEG-Si (3400 MW)) in 95% ethanol for 18 hr [157]. After glass was rinsed with ethanol and water, flow chambers were prepared as described previously [167].

5.4.4 TIRF microscopy (TIRFM) and analysis

Time-lapse TIRFM movies were obtained using an Olympus IX-71 microscope with through-the-objective TIRF illumination, iXon EMCCD camera (Andor Technology), and a cellTIRF 4Line system (Olympus). Flow chambers were incubated with HEK-BSA for 3 min before

adding 1 mg/ml neutravidin. After a 2 min streptavidin (1.8 μM) incubation, the chamber was washed with HEK-BSA followed by 1X TIRF buffer (Table 5.1). Following, Mg-ATP-actin (10% Alexa 488-labeled, 0.5% biotin-actin (Cytoskeleton)) was added to a polymerization mix (10 mM imidazole (pH 7.0), 50 mM KCl, 1 mM $MgCl_2$, 1 mM EGTA, 50 mM DTT, 0.2 mM ATP, 50 μM $CaCl_2$, 15 mM glucose, 20 μg/mL catalase, 100 μg/mL glucose oxidase, and 0.5% (400 centipoise) methylcellulose) to induce F-actin assembly. The mixture was added to the prepared flow chamber and allowed to polymerize for 10-15 min. Following, the actin binding proteins (ABPs) of interest were added to a polymerization mix in the absence of actin, flowed into the chamber, and imaged at room temperature at 5 s intervals.

To determine the barbed end depolymerization rate, the length for depolymerizing filaments that did not exhibit breakage events was manually tracked every frame for a minimum of 10 frames. These lengths were plotted against the time and a line of best-fit was found, where the slope is equal to the depolymerization rate.

Buffer name	Recipe	Reference
1X TIRF	1X KMEI, 100 mM DTT, 0.2 mM ATP, 30 mM glucose, 1% methylcellulose	[120]
Talon Extraction (Twinfilin, CAP1)	50 mM NaH_2PO_4, 500 mM NaCl, 10% glycerol, 10 mM imidazole, 1 Roche protease inhibitor tablet, 10mM β-mercaptoethanol	[28]
Talon Elution	50 mM NaH_2PO_4, 500 mM NaCl, 10% glycerol, 250 mM imidazole, 10 mM β-mercaptoethanol	[28]
Twinfilin Storage	20 mM HEPES pH 7.5, 1 mM EDTA, 50 mM KCl, 1 mM DTT	[57]
Coronin Extraction	20 mM HEPES pH 7.5, 150 mM KCl, 20 mM imidazole, 10 mM β-mercaptoethanol, 0.5 mM PMSF, 1 Roche protease inhibitor tablet	Adapted from [50, 97]
Coronin Elution	20 mM HEPES pH 7.5, 150 mM KCl, 250 mM imidazole, 10 mM β-mercaptoethanol	Adapted from [50, 97]
Coronin QA	20 mM HEPES pH 7.5, 50 mM KCl, 1 mM DTT	[50]
Coronin QB	20 mM HEPES pH 7.5, 500 mM KCl, 1 mM DTT	[50]
CAP1 Storage	20 mM Tris-HCl pH 8.0, 100 mM NaCl, 1 mM DTT	[57]

Table 5.1: **Buffers used in Chapter 5.**

CHAPTER 6

DISCUSSION AND FUTURE DIRECTIONS

6.1 Fission yeast Arp2/3 complex rapidly initiates both branched and linear F-actin

In this work, we engineered and tested multiple fluorescently-tagged Arp2/3 complex constructs. As direct visualization for the Arp2/3 complex mechanistic pathways has been limited to only two studies [134, 135], it is crucial to further our understanding of this key actin nucleator, as well as develop a construct for fission yeast protein mechanistic studies. Here, we found that a fluorescently tagged Arp2/3 complex, ArpC5-Halo (Halo-Arp2/3 complex) exhibited no growth or F-actin network defects in vivo (Figure 2.5, 2.2) was activated by all classes of nucleation promoting factors found in fission yeast (Figure 2.1, 2.7, 2.9), and was visible at the single molecule level (Figure 2.4, 2.7, 2.9). Additionally, we demonstrated that the time to nucleation (time delay between Arp2/3 complex binding and branch elongation) was extremely rapid, occurring 2.1 seconds after binding (Figure 2.9), similar to rates previously seen in budding yeast [134].

Last, we showed that Arp2/3 complex binding to F-actin is 3-fold increased in the presence of VCA (Figure 2.8). Interestingly, the total amount of Arp2/3 complex in frame also increased in the presence of VCA, but this increase was dependent on the presence of F-actin. While it is unclear why this might occur, we hypothesize that VCA increases Arp2/3 complex's "sampling of actin filaments. As VCA induces a conformational change in the short pitch of Arp2/3 complex [38, 168], this conformation may be more favorable for Arp2/3 complex interactions with F-actin. Thus, as more Arp2/3 complex molecules are sampling F-actin, more molecules will be present around the network, though more work must be done to conclusively demonstrate this.

This critical, much needed tool that we have developed will provide useful in many

different mechanistic studies across multiple systems. Future work will investigate the mechanisms that drive profilin inhibition of Arp2/3 complex branching (Section 6.4.1), where direct visualization is critical to distinguishing the mechanism by which inhibition occurs. Further, recent studies have demonstrated the synergistic activation of Arp2/3 complex by both Wsp1 and Dip1 in vivo and in vitro [4], yet the temporal order or pathway for this is not known. Single molecule investigation in which all proteins are directly visualized will reveal how these two different Arp2/3 complex activators can synergize to increase actin nucleation and branching. Additionally, it is still unknown the mechanisms by which Arp2/3 complex branches are severed by de-branching proteins, and this tool will allow direct visualization of the de-branching process.

6.2 Actin binding proteins are tailored for their specific functions and F-actin networks

In this dissertation, we have demonstrated multiple ways in which actin binding proteins (1) are tailored for specific functions and (2) can cooperate or compete with one another to associate with their specific F-actin networks.

6.2.1 Fission yeast Cdc12 is tailored for its role in cytokinesis

Our lab found that the fission yeast formin, Cdc12, is specifically tailored for its role during cytokinesis. When the Cdc12 FH1 and FH2 domains were replaced with these domains from formins with different elongation and nucleation properties, we discovered that cytokinesis either was delayed or initiated by a different pathway (Figure 3.6). Further, the formin chimeras with nucleation properties most similar to Cdc12 exhibited less cytokinetic defects than poor nucleators (Figure 3.6, 3.7). Computational modeling confirmed that nucleation, rather than elongation, is the key factor driving proper contractile ring formation.

Future work will further investigate mechanisms which uniquely tailor Cdc12 for its role in fission yeast cytokinesis. While monomer competition and monomer to profilin ratios play a role in regulating Cdc12-mediated actin nucleation and elongation, proteins which regulate Cdc12 localization, and activity within fission yeast, are still unknown, as common formin inhibition by Rho GTPases through their conserved DID and DAD domains did not alter Cdc12 activity [165]. Thus, the exact mechanisms for Cdc12 regulation are a ripe area for future work.

6.2.2 Fission yeast disassembly proteins

In addition to understanding the mechanisms of Cdc12's specificity for contractile ring formation, our lab has begun working to elucidate the mechanisms of fission yeast disassembly proteins. Despite the importance of regulated F-actin disassembly for network dynamic turnover and function, little work has been done to examine the exact mechanisms for these proteins in vitro.

Fission yeast contains multiple disassembly proteins that all work alone or in concert with other factors to drive rapid, highly regulated network disassembly. The mechanisms for cofilin-driven disassembly in fission yeast and other systems has been studied extensively. Our lab found that the fission yeast disassembly protein twinfilin (Twf1), with its cofactor Cyclase associated protein 1 (CAP1), rapidly depolymerize actin filaments at both the barbed and pointed end, similar to mechanisms for their budding yeast homologs (Figure 5.1, 5.3). While purifying cofilin's cofactor, coronin, proved difficult, future work will focus on optimizing this purification to understand the mechanisms of how coronin, along with AIP1 can enhance cofilin-mediated disassembly.

Future work will focus on mechanistic investigations of these proteins alone and in concert. Additionally, our lab has previously shown the role of cofilin in actin binding protein sorting for the actin patch protein fimbrin and the contractile ring protein tropomyosin [28].

Understanding how disassembly proteins and their role in F-actin turnover fit into actin binding protein sorting between networks will be a critical step towards understanding a full view of actin cytoskeleton self-organization.

6.2.3 Competitive and cooperative interactions of actin binding proteins contribute to F-actin network identity

Previous work from our lab has looked at understanding how competitive and cooperative interactions between actin binding proteins can directly influence their association with F-actin and their sorting to F-actin networks [133, 28]. Here, we demonstrated that the actin crosslinking proteins fimbrin Fim1 (actin patches) and α-actinin Ain1 compete for binding to F-actin both in vivo and in vitro [29]. As they are thought to associate with similar sites on F-actin, this presents a key reason for why these two crosslinking proteins could compete. We found that Fim1 out-competed Ain1 for association with F-actin due to its increased residence time on actin filaments. Additionally, the presence of Fim1 competitor, the contractile ring protein tropomyosin Cdc8, shifts the competition in favor of Ain1. Cdc8 enhances bundling of Ain1 by increasing the residence time of Ain1 on F-actin.

Despite out-competing both Ain1 or Cdc8 alone, when both are present, the two proteins can prevent Fim1 association with F-actin. This provides a key mechanistic detail for how a robust, highly expressed protein such as Fim1 is prevented from contractile ring association in vivo. In future studies it will be critical to understand how other non-mutually exclusive factors, such as mechanical stress, inhibitor/activating proteins, or post-translational modifications may influence actin binding protein sorting beyond these intrinsic factors we have observed so far.

6.3 Initiation of F-actin network self-organization relies on multiple, complex factors.

Our lab has long focused on understanding how multiple actin networks in a shared, common cytoplasm can self-organize to perform diverse, specialized functions at both the right place and time. Previous work from our lab has shown how actin monomer competition and the monomer to profilin ratio within cells can drive F-actin network formation and maintenance during steady-state homeostatic conditions [17, 141, 142]. Here, we investigated how actin cytoskeleton self-organization is initially established. We optimized a microfluidic system for Latrunculin A drug treatments to mimic the "initial" disassembled state, while allowing for rapid, temporal control of both disassembly and re-assembly initiation.

We found that, despite being a dynamic network with high turnover, endocytic actin patches were the last network to disassemble, yet the first to re-assemble. Further, while endocytic actin patches intially assemble at the cell poles, they then depolarize throughout the cell and do not re-polarize until formin-mediated actin cables or the contractile ring are assembled. This result provides further evidence to the long-standing role of actin cables in cell polarization, despite cables being a difficult network to study.

Interestingly, if actin patch re-assembly is inhibited by the small molecule Arp2/3 complex inhibitor, CK-666, formin-mediated F-actin networks, or ectopic F-actin do not assemble until CK-666 is washed out. This unexpected result suggests that either (1) the presence of endocytic actin patches are required for initial formin-mediated F-actin network assembly, or (2) the actin monomer to profilin ratio must be re-adjusted for the excess actin monomers. However, due to limitations in available technology and genetic tools, many of these possibilities proved difficult to directly test. Future work should aim to directly investigate these possible mechanisms using new technologies such as auxin inducible degron systems (Section 6.4.5).

6.4 Future directions

6.4.1 Profilin inhibition of Arp2/3 complex branching

Previous work from our lab has demonstrated how F-actin network homeostasis is maintained through a delicate ratio of actin monomers to the monomer binding protein profilin [142, 141]. Our lab found that, in the presence of profilin, Arp2/3 complex branching is inhibited, resulting in less branches in vitro [141]. We have hypothesized that this Arp2/3 complex branch inhibition is due to actin monomer competition between profilin and the nucleation promoting factor, Wasp. As Wasp must bind to actin monomers and Arp2/3 complex before this tertiary structure can interact with F-actin to nucleate branches, profilin binding of actin monomers decreases the available monomer pool for Wasp binding [141].In support of this, profilin mutants that increase or decrease the ability of profilin to bind to actin monomers changes the level of branching inhibition observed in vitro [141]. However, another possible mechanism for how profilin inhibits Arp2/3 complex is through competition for barbed end binding. Arp2/3 complex has been observed to bind to or near the barbed end and nucleate F-actin branches, though these two cannot be distinguished from one another at currently available dynamic microscopy resolution [134].

As we have successfully engineered a fluorescently tagged Arp2/3 complex, we aim to distinguish between these two possible mechanisms for profilin-mediated branch inhibition. By direct visualization of Arp2/3 complex binding and branch formation, we can investigate whether profilin inhibition of branching results from barbed end competition (less barbed end binding events) or actin monomer competition (less total and side branching events).

6.4.2 Mechanisms of de-branching

How Arp2/3 complex branches are severed and broken down ('de-branching') is an understudied area of cell biology and protein biochemistry. De-branching proteins such as GMF are

critical for network turnover at the leading edge of motile cells, but the mechanisms that drive this process are still poorly understood. Work in recent years has shown how Arp2/3 complex branches can be protected from de-branching [52] and how force and phosphate state can influence branch dissociation [102], but no studies directly visualize the de-branching process with labeled Arp2/3 complex. Just a few questions that remain unclear are (1) if Arp2/3 complex leaves the branch site before branch break, (2) where de-branching proteins bind and the mechanisms behind their action (cooperativity, structure changes, direct Arp2/3 complex binding), (3) if Arp2/3 complex remains bound to the pointed end of the daughter filament post-break, similar to its pointed end binding with Dip1 linear actin nucleation processes. Future work should investigate the ordering, mechanisms, and kinetics of de-branching processes, both under force (breakage) or in the presence of de-branching proteins utilizing labeled Arp2/3 complex to begin to address such questions.

6.4.3 Actin binding protein sorting: other competitors and the role of tension

We found that α-actinin Ain1 and Cdc8 can synergize to enhance Ain1-mediated bundling and compete with fimbrin for association with F-actin [29]. Additionally, we found that the actin patch protein fimbrin can displace the contractile ring protein α-actinin from the ring when patches are inhibited by CK-666 treatment [29].

Interestingly though, despite previous work from our lab showing that fimbrin also competes with the contractile ring protein tropomyosin Cdc8 in vitro [28], when fimbrin is displaced from actin patches through CK-666 treatment, Cdc8 is not displaced from the contractile ring [29]. This implies that other mechanisms must be in place to help maintain Cdc8 at the contractile ring. Future work should focus on a large, actin binding protein screen to identify other possible actin binding protein competitors that allow Cdc8 to remain at the contractile ring even in the presence of its known competitor fimbrin.

Further, it is unclear the role tension and force play in actin binding protein sorting. The

contractile ring tension may allow Cdc8 to be a better competitor against fimbrin, creating individual domains on the contractile ring. It will be crucial to understand how force influences both actin binding protein activity and their competitive and cooperative mechanisms to begin to understand the mechanisms of self-organization at work in cells. A combination of in vivo tension mutants to screen for possible changes in competitive and cooperative localization, similar to the screens performed in [29], with in vitro mechanistic studies using microfluidic devices to precisely control tension while monitoring protein binding and activity [20, 159] will allow for a better understanding of the role force plays in actin binding protein sorting and self-organization as a whole.

6.4.4 Fission yeast actin

In all of our studies, actin binding proteins are purified either directly from fission yeast or recombinantly expressed and purified from bacterial or insect cell expression systems. However, the actin itself used in our in vitro studies is purified from chicken skeletal muscle, similar to historical experiments [137]. This is largely due to the fact that previous attempts to purify fission yeast actin from either fission yeast or recombinant systems have been difficult to reproduce or resulted in low yield due to extensive protein degradation [146, 148, 54].

Despite this, there is significant evidence to suggest that specific actin isoforms can influence the activity of actin binding proteins [121, 93]. Work in budding yeast has demonstrated that the actin isoform expressed is critical to proper F-actin network self-organization and network function [121]. Additionally, evidence suggests that mammalian actin isoforms have functionally distinct interactions with various myosins [93]. Thus, while initial studies and inferences can be made using our current actin source, it is critical to repeat key findings with fission yeast actin to fully understand actin binding protein mechanisms as well as sorting pathways.

To address the influence of fission yeast actin on our actin binding proteins mechanisms or sorting, our lab is involved in a collaboration to engineer a stable, high yield fission yeast actin construct. To address the issue of protein degradation, we have introduced a single point mutation (Y371H). Our lab introduced this point mutation into fission yeast and found that it did not influence fission yeast growth or F-actin networks in vivo (6.1A-D). Further, we have engineered an actin and thymosin β-4 chimera, linked by a TEV protease site with a histidine tag on the C-terminus (Actin(Y371H)-TEV linker-Thymosin β-4-6xHis). I successfully purified this construct from insect cells (6.1E) and future work will begin to investigate how the actin binding protein mechanisms examined throughout this dissertation are affected by their native actin isoform.

6.4.5 Auxin inducible degron systems

While fission yeast has a multitude of genetic tools, the system is often limited in high temporal control for protein expression and degradation. Systems to over- or under-express proteins are often limited to nutrient-inducible promoters, which require hours for increased expression or shut-off. Work in other systems has demonstrated the power of an auxin inducible degron (AID) system, by which the addition of auxin leads to rapid, targeted protein degradation [128, 77]. The AID system involves fusing an auxin-inducible destabilizing domain ('degron') to a protein of interest and the expression of degradation-targeting proteins from the auxin-mediated pathway in plants [128]. By the addition of the small molecule auxin, targeted degradation of the protein of interest can be reliably introduced with high temporal control [128].

In studies, such as our work to look at the initiation of self-organization, a tool like this would be critical for demonstrating the importance of Arp2/3 complex or other endocytic proteins, as mutants to do this are either unreliable or attempts to design them have proven unsuccessful. Recent work has engineered fission yeast AID strains for proteins with nuclear

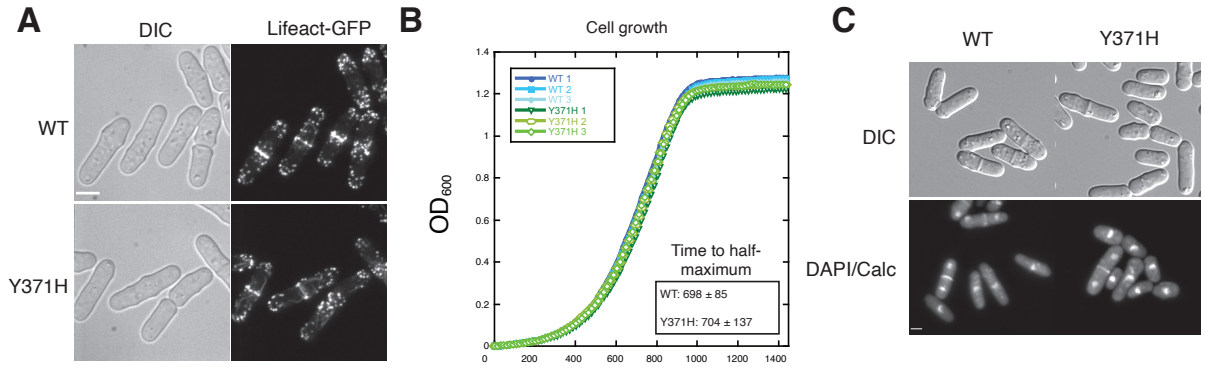

D

	WT	Y371H
Cells with one nucleus (%)	77.3 ± 1.7	78.6 ± 1.8*
Cells with 2 nuclei (%)	22.7 ± 1.7	20.8 ± 1.9**
Cells with >2 nuclei (%)	0	.60 ± .06***
Cells with normal septa (%)	100	100
Cells with abnormal septa (%)	0	0

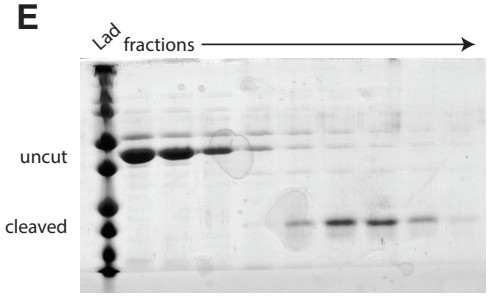

Figure 6.1: **Fission yeast actin Y371H mutation does not affect cells in vivo and produces protein at a high yield. A.** Micrographs of wild-type (WT) and actin mutant Y371H fission yeast cells showing morphology (DIC) and organization of actin networks (Lifeact-GFP). Scale bar, 5 μm. **B.** Growth curve of WT and Y371H actin mutant strains. 3 replicates of each strain are shown. Average time to half-maximum OD_{600} of each strain was calculated from 15 replicates each. For the average time to half-maximums, a two-tailed t-test for data sets with unequal variance yielded a p-value of 0.87. **C.** Micrographs of WT and Y371H actin mutant cells including DIC (morphology) and methanol fixed cells stained with DAPI (nuclei) and Calcofluor (septa). Scale bar, 5 μm. **D.** Table of quantification of cells shown in (C). Percentage of cells with 1, 2, and greater than 2 nuclei as well as the percentage of cells exhibiting normal and abnormal (misplaced, unusually broad, or misshapen) septa are shown. 2 replicates were analyzed, n $\geq$ 300 for each replicate. To compare WT and Y371H, two-tailed t-tests for data sets with unequal variance were conducted, yielding p-values of: *p-value=0.66, **p-value=0.53, ***p-value=0.061. **E.** SDS-PAGE protein gel showing purified fission yeast actin after anion exchange.

localization [66]. Development of an AID system for cytosolic proteins will prove a crucial tool for future mechanistic studies in many different fields beyond our own work.

6.4.6 Disassembly proteins: the role in self-organization

In this work, I began to investigate the disassembly mechanisms of the fission yeast disassembly protein twinfilin (Twf1) and its cofactor cyclase associates protein (CAP1) as well as optimization for purification of the disassembly cofactors coronin 1 (Crn1) and actin interacting protein 1 (AIP1). While preliminary investigation suggests that Twf1 and CAP1 use mechanisms in fission yeast similar to their budding yeast homologs, there are still many questions left to be explored with these proteins.

In addition to understanding the mechanisms of these proteins alone and with associated cofactors, future work should focus on how disassembly proteins influence actin cytoskeleton self-organization. Disassembly of F-actin networks is a crucial component to the dynamic cycle that maintains self-organization, yet little work has been done to understand its role. Previous work from our lab found that competition between ADF/cofilin and fimbrin leads to a synergy that enhances both their activities, as well as allows them to compete with and displace tropomyosin Cdc8 from actin filaments in vitro [28]. Additionally, studies have debated the capping/uncapping role of twinfilin [61, 53]. Recent structural work has revealed that twinfilin may bind to actin and capping protein at the barbed end to promote filament uncapping for a further mechanism of rapid actin disassembly [92], yet how this novel disassembly mechanism fits into the larger picture of actin turnover and self-organization is still unclear.

Future work should focus on the role disassembly factors in influencing actin monomer competition and actin binding protein sorting to obtain a more complete picture of self-organization. Using a combinatorial approach of in vivo and in vitro, similar to our work in [29], will be critical for addressing this question. By examining both how mutants in fission

yeast change the localization of other actin binding proteins in vivo and how combinations of actin binding proteins can influence one another's activity or F-actin association, we can further get a clear picture of how disassembly influences network self-organization.

References

[1] Rajesh Arasada, Wasim A. Sayyad, Julien Berro, and Thomas D. Pollard. High-speed superresolution imaging of the proteins in fission yeast clathrin-mediated endocytic actin patches. *Molecular Biology of the Cell*, 29(3):295–303, February 2018.

[2] D. Axelrod, N. L. Thompson, and T. P. Burghardt. Total internal inflection fluorescent microscopy. *Journal of Microscopy*, 129(Pt 1):19–28, January 1983.

[3] M. K. Balasubramanian, D. McCollum, L. Chang, K. C. Wong, N. I. Naqvi, X. He, S. Sazer, and K. L. Gould. Isolation and characterization of new fission yeast cytokinesis mutants. *Genetics*, 149(3):1265–1275, July 1998.

[4] Connor J Balzer, Michael L James, Heidy Y Narvaez-Ortiz, Luke A Helgeson, Vladimir Sirotkin, and Brad J Nolen. Synergy between Wsp1 and Dip1 may initiate assembly of endocytic actin networks. *eLife*, 9, 2020.

[5] Connor J. Balzer, Andrew R. Wagner, Luke A. Helgeson, and Brad J. Nolen. Dip1 Co-opts Features of Branching Nucleation to Create Linear Actin Filaments that Activate WASP-Bound Arp2/3 Complex. *Current biology: CB*, 28(23):3886–3891.e4, 2018.

[6] James R. Bartles. Parallel Actin Bundles and Their Multiple Actin-bundling Proteins. *Current opinion in cell biology*, 12(1):72–78, February 2000.

[7] Roshni Basu and Fred Chang. Characterization of dip1p reveals a switch in Arp2/3-dependent actin assembly for fission yeast endocytosis. *Current biology : CB*, 21(11):905–916, June 2011.

[8] Christopher C. Beltzner and Thomas D. Pollard. Identification of functionally important residues of Arp2/3 complex by analysis of homology models from diverse species. *Journal of Molecular Biology*, 336(2):551–565, February 2004.

[9] Christopher C. Beltzner and Thomas D. Pollard. Pathway of actin filament branch formation by Arp2/3 complex. *The Journal of Biological Chemistry*, 283(11):7135–7144, March 2008.

[10] Alexander Belyy, Felipe Merino, Oleg Sitsel, and Stefan Raunser. Structure of the Lifeact–F-actin complex. *bioRxiv*, page 2020.02.16.951269, February 2020. Publisher: Cold Spring Harbor Laboratory Section: New Results.

[11] Julien Berro, Vladimir Sirotkin, and Thomas D. Pollard. Mathematical modeling of endocytic actin patch kinetics in fission yeast: disassembly requires release of actin filament fragments. *Molecular Biology of the Cell*, 21(16):2905–2915, August 2010.

[12] Ingrid Billault-Chaumartin and Sophie G. Martin. Capping Protein Insulates Arp2/3-Assembled Actin Patches from Formins. *Current Biology*, 29(19):3165–3176.e6, October 2019.

[13] L. Blanchoin and T. D. Pollard. Mechanism of interaction of Acanthamoeba actophorin (ADF/Cofilin) with actin filaments. *The Journal of Biological Chemistry*, 274(22):15538–15546, May 1999.

[14] Laurent Blanchoin, Rajaa Boujemaa-Paterski, Cécile Sykes, and Julie Plastino. Actin dynamics, architecture, and mechanics in cell motility. *Physiological Reviews*, 94(1):235–263, January 2014.

[15] Laurent Blanchoin, Thomas D. Pollard, and R. Dyche Mullins. Interactions of ADF/cofilin, Arp2/3 complex, capping protein and profilin in remodeling of branched actin filament networks. *Current Biology*, 10(20):1273–1282, October 2000. Publisher: Elsevier.

[16] Dennis Breitsprecher and Bruce L. Goode. Formins at a glance. *Journal of Cell Science*, 126(1):1–7, January 2013.

[17] Thomas A. Burke, Jenna R. Christensen, Elisabeth Barone, Cristian Suarez, Vladimir Sirotkin, and David R. Kovar. Homeostatic actin cytoskeleton networks are regulated by assembly factor competition for monomers. *Current biology: CB*, 24(5):579–585, March 2014.

[18] Liang Cai, Alexander M. Makhov, and James E. Bear. F-actin binding is essential for coronin 1B function in vivo. *Journal of Cell Science*, 120(10):1779–1790, May 2007.

[19] Liang Cai, Thomas W. Marshall, Andrea C. Uetrecht, Dorothy A. Schafer, and James E. Bear. Coronin 1B Coordinates Arp2/3 Complex and Cofilin Activities at the Leading Edge. *Cell*, 128(5):915–929, March 2007.

[20] Luyan Cao, Mikael Kerleau, Emiko L. Suzuki, Hugo Wioland, Sandy Jouet, Berengere Guichard, Martin Lenz, Guillaume Romet-Lemonne, and Antoine Jegou. Modulation of formin processivity by profilin and mechanical tension. *eLife*, 7:e34176, May 2018. Publisher: eLife Sciences Publications, Ltd.

[21] Luyan Cao, Amina Yonis, Malti Vaghela, Elias H. Barriga, Priyamvada Chugh, Matthew B. Smith, Julien Maufront, Geneviève Lavoie, Antoine Méant, Emma Ferber, Miia Bovellan, Art Alberts, Aurélie Bertin, Roberto Mayor, Ewa K. Paluch, Philippe P. Roux, Antoine Jégou, Guillaume Romet-Lemonne, and Guillaume Charras. SPIN90 associates with mDia1 and the Arp2/3 complex to regulate cortical actin organization. *Nature Cell Biology*, 22(7):803–814, July 2020. Number: 7 Publisher: Nature Publishing Group.

[22] Wenxiang Cao, Jim P. Goodarzi, and Enrique M. De La Cruz. Energetics and kinetics of cooperative cofilin-actin filament interactions. *Journal of Molecular Biology*, 361(2):257–267, August 2006.

[23] M. F. Carlier and D. Pantaloni. Direct evidence for ADP-inorganic phosphate-F-actin as the major intermediate in ATP-actin polymerization. Rate of dissociation of

inorganic phosphate from actin filaments. *Biochemistry*, 25(24):7789–7792, December 1986.

[24] Dimitra Chalkia, Nikolas Nikolaidis, Wojciech Makalowski, Jan Klein, and Masatoshi Nei. Origins and Evolution of the Formin Multigene Family That Is Involved in the Formation of Actin Filaments. *Molecular Biology and Evolution*, 25(12):2717–2733, December 2008.

[25] F. Chang, D. Drubin, and P. Nurse. cdc12p, a protein required for cytokinesis in fission yeast, is a component of the cell division ring and interacts with profilin. *The Journal of Cell Biology*, 137(1):169–182, April 1997.

[26] Qian Chen and Thomas D. Pollard. Actin filament severing by cofilin dismantles actin patches and produces mother filaments for new patches. *Current biology: CB*, 23(13):1154–1162, July 2013.

[27] David Chereau, Frederic Kerff, Philip Graceffa, Zenon Grabarek, Knut Langsetmo, and Roberto Dominguez. Actin-bound structures of Wiskott-Aldrich syndrome protein (WASP)-homology domain 2 and the implications for filament assembly. *Proceedings of the National Academy of Sciences of the United States of America*, 102(46):16644–16649, November 2005.

[28] Jenna R. Christensen, Glen M. Hocky, Kaitlin E. Homa, Alisha N. Morganthaler, Sarah E. Hitchcock-DeGregori, Gregory A. Voth, and David R. Kovar. Competition between Tropomyosin, Fimbrin, and ADF/Cofilin drives their sorting to distinct actin filament networks. *eLife*, 6, 2017.

[29] Jenna R Christensen, Kaitlin E Homa, Alisha N Morganthaler, Rachel R Brown, Cristian Suarez, Alyssa J Harker, Meghan E O'Connell, and David R Kovar. Cooperation between tropomyosin and α-actinin inhibits fimbrin association with actin filament networks in fission yeast. *eLife*, 8:e47279, June 2019. Publisher: eLife Sciences Publications, Ltd.

[30] Joseph E. Clayton, Matthew R. Sammons, Benjamin C. Stark, Alex R. Hodges, and Matthew Lord. Differential regulation of unconventional fission yeast myosins via the actin track. *Current biology: CB*, 20(16):1423–1431, August 2010.

[31] Valerie C. Coffman, Jennifer A. Sees, David R. Kovar, and Jian-Qiu Wu. The formins Cdc12 and For3 cooperate during contractile ring assembly in cytokinesis. *The Journal of Cell Biology*, 203(1):101–114, October 2013.

[32] John A. Cooper, E. Loren Buhle, Simon B. Walker, Tian Y. Tsong, and Thomas D. Pollard. Kinetic evidence for a monomer activation step in actin polymerization. *Biochemistry*, 22(9):2193–2202, April 1983.

[33] Naomi Courtemanche, Thomas D. Pollard, and Qian Chen. Avoiding artefacts when counting polymerized actin in live cells with LifeAct fused to fluorescent proteins. *Nature Cell Biology*, 18(6):676–683, June 2016. Number: 6 Publisher: Nature Publishing Group.

[34] S. Cranz-Mileva, B. MacTaggart, J. Russell, and S. E. Hitchcock-DeGregori. Evolutionarily conserved sites in yeast tropomyosin function in cell polarity, transport and contractile ring formation. *Biology Open*, 4(8):1040–1051, August 2015.

[35] Mark J. Dayel and R. Dyche Mullins. Activation of Arp2/3 complex: addition of the first subunit of the new filament by a WASP protein triggers rapid ATP hydrolysis on Arp2. *PLoS biology*, 2(4):E91, April 2004.

[36] Marc Edwards, Adam Zwolak, Dorothy A. Schafer, David Sept, Roberto Dominguez, and John A. Cooper. Capping protein regulators fine-tune actin assembly dynamics. *Nature Reviews. Molecular Cell Biology*, 15(10):677–689, October 2014.

[37] C. Egile, T. P. Loisel, V. Laurent, R. Li, D. Pantaloni, P. J. Sansonetti, and M. F. Carlier. Activation of the CDC42 effector N-WASP by the Shigella flexneri IcsA protein promotes actin nucleation by Arp2/3 complex and bacterial actin-based motility. *The Journal of Cell Biology*, 146(6):1319–1332, September 1999.

[38] Sofia Espinoza-Sanchez, Lauren Ann Metskas, Steven Z. Chou, Elizabeth Rhoades, and Thomas D. Pollard. Conformational changes in Arp2/3 complex induced by ATP, WASp-VCA, and actin filaments. *Proceedings of the National Academy of Sciences*, 115(37):E8642–E8651, September 2018. ISBN: 9781717594112 Publisher: National Academy of Sciences Section: PNAS Plus.

[39] B. Feierbach and F. Chang. Roles of the fission yeast formin for3p in cell polarity, actin cable formation and symmetric cell division. *Current biology: CB*, 11(21):1656–1665, October 2001.

[40] Kenneth N. Fish. Total Internal Reflection Fluorescence (TIRF) Microscopy. *Current protocols in cytometry / editorial board, J. Paul Robinson, managing editor ... [et al.]*, 0 12:Unit12.18, October 2009.

[41] Yannick Gachet and Jeremy S. Hyams. Endocytosis in fission yeast is spatially associated with the actin cytoskeleton during polarised cell growth and cytokinesis. *Journal of Cell Science*, 118(Pt 18):4231–4242, September 2005.

[42] Meghal Gandhi, Vérane Achard, Laurent Blanchoin, and Bruce L. Goode. Coronin switches roles in actin disassembly depending on the nucleotide state of actin. *Molecular cell*, 34(3):364–374, May 2009.

[43] Lina Gao and Anthony Bretscher. Analysis of Unregulated Formin Activity Reveals How Yeast Can Balance F-Actin Assembly between Different Microfilament-based Organizations. *Molecular Biology of the Cell*, 19(4):1474–1484, April 2008.

[44] M.A. Geeves. 4.13 Thin Filament Regulation. In *Comprehensive Biophysics*, pages 251–267. Elsevier, 2012.

[45] Erin D. Goley, Stacia E. Rodenbusch, Adam C. Martin, and Matthew D. Welch. Critical conformational changes in the Arp2/3 complex are induced by nucleotide and nucleation promoting factor. *Molecular Cell*, 16(2):269–279, October 2004.

[46] Erin D. Goley and Matthew D. Welch. The ARP2/3 complex: an actin nucleator comes of age. *Nature Reviews. Molecular Cell Biology*, 7(10):713–726, October 2006.

[47] B. L. Goode, D. G. Drubin, and P. Lappalainen. Regulation of the cortical actin cytoskeleton in budding yeast by twinfilin, a ubiquitous actin monomer-sequestering protein. *The Journal of Cell Biology*, 142(3):723–733, August 1998.

[48] Bruce L. Goode and Michael J. Eck. Mechanism and Function of Formins in the Control of Actin Assembly. *Annual Review of Biochemistry*, 76(1):593–627, June 2007.

[49] Bruce L. Goode, Julian A. Eskin, and Beverly Wendland. Actin and endocytosis in budding yeast. *Genetics*, 199(2):315–358, February 2015.

[50] Bruce L. Goode, Jonathan J. Wong, Anne-Christine Butty, Matthias Peter, Ashley L. McCormack, John R. Yates, David G. Drubin, and Georjana Barnes. Coronin Promotes the Rapid Assembly and Cross-linking of Actin Filaments and May Link the Actin and Microtubule Cytoskeletons in Yeast. *The Journal of Cell Biology*, 144(1):83–98, January 1999.

[51] Peter W. Gunning, Umesh Ghoshdastider, Shane Whitaker, David Popp, and Robert C. Robinson. The evolution of compositionally and functionally distinct actin filaments. *Journal of Cell Science*, 128(11):2009–2019, June 2015.

[52] Siyang Guo, Olga S. Sokolova, Johnson Chung, Shae Padrick, Jeff Gelles, and Bruce L. Goode. Abp1 promotes Arp2/3 complex-dependent actin nucleation and stabilizes branch junctions by antagonizing GMF. *Nature Communications*, 9(1):2895, July 2018. Bandiera_abtest: a Cc_license_type: cc_by Cg_type: Nature Research Journals Number: 1 Primary_atype: Research Publisher: Nature Publishing Group Subject_term: Actin;Cytoskeletal proteins Subject_term_id: actin;cytoskeletal-proteins.

[53] Markku Hakala, Hugo Wioland, Mari Tolonen, Antoine Jegou, Guillaume Romet-Lemonne, and Pekka Lappalainen. Twinfilin uncaps filament barbed ends to promote turnover of lamellipodial actin networks. *bioRxiv*, page 864769, December 2019. Publisher: Cold Spring Harbor Laboratory Section: New Results.

[54] Tomoyuki Hatano, Salvatore Alioto, Emanuele Roscioli, Saravanan Palani, Scott T. Clarke, Anton Kamnev, Juan Ramon Hernandez-Fernaud, Lavanya Sivashanmugam, Bernardo Chapa-Y-Lazo, Alexandra M. E. Jones, Robert C. Robinson, Karuna Sampath, Masanori Mishima, Andrew D. McAinsh, Bruce L. Goode, and Mohan K. Balasubramanian. Rapid production of pure recombinant actin isoforms in Pichia pastoris. *Journal of Cell Science*, 131(8), April 2018.

[55] Henry N. Higgs and Kevin J. Peterson. Phylogenetic Analysis of the Formin Homology 2 Domain. *Molecular Biology of the Cell*, 16(1):1–13, January 2005.

[56] Henry N. Higgs and Thomas D. Pollard. Regulation of Actin Polymerization by Arp2/3 Complex and WASp/Scar Proteins *. *Journal of Biological Chemistry*, 274(46):32531–32534, November 1999. Publisher: Elsevier.

[57] Denise M. Hilton, Rey M. Aguilar, Adam B. Johnston, and Bruce L. Goode. Species-Specific Functions of Twinfilin in Actin Filament Depolymerization. *Journal of Molecular Biology*, 430(18, Part B):3323–3336, September 2018.

[58] Junqi Huang, Yinyi Huang, Haochen Yu, Dhivya Subramanian, Anup Padmanabhan, Rahul Thadani, Yaqiong Tao, Xie Tang, Roland Wedlich-Soldner, and Mohan K. Balasubramanian. Nonmedially assembled F-actin cables incorporate into the actomyosin ring in fission yeast. *The Journal of Cell Biology*, 199(5):831–847, November 2012.

[59] Silvia Jansen, Agnieszka Collins, Samantha M. Chin, Casey A. Ydenberg, Jeff Gelles, and Bruce L. Goode. Single-molecule imaging of a three-component ordered actin disassembly mechanism. *Nature Communications*, 6(1):7202, May 2015. Number: 1 Publisher: Nature Publishing Group.

[60] Adam B. Johnston, Agnieszka Collins, and Bruce L. Goode. High-speed depolymerization at actin filament ends jointly catalysed by Twinfilin and Srv2/CAP. *Nature Cell Biology*, 17(11):1504–1511, November 2015.

[61] Adam B Johnston, Denise M Hilton, Patrick McConnell, Britney Johnson, Meghan T Harris, Avital Simone, Gaya K Amarasinghe, John A Cooper, and Bruce L Goode. A novel mode of capping protein-regulation by twinfilin. *eLife*, 7:e41313, October 2018. Publisher: eLife Sciences Publications, Ltd.

[62] D. A. Kaiser, V. K. Vinson, D. B. Murphy, and T. D. Pollard. Profilin is predominantly associated with monomeric actin in Acanthamoeba. *Journal of Cell Science*, 112 (Pt 21):3779–3790, November 1999.

[63] Tomoko Kamasaki, Ritsuko Arai, Masako Osumi, and Issei Mabuchi. Directionality of F-actin cables changes during the fission yeast cell cycle. *Nature Cell Biology*, 7(9):916–917, September 2005.

[64] Tomoko Kamasaki, Masako Osumi, and Issei Mabuchi. Three-dimensional arrangement of F-actin in the contractile ring of fission yeast. *The Journal of Cell Biology*, 178(5):765–771, August 2007.

[65] Hyeran Kang, Michael J. Bradley, Brannon R. McCullough, Anaëlle Pierre, Elena E. Grintsevich, Emil Reisler, and Enrique M. De La Cruz. Identification of cation-binding sites on actin that drive polymerization and modulate bending stiffness. *Proceedings of the National Academy of Sciences of the United States of America*, 109(42):16923–16927, October 2012.

[66] Mai Kanke, Kohei Nishimura, Masato Kanemaki, Tatsuo Kakimoto, Tatsuro S. Takahashi, Takuro Nakagawa, and Hisao Masukata. Auxin-inducible protein depletion system in fission yeast. *BMC cell biology*, 12:8, February 2011.

[67] Taekyung Kim, John A. Cooper, and David Sept. The interaction of capping protein with the barbed end of the actin filament. *Journal of Molecular Biology*, 404(5):794–802, December 2010.

[68] Tommi Kotila, Hugo Wioland, Giray Enkavi, Konstantin Kogan, Ilpo Vattulainen, Antoine Jégou, Guillaume Romet-Lemonne, and Pekka Lappalainen. Mechanism of synergistic actin filament pointed end depolymerization by cyclase-associated protein and cofilin. *Nature Communications*, 10, November 2019.

[69] David R. Kovar, Elizabeth S. Harris, Rachel Mahaffy, Henry N. Higgs, and Thomas D. Pollard. Control of the assembly of ATP- and ADP-actin by formins and profilin. *Cell*, 124(2):423–435, January 2006.

[70] David R. Kovar, Jeffrey R. Kuhn, Andrea L. Tichy, and Thomas D. Pollard. The fission yeast cytokinesis formin Cdc12p is a barbed end actin filament capping protein gated by profilin. *The Journal of Cell Biology*, 161(5):875–887, June 2003.

[71] David R. Kovar, Vladimir Sirotkin, and Matthew Lord. Three's company: The fission yeast actin cytoskeleton. *Trends in cell biology*, 21(3):177–187, March 2011.

[72] David R. Kovar, Jian-Qiu Wu, and Thomas D. Pollard. Profilin-mediated Competition between Capping Protein and Formin Cdc12p during Cytokinesis in Fission Yeast. *Molecular Biology of the Cell*, 16(5):2313–2324, May 2005.

[73] Shusaku Kurisu and Tadaomi Takenawa. The WASP and WAVE family proteins. *Genome Biology*, 10(6):226, 2009.

[74] I.-Ju Lee, Valerie C. Coffman, and Jian-Qiu Wu. Contractile-ring assembly in fission yeast cytokinesis: Recent advances and new perspectives. *Cytoskeleton (Hoboken, N.J.)*, 69(10):751–763, October 2012.

[75] W. L. Lee, M. Bezanilla, and T. D. Pollard. Fission yeast myosin-I, Myo1p, stimulates actin assembly by Arp2/3 complex and shares functions with WASp. *The Journal of Cell Biology*, 151(4):789–800, November 2000.

[76] Fang Li and Henry N. Higgs. The Mouse Formin mDia1 Is a Potent Actin Nucleation Factor Regulated by Autoinhibition. *Current Biology*, 13(15):1335–1340, August 2003.

[77] Shiqian Li, Xavier Prasanna, Veijo T. Salo, Ilpo Vattulainen, and Elina Ikonen. An efficient auxin-inducible degron system with low basal degradation in human cells. *Nature Methods*, 16(9):866–869, September 2019. Number: 9 Publisher: Nature Publishing Group.

[78] Yujie Li, Jenna R. Christensen, Kaitlin E. Homa, Glen M. Hocky, Alice Fok, Jennifer A. Sees, Gregory A. Voth, and David R. Kovar. The F-actin bundler α-actinin Ain1 is tailored for ring assembly and constriction during cytokinesis in fission yeast. *Molecular Biology of the Cell*, 27(11):1821–1833, 2016.

[79] J. Lu and T. D. Pollard. Profilin binding to poly-L-proline and actin monomers along with ability to catalyze actin nucleotide exchange is required for viability of fission yeast. *Molecular Biology of the Cell*, 12(4):1161–1175, April 2001.

[80] Qing Luan, Su-Ling Liu, Luke A Helgeson, and Brad J Nolen. Structure of the nucleation-promoting factor SPIN90 bound to the actin filament nucleator Arp2/3 complex. *The EMBO Journal*, 37(22):e100005, November 2018. Publisher: John Wiley & Sons, Ltd.

[81] Laura M. Machesky, R. Dyche Mullins, Henry N. Higgs, Donald A. Kaiser, Laurent Blanchoin, Robin C. May, Margaret E. Hall, and Thomas D. Pollard. Scar, a WASp-related protein, activates nucleation of actin filaments by the Arp2/3 complex. *Proceedings of the National Academy of Sciences*, 96(7):3739–3744, March 1999.

[82] J. B. Marchand, D. A. Kaiser, T. D. Pollard, and H. N. Higgs. Interaction of WASP/Scar proteins with actin and vertebrate Arp2/3 complex. *Nature Cell Biology*, 3(1):76–82, January 2001.

[83] Sophie G. Martin and Fred Chang. Dynamics of the formin for3p in actin cable assembly. *Current biology: CB*, 16(12):1161–1170, June 2006.

[84] P. Matsudaira. Modular organization of actin crosslinking proteins. *Trends in Biochemical Sciences*, 16(3):87–92, March 1991.

[85] D. McCollum, A. Feoktistova, M. Morphew, M. Balasubramanian, and K. L. Gould. The Schizosaccharomyces pombe actin-related protein, Arp3, is a component of the cortical actin cytoskeleton and interacts with profilin. *The EMBO Journal*, 15(23):6438–6446, December 1996. Publisher: John Wiley & Sons, Ltd.

[86] A. McGough, B. Pope, W. Chiu, and A. Weeds. Cofilin changes the twist of F-actin: implications for actin filament dynamics and cellular function. *The Journal of Cell Biology*, 138(4):771–781, August 1997.

[87] Alphée Michelot and David G. Drubin. Building Distinct Actin Filament Networks in a Common Cytoplasm. *Current Biology*, 21(14):R560–R569, July 2011.

[88] Mouna A. Mikati, Dennis Breitsprecher, Silvia Jansen, Emil Reisler, and Bruce L. Goode. Coronin enhances actin filament severing by recruiting cofilin to filament sides and altering F-actin conformation. *Journal of molecular biology*, 427(19):3137–3147, September 2015.

[89] Fumio Motegi, Ritsuko Arai, and Issei Mabuchi. Identification of Two Type V Myosins in Fission Yeast, One of Which Functions in Polarized Cell Growth and Moves Rapidly in the Cell. *Molecular Biology of the Cell*, 12(5):1367–1380, May 2001. Publisher: American Society for Cell Biology (mboc).

[90] R. D. Mullins, J. A. Heuser, and T. D. Pollard. The interaction of Arp2/3 complex with actin: nucleation, high affinity pointed end capping, and formation of branching networks of filaments. *Proceedings of the National Academy of Sciences of the United States of America*, 95(11):6181–6186, May 1998.

[91] Lise N. Munsie, Nicholas Caron, Carly R. Desmond, and Ray Truant. Lifeact cannot visualize some forms of stress-induced twisted f-actin. *Nature Methods*, 6(5):317–317, May 2009. Number: 5 Publisher: Nature Publishing Group.

[92] Dennis M. Mwangangi, Edward Manser, and Robert C. Robinson. The structure of the actin filament uncapping complex mediated by twinfilin. *Science Advances*, 7(5):eabd5271, January 2021. Publisher: American Association for the Advancement of Science Section: Research Article.

[93] Mirco Müller, Ralph P. Diensthuber, Igor Chizhov, Peter Claus, Sarah M. Heissler, Matthias Preller, Manuel H. Taft, and Dietmar J. Manstein. Distinct Functional Interactions between Actin Isoforms and Nonsarcomeric Myosins. *PLoS ONE*, 8(7):e70636, July 2013.

[94] Kentaro Nakano, Jun Imai, Ritsuko Arai, Akio Toh-E, Yasushi Matsui, and Issei Mabuchi. The small GTPase Rho3 and the diaphanous/formin For3 function in polarized cell growth in fission yeast. *Journal of Cell Science*, 115(Pt 23):4629–4639, December 2002.

[95] Kentaro Nakano and Issei Mabuchi. Actin-depolymerizing protein Adf1 is required for formation and maintenance of the contractile ring during cytokinesis in fission yeast. *Molecular Biology of the Cell*, 17(4):1933–1945, April 2006.

[96] Brad J. Nolen and Thomas D. Pollard. Insights into the influence of nucleotides on actin family proteins from seven new structures of Arp2/3 complex. *Molecular cell*, 26(3):449–457, May 2007.

[97] Maya A. Olshina, Fiona Angrisano, Danushka S. Marapana, David T. Riglar, Kartik Bane, Wilson Wong, Bruno Catimel, Meng-Xin Yin, Andrew B. Holmes, Friedrich Frischknecht, David R. Kovar, and Jake Baum. Plasmodium falciparum coronin organizes arrays of parallel actin filaments potentially guiding directional motility in invasive malaria parasites. *Malaria Journal*, 14(1):280, July 2015.

[98] Shoichiro Ono and Kanako Ono. Tropomyosin inhibits ADF/cofilin-dependent actin filament dynamics. *The Journal of Cell Biology*, 156(6):1065–1076, March 2002.

[99] Takanori Otomo, Chinatsu Otomo, Diana R. Tomchick, Mischa Machius, and Michael K. Rosen. Structural Basis of Rho GTPase-Mediated Activation of the Formin mDia1. *Molecular Cell*, 18(3):273–281, April 2005.

[100] Shae B. Padrick, Lynda K. Doolittle, Chad A. Brautigam, David S. King, and Michael K. Rosen. Arp2/3 complex is bound and activated by two WASP proteins. *Proceedings of the National Academy of Sciences*, 108(33):13367–13368, August 2011. Publisher: National Academy of Sciences Section: PNAS Plus.

[101] Shae B. Padrick and Michael K. Rosen. Physical mechanisms of signal integration by WASP family proteins. *Annual Review of Biochemistry*, 79:707–735, 2010.

[102] Nandan G. Pandit, Wenxiang Cao, Jeffrey Bibeau, Eric M. Johnson-Chavarria, Edwin W. Taylor, Thomas D. Pollard, and Enrique M. De La Cruz. Force and phosphate release from Arp2/3 complex promote dissociation of actin filament branches. *Proceedings of the National Academy of Sciences*, 117(24):13519–13528, June 2020.

[103] D. Pantaloni, R. Boujemaa, D. Didry, P. Gounon, and M. F. Carlier. The Arp2/3 complex branches filament barbed ends: functional antagonism with capping proteins. *Nature Cell Biology*, 2(7):385–391, July 2000.

[104] Aditya S. Paul, Aditya Paul, Thomas D. Pollard, and Thomas Pollard. The role of the FH1 domain and profilin in formin-mediated actin-filament elongation and nucleation. *Current biology: CB*, 18(1):9–19, January 2008.

[105] Aditya S. Paul and Thomas D. Pollard. Review of the mechanism of processive actin filament elongation by formins. *Cell Motility and the Cytoskeleton*, 66(8):606–617, August 2009.

[106] Robert J. Pelham and Fred Chang. Actin dynamics in the contractile ring during cytokinesis in fission yeast. *Nature*, 419(6902):82–86, September 2002.

[107] J. Petersen, D. Weilguny, R. Egel, and O. Nielsen. Characterization of fus1 of Schizosaccharomyces pombe: a developmentally controlled function needed for conjugation. *Molecular and Cellular Biology*, 15(7):3697–3707, July 1995.

[108] Janni Petersen, Olaf Nielsen, Richard Egel, and Iain M. Hagan. FH3, A Domain Found in Formins, Targets the Fission Yeast Formin Fus1 to the Projection Tip During Conjugation. *The Journal of Cell Biology*, 141(5):1217–1228, June 1998.

[109] T. D. Pollard. Rate constants for the reactions of ATP- and ADP-actin with the ends of actin filaments. *The Journal of Cell Biology*, 103(6 Pt 2):2747–2754, December 1986.

[110] Thomas D. Pollard. Actin and Actin-Binding Proteins. *Cold Spring Harbor Perspectives in Biology*, 8(8), 2016.

[111] Thomas D. Pollard and Gary G. Borisy. Cellular motility driven by assembly and disassembly of actin filaments. *Cell*, 112(4):453–465, February 2003.

[112] Thomas D. Pollard and John A. Cooper. Quantitative analysis of the effect of Acanthamoeba profilin on actin filament nucleation and elongation. *Biochemistry*, 23(26):6631–6641, December 1984.

[113] Thomas D. Pollard and Jian-Qiu Wu. Understanding cytokinesis: lessons from fission yeast. *Nature Reviews. Molecular Cell Biology*, 11(2):149–155, February 2010.

[114] Francisco Rivero, Tetsuya Muramoto, Ann-Kathrin Meyer, Hideko Urushihara, Taro Q. P. Uyeda, and Chikako Kitayama. A comparative sequence analysis reveals a common GBD/FH3-FH1-FH2-DAD architecture in formins from Dictyostelium, fungi and metazoa. *BMC genomics*, 6:28, March 2005.

[115] Avital A. Rodal, Amity L. Manning, Bruce L. Goode, and David G. Drubin. Negative regulation of yeast WASp by two SH3 domain-containing proteins. *Current biology: CB*, 13(12):1000–1008, June 2003.

[116] Stéphane Romero, Christophe Le Clainche, Dominique Didry, Coumaran Egile, Dominique Pantaloni, and Marie-France Carlier. Formin is a processive motor that requires profilin to accelerate actin assembly and associated ATP hydrolysis. *Cell*, 119(3):419–429, October 2004.

[117] Klemens Rottner, Jan Hänisch, and Kenneth G. Campellone. WASH, WHAMM and JMY: regulation of Arp2/3 complex and beyond. *Trends in Cell Biology*, 20(11):650–661, November 2010.

[118] Jeremy D. Rotty, Congying Wu, Elizabeth M. Haynes, Cristian Suarez, Jonathan D. Winkelman, Heath E. Johnson, Jason M. Haugh, David R. Kovar, and James E. Bear. Profilin-1 Serves as a Gatekeeper for Actin Assembly by Arp2/3-Dependent and -Independent Pathways. *Developmental Cell*, 32(1):54–67, January 2015.

[119] Marco B. Rust, Sharof Khudayberdiev, Silvia Pelucchi, and Elena Marcello. CAPt'n of Actin Dynamics: Recent Advances in the Molecular, Developmental and Physiological Functions of Cyclase-Associated Protein (CAP). *Frontiers in Cell and Developmental Biology*, 8, September 2020.

[120] Alberto Sanchez-Diaz and Pilar Perez, editors. *Yeast Cytokinesis: Methods and Protocols*. Methods in Molecular Biology. Humana Press, 2016.

[121] Micaela Boiero Sanders, Christopher P. Toret, Adrien Antkowiak, Robert C. Robinson, and Alphée Michelot. Specialization of actin isoforms derived from the loss of key interactions with regulatory factors. *bioRxiv*, page 2021.02.09.430555, February 2021. Publisher: Cold Spring Harbor Laboratory Section: New Results.

[122] Kenneth E. Sawin and Paul Nurse. Regulation of Cell Polarity by Microtubules in Fission Yeast. *The Journal of Cell Biology*, 142(2):457–471, July 1998.

[123] Johannes Schindelin, Ignacio Arganda-Carreras, Erwin Frise, Verena Kaynig, Mark Longair, Tobias Pietzsch, Stephan Preibisch, Curtis Rueden, Stephan Saalfeld, Benjamin Schmid, Jean-Yves Tinevez, Daniel James White, Volker Hartenstein, Kevin Eliceiri, Pavel Tomancak, and Albert Cardona. Fiji - an Open Source platform for biological image analysis. *Nature methods*, 9(7), June 2012.

[124] Caroline A. Schneider, Wayne S. Rasband, and Kevin W. Eliceiri. NIH Image to ImageJ: 25 years of Image Analysis. *Nature methods*, 9(7):671–675, July 2012.

[125] André Schönichen and Matthias Geyer. Fifteen formins for an actin filament: A molecular view on the regulation of human formins. *Biochimica et Biophysica Acta (BBA) - Molecular Cell Research*, 1803(2):152–163, February 2010.

[126] Bonnie J. Scott, Erin M. Neidt, and David R. Kovar. The functionally distinct fission yeast formins have specific actin-assembly properties. *Molecular Biology of the Cell*, 22(20):3826–3839, October 2011.

[127] Shashank Shekhar, Johnson Chung, Jane Kondev, Jeff Gelles, and Bruce L. Goode. Synergy between Cyclase-associated protein and Cofilin accelerates actin filament depolymerization by two orders of magnitude. *Nature Communications*, 10, November 2019.

[128] Ameet Shetty, Natalia I. Reim, and Fred Winston. Auxin-Inducible Degron System for Depletion of Proteins in Saccharomyces cerevisiae. *Current Protocols in Molecular Biology*, 128(1):e104, September 2019.

[129] Vladimir Sirotkin, Christopher C. Beltzner, Jean-Baptiste Marchand, and Thomas D. Pollard. Interactions of WASp, myosin-I, and verprolin with Arp2/3 complex during actin patch assembly in fission yeast. *The Journal of Cell Biology*, 170(4):637–648, August 2005.

[130] Vladimir Sirotkin, Julien Berro, Keely Macmillan, Lindsey Zhao, and Thomas D. Pollard. Quantitative Analysis of the Mechanism of Endocytic Actin Patch Assembly and Disassembly in Fission Yeast. *Molecular Biology of the Cell*, 21(16):2894–2904, August 2010.

[131] B. Sjöblom, A. Salmazo, and K. Djinović-Carugo. Alpha-actinin structure and regulation. *Cellular and molecular life sciences: CMLS*, 65(17):2688–2701, September 2008.

[132] Colleen T. Skau, David S. Courson, Andrew J. Bestul, Jonathan D. Winkelman, Ronald S. Rock, Vladimir Sirotkin, and David R. Kovar. Actin Filament Bundling by Fimbrin Is Important for Endocytosis, Cytokinesis, and Polarization in Fission Yeast. *The Journal of Biological Chemistry*, 286(30):26964–26977, July 2011.

[133] Colleen T. Skau and David R. Kovar. Competition between fimbrin and tropomyosin regulates endocytosis and cytokinesis kinetics in fission yeast. *Current biology : CB*, 20(16):1415–1422, August 2010.

[134] Benjamin A. Smith, Karen Daugherty-Clarke, Bruce L. Goode, and Jeff Gelles. Pathway of actin filament branch formation by Arp2/3 complex revealed by single-molecule imaging. *Proceedings of the National Academy of Sciences of the United States of America*, 110(4):1285–1290, January 2013.

[135] Benjamin A. Smith, Shae B. Padrick, Lynda K. Doolittle, Karen Daugherty-Clarke, Ivan R. Corrêa, Ming-Qun Xu, Bruce L. Goode, Michael K. Rosen, and Jeff Gelles. Three-color single molecule imaging shows WASP detachment from Arp2/3 complex triggers actin filament branch formation. *eLife*, 2:e01008, September 2013.

[136] Hilary A Snaith, Itaru Samejima, and Kenneth E Sawin. Multistep and multimode cortical anchoring of tea1p at cell tips in fission yeast. *The EMBO Journal*, 24(21):3690–3699, November 2005.

[137] J. A. Spudich and S. Watt. The regulation of rabbit skeletal muscle contraction. I. Biochemical studies of the interaction of the tropomyosin-troponin complex with actin and the proteolytic fragments of myosin. *The Journal of Biological Chemistry*, 246(15):4866–4871, August 1971.

[138] Benjamin C. Stark, Thomas E. Sladewski, Luther W. Pollard, and Matthew Lord. Tropomyosin and myosin-II cellular levels promote actomyosin ring assembly in fission yeast. *Molecular Biology of the Cell*, 21(6):989–1000, March 2010.

[139] J. Strand, M. Nili, E. Homsher, and L. S. Tobacman. Modulation of myosin function by isoform-specific properties of Saccharomyces cerevisiae and muscle tropomyosins. *The Journal of Biological Chemistry*, 276(37):34832–34839, September 2001.

[140] F. B. Straub and G. Feuer. [Adenosine triphosphate, the functional group of actin]. *Kiserletes Orvostudomany*, 2(2):141–151, 1950.

[141] Cristian Suarez, Robert T. Carroll, Thomas A. Burke, Jenna R. Christensen, Andrew J. Bestul, Jennifer A. Sees, Michael L. James, Vladimir Sirotkin, and David R. Kovar. Profilin regulates F-actin network homeostasis by favoring formin over Arp2/3 complex. *Developmental Cell*, 32(1):43–53, January 2015.

[142] Cristian Suarez and David R. Kovar. Internetwork competition for monomers governs actin cytoskeleton organization. *Nature reviews. Molecular cell biology*, 17(12):799–810, December 2016.

[143] Cristian Suarez, Jérémy Roland, Rajaa Boujemaa-Paterski, Hyeran Kang, Brannon R. McCullough, Anne-Cécile Reymann, Christophe Guérin, Jean-Louis Martiel, Enrique M. De la Cruz, and Laurent Blanchoin. Cofilin tunes the nucleotide state of actin filaments and severs at bare and decorated segment boundaries. *Current biology: CB*, 21(10):862–868, May 2011.

[144] Yidi Sun, Johannes Schöneberg, Xuyan Chen, Tommy Jiang, Charlotte Kaplan, Ke Xu, Thomas D. Pollard, and David G. Drubin. Direct comparison of clathrin-mediated

endocytosis in budding and fission yeast reveals conserved and evolvable features. *eLife*, 8, December 2019.

[145] T. M. Svitkina and G. G. Borisy. Arp2/3 complex and actin depolymerizing factor/cofilin in dendritic organization and treadmilling of actin filament array in lamellipodia. *The Journal of Cell Biology*, 145(5):1009–1026, May 1999.

[146] Masak Takaine and Issei Mabuchi. Properties of Actin from the Fission Yeast Schizosaccharomyces pombe and Interaction with Fission Yeast Profilin *. *Journal of Biological Chemistry*, 282(30):21683–21694, July 2007. Publisher: Elsevier.

[147] Kotaro Tanaka, Shuichi Takeda, Kaoru Mitsuoka, Toshiro Oda, Chieko Kimura-Sakiyama, Yuichiro Maéda, and Akihiro Narita. Structural basis for cofilin binding and actin filament disassembly. *Nature Communications*, 9(1):1860, May 2018. Number: 1 Publisher: Nature Publishing Group.

[148] Shih-Chieh Ti and Thomas D. Pollard. Purification of actin from fission yeast Schizosaccharomyces pombe and characterization of functional differences from muscle actin. *The Journal of Biological Chemistry*, 286(7):5784–5792, February 2011.

[149] Ei-Ichi Ueda, Jun Kashiwazaki, Saki Inoué, and Issei Mabuchi. Fission yeast Adf1 is necessary for reassembly of actin filaments into the contractile ring during cytokinesis. *Biochemical and Biophysical Research Communications*, 506(2):330–338, November 2018.

[150] D. Vavylonis, J.-Q. Wu, S. Hao, B. O'Shaughnessy, and T. D. Pollard. Assembly Mechanism of the Contractile Ring for Cytokinesis by Fission Yeast. *Science*, 319(5859):97–100, January 2008.

[151] Luis Vidali, Peter A. C. van Gisbergen, Christophe Guérin, Paula Franco, Ming Li, Graham M. Burkart, Robert C. Augustine, Laurent Blanchoin, and Magdalena Bezanilla. Rapid formin-mediated actin-filament elongation is essential for polarized plant cell growth. *Proceedings of the National Academy of Sciences*, 106(32):13341–13346, August 2009. Publisher: National Academy of Sciences Section: Biological Sciences.

[152] Ana Virel and Lars Backman. Molecular evolution and structure of alpha-actinin. *Molecular Biology and Evolution*, 21(6):1024–1031, June 2004.

[153] Andrew R. Wagner, Qing Luan, Su-Ling Liu, and Brad J. Nolen. Dip1 defines a class of Arp2/3 complex activators that function without preformed actin filaments. *Current biology: CB*, 23(20):1990–1998, October 2013.

[154] Andrew R. Wagner, Qing Luan, Su-Ling Liu, and Brad J. Nolen. WISH/DIP/SPIN90 proteins form a class of Arp2/3 complex activators that function without preformed actin filaments. *Current biology : CB*, 23(20):1990–1998, October 2013.

[155] M. D. Welch, J. Rosenblatt, J. Skoble, D. A. Portnoy, and T. J. Mitchison. Interaction of human Arp2/3 complex and the Listeria monocytogenes ActA protein in actin filament nucleation. *Science (New York, N.Y.)*, 281(5373):105–108, July 1998.

[156] T.Z. Win, Y. Gachet, D.P. Mulvihill, K.M. May, and J.S. Hyams. Two type V myosins with non-overlapping functions in the fission yeast Schizosaccharomyces pombe: Myo52 is concerned with growth polarity and cytokinesis, Myo51 is a component of the cytokinetic actin ring. *Journal of Cell Science*, 114(1):69–79, January 2001.

[157] Jonathan D. Winkelman, Colleen G. Bilancia, Mark Peifer, and David R. Kovar. Ena/VASP Enabled is a highly processive actin polymerase tailored to self-assemble parallel-bundled F-actin networks with Fascin. *Proceedings of the National Academy of Sciences of the United States of America*, 111(11):4121–4126, March 2014.

[158] D. Winter, T. Lechler, and R. Li. Activation of the yeast Arp2/3 complex by Bee1p, a WASP-family protein. *Current biology: CB*, 9(9):501–504, May 1999.

[159] Hugo Wioland, Antoine Jegou, and Guillaume Romet-Lemonne. Torsional stress generated by ADF/cofilin on cross-linked actin filaments boosts their severing. *Proceedings of the National Academy of Sciences*, 116(7):2595–2602, February 2019. Publisher: National Academy of Sciences Section: PNAS Plus.

[160] J. Q. Wu, J. Bähler, and J. R. Pringle. Roles of a fimbrin and an alpha-actinin-like protein in fission yeast cell polarization and cytokinesis. *Molecular Biology of the Cell*, 12(4):1061–1077, April 2001.

[161] Jian-Qiu Wu, Jeffrey R. Kuhn, David R. Kovar, and Thomas D. Pollard. Spatial and temporal pathway for assembly and constriction of the contractile ring in fission yeast cytokinesis. *Developmental Cell*, 5(5):723–734, November 2003.

[162] Jian-Qiu Wu and Thomas D. Pollard. Counting cytokinesis proteins globally and locally in fission yeast. *Science (New York, N.Y.)*, 310(5746):310–314, October 2005.

[163] Jian-Qiu Wu, Vladimir Sirotkin, David R. Kovar, Matthew Lord, Christopher C. Beltzner, Jeffrey R. Kuhn, and Thomas D. Pollard. Assembly of the cytokinetic contractile ring from a broad band of nodes in fission yeast. *The Journal of Cell Biology*, 174(3):391–402, July 2006.

[164] Jingyuan Xu, Denis Wirtz, and Thomas D. Pollard. Dynamic Cross-linking by α-Actinin Determines the Mechanical Properties of Actin Filament Networks. *Journal of Biological Chemistry*, 273(16):9570–9576, April 1998.

[165] Ann Yonetani, Raymond J. Lustig, James B. Moseley, Tetsuya Takeda, Bruce L. Goode, and Fred Chang. Regulation and targeting of the fission yeast formin cdc12p in cytokinesis. *Molecular Biology of the Cell*, 19(5):2208–2219, May 2008.

[166] Dennis Zimmermann, Kaitlin E. Homa, Glen M. Hocky, Luther W. Pollard, Enrique M. De La Cruz, Gregory A. Voth, Kathleen M. Trybus, and David R. Kovar. Mechanoregulated inhibition of formin facilitates contractile actomyosin ring assembly. *Nature Communications*, 8(1), December 2017.

[167] Dennis Zimmermann, Alisha N. Morganthaler, David R. Kovar, and Cristian Suarez. In Vitro Biochemical Characterization of Cytokinesis Actin-Binding Proteins. *Methods in Molecular Biology (Clifton, N.J.)*, 1369:151–179, 2016.

[168] Austin Zimmet, Trevor Van Eeuwen, Malgorzata Boczkowska, Grzegorz Rebowski, Kenji Murakami, and Roberto Dominguez. Cryo-EM structure of NPF-bound human Arp2/3 complex and activation mechanism. *Science Advances*, 6(23):eaaz7651, June 2020. Publisher: American Association for the Advancement of Science Section: Research Article.

APPENDIX A

PROTOCOLS

A.1 Tethered filament disassembly assay

1) Assemble flow chambers using 1:1000 PEG-Silane:Biotin-PEG-Silane glass

2) Flow HEK-BSA and incubate 3 min.

3) Flow 1.8 μM streptavidin and incubate 30s-1 min.

4) Wash with HEK-BSA

5) Wash 2x with 1X TIRF buffer

6) Flow reaction (actin should contain 0.5% biotin actin) to pre-assemble filaments (usually no proteins of interest, but depends on reaction) and assemble until desired length

7) Flow reaction with proteins of interest and no actin to induce depolymerization/disassembly conditions.

A.2 Fission yeast microfluidic drug treatment assay

1) Assemble CellASIC ONIX microfluidic plate with well 1 on all rows being used that day filled with YE5S + 1% Pluronic F-127. Flow 6 psi into chamber for 10 min and then continuously incubate 50 min at 3 psi. This pre-coats the chamber to avoid small molecules adsorbing to the PDMS.

2) Put cells that have been grown in media + 0.1 % Pluronic F-127 into cell loading well of only the chamber being images.

3) Load cells at 8 psi for 3 seconds. Check cell capture rate/density, and repeat if needed. From here on, image at all steps/media changes.

4) For media rounds and treatments, flow at 6 psi for 10 min and then 3 psi for remaining time. Use this same pressure and timing for each drug treatment / wash switching step.

A.3 Tethered filament binding assay

1) Assemble flow chambers using 1:1000 PEG-Silane:Biotin-PEG-Silane glass

2) Flow HEK-BSA and incubate 3 min.

3) Flow 1 mg/mL neutravidin and incubate 2 min.

4) Wash with HEK-BSA

5) Wash 2x with 1X TIRF buffer

6) Flow reaction with actin alone (at least 0.5% biotin actin) and let filaments pre-assemble to desired length.

7) Flow reaction containing actin, capping protein (to prevent new polymerization), and proteins of interest. Image as rapidly as scope / protein visibility allows.